

**UNIVERSIDADE DE SÃO PAULO
INSTITUTO DE QUÍMICA
Programa de Pós-Graduação em Química**

LAURA MORTARA

**Structure and stability of synthetic surfactant aggregates:
ion association selectivity to interfaces and vesicle
formation**

Versão corrigida da Tese conforme Resolução CoPGr 5890
O original se encontra disponível na Secretaria de Pós-Graduação do IQ-USP

São Paulo

Data do Depósito na SPG

02/06/2023

LAURA MORTARA

Estrutura e estabilidade de agregados de surfactantes sintéticos: seletividade na associação de íons a interfaces e formação de vesículas

Tese apresentada ao Instituto de Química da Universidade de São Paulo para obtenção do Título de Doutora em Ciências (Química)

*Orientador: Prof Dr Hernan Chaimovich
Coorientador: Prof Dr Filipe da Silva Lima*

São Paulo
2023

Autorizo a reprodução e divulgação total ou parcial deste trabalho, por qualquer meio convencional ou eletrônico, para fins de estudo e pesquisa, desde que citada a fonte.

Ficha Catalográfica elaborada eletronicamente pelo autor, utilizando o programa desenvolvido pela Seção Técnica de Informática do ICMC/USP e adaptado para a Divisão de Biblioteca e Documentação do Conjunto das Químicas da USP

Bibliotecária responsável pela orientação de catalogação da publicação:
Marlene Aparecida Vieira - CRB - 8/5562

M827e Mortara, Laura
Estrutura e estabilidade de agregados de surfactantes sintéticos: seletividade na associação de íons a interfaces e formação de vesículas / Laura Mortara. - São Paulo, 2023.
141 p.

Tese (doutorado) - Instituto de Química da Universidade de São Paulo. Departamento de Química Fundamental.
Orientador: Chaimovich, Hernan
Coorientador: da Silva Lima, Filipe

1. Efeito específico de íons. 2. Surfactantes zwitteriônicos. 3. Dinâmica molecular. I. T. II. Chaimovich, Hernan, orientador. III. da Silva Lima, Filipe, coorientador.



Universidade de São Paulo
Instituto de Química

"Estrutura e estabilidade de agregados de surfactantes sintéticos:
seletividade na associação de íons a interfaces e formação de
vesículas"

LAURA MORTARA

Tese de Doutorado submetida ao Instituto de Química da Universidade de São Paulo como parte dos requisitos necessários à obtenção do grau de Doutora em Ciências - no Programa de Química.

Prof. Dr. Hernan Chaimovich Guralnik
(Orientador e Presidente)

APROVADO(A) POR:

Prof. Dr. Mauro Carlos Costa Ribeiro
IQ - USP

Prof. Dr. Luis Gustavo Dias *(por videoconferência)*
FFCLRP - USP

Profa. Dra. Eneida de Paula *(por videoconferência)*
IB - UNICAMP

SÃO PAULO
24 de agosto de 2023

Aos meus pais, Maria e Roberto

Acknowledgments

I would like to thank my supervisors, Prof. Hernan and Prof. Filipe, as also Profa. Iolanda (although not officially my supervisor, you were as important to me as they were on this journey). You taught me how to be a researcher, how to think critically, and, most importantly, how beautiful science can be.

I am also grateful to Prof. Schneck and Prof. van der Vegt, my supervisors during my exchange period in Germany. Thank you for all the valuable scientific knowledge I acquired and for the warm welcome during these challenging pandemic times.

I would also like to thank Profa. Shirley for her helpful discussions on the results during our weekly seminars.

Of course, I would like to express my gratitude to my parents, Maria and Roberto, my siblings Vitor and Sofia, and my grandmother, Gláucia, for the unwavering support they provided me throughout these years.

I am also thankful for all the help I received, both in terms of scientific matters and everyday lab life, from Gustavo and Caroline, who played significant roles in the work carried out here.

I would like to acknowledge all my lab friends, Peter, Matheus, Tarcillo, Norma, Ray, Bea, Bia, Mika, Dani, Liti, Profa Flávia, Lori, Amanda. You made the everyday life so much better.

To Márcia, thank you for all the assistance in the lab (and for the coffees, breakfasts, cakes, and lunches).

I am also grateful to my friends in Germany, Tetiana and Julio, who were incredibly welcoming and provided valuable experimental help. Additionally, I want to express my gratitude to Madhu and Srijita for the delicious meals and great friendship.

I am also thankful for my friends, who always cheered me up when needed!

I would like to acknowledge Lichtenberg II cluster of the TU Darmstadt (Darmstadt, Germany) (Project ID 1544) Santos Dumont cluster of National Laboratory of Scientific Computation (LNCC) (Petrópolis, Brazil) (Project Number 224709) for the computer time for simulations.

Lastly, but most importantly, I would like to thank the funding agencies, FAPESP (process n°2018/19838-8 and n°2019/27381-0) and CNPq, for the scholarships that made all of this possible.

“The more clearly we can focus our attention on the wonders and realities of the universe about us, the less taste we shall have for destruction.”

Rachel Carson

Abstract

Mortara, L. **Structure and stability of synthetic surfactant aggregates: Ion association selectivity to interfaces and vesicle formation.** 2023. (141p.) Ph.D. Thesis – Graduate Program in Chemistry. Instituto de Química, Universidade de São Paulo, São Paulo.

Specific ion effect defines a variety of phenomena in physical chemistry and biology, from the stability of colloidal suspensions to enzymatic activity and ligand-receptor binding. Establishing a rigorous scientific interpretation of these effects has kept scientists busy for over a century. Nevertheless, a complete description of the specificities of ion interactions with the solute surface still needs to be completed.

In the spontaneous aggregation of amphiphiles, the hydrophobic effect depends, almost exclusively, on the difference of free energy between the exposed areas of the hydrocarbon chains of the natural lipid or synthetic surfactant in solution or in the aggregate. The detailed structure of the aggregate, the chain order, and the viscosity depend critically on the surfactant's molecular structure and the medium composition.

We showed that, for zwitterionic micelles, there is no specific anion effect on the overall micelle hydration, but there is a specific anion effect on the thermodynamics of micelle formation. We also showed that the degree of counterion partitioning in these zwitterionic micelles could be directly correlated to the dehydration of apolar moieties of hydrotropic anions upon interface interaction. Still, on ion effects, the competition between chloride and bromide interaction in cationic surfactant monolayers was directly quantified and modeled. Lastly, we showed the formation of vesicular aggregates by a novel imidazolium-based surfactant. Thermal phase behavior of this surfactant was characterized and the phase

transition temperature significantly differed from a similar commercially available surfactant with the same alkyl tail length.

The work developed in this thesis, using two different systems, i.e., zwitterionic and cationic surfactants, has clarified aspects related to specific ion effects and the formation of micellar and vesicular aggregates.

Keywords: micelles, salt effect, hydrophobic effect, hydrotropic anion, molecular dynamics, vesicles

Resumo

Mortara, L. **Estrutura e Estabilidade de Agregados de Surfactantes Sintéticos: Seletividade na Associação de Íons a Interfaces e Formação de Vesículas.** 2023. (141p.). Tese – Programa de Pós-Graduação em Química. Instituto de Química, Universidade de São Paulo, São Paulo.

O efeito específico de íons define uma variedade de fenômenos em físico-química e biologia, desde a estabilidade de suspensões coloidais até atividade enzimática e ligação ligante-receptor. Estabelecer uma interpretação científica rigorosa desses efeitos mantém os cientistas ocupados por mais de um século. No entanto, uma descrição completa das especificidades das interações iônicas com as superfícies dos solutos ainda precisa ser concluída.

Na agregação espontânea de anfifílicos, o efeito hidrofóbico depende, quase exclusivamente, da diferença de energia livre entre as áreas expostas das cadeias de hidrocarbonos do lipídio natural ou do surfactante sintético em solução, ou nos agregados. A estrutura detalhada do agregado, a ordem das cadeias e a viscosidade dependem criticamente da estrutura molecular do surfactante e da composição do meio.

Nesta Tese mostramos que, para micelas zwitteriônicas, não há efeito específico de ânions na hidratação da micela, mas há um efeito específico do ânion na termodinâmica de formação dos agregados. Também evidenciamos que o grau de partição de contraíons nessas micelas zwitteriônicas pode estar diretamente correlacionado com a desidratação de porções apolares dos ânions hidrotrópicos na interação com a interface. Ainda sobre os efeitos dos íons, a competição entre a interação cloreto e brometo em monocamadas de

surfactantes catiônicos foi experimentalmente quantificada e modelada usando dinâmica molecular. Por fim, mostramos a formação de agregados vesiculares por um novo surfactante à base de imidazol. O comportamento deste surfactante com a temperatura foi caracterizado, e a temperatura de transição de fase diferiu significativamente de um surfactante similar disponível comercialmente com o mesmo comprimento de cauda de alquílica.

O trabalho desenvolvido nesta tese, utilizando dois sistemas diferentes, ou seja, tensoativos zwitteriônicos e catiônicos, esclareceu aspectos relacionados aos efeitos de íons específicos e à formação de agregados micelares e vesiculares.

Palavras-chave: micelas, efeito de sal, anion hidrotrópico, dinâmica molecular, vesículas

Table of Contents

1 Introduction.....	15
2 Objectives.....	31
3 Material and Methods.....	33
4 Results.....	35
4.1 Specific Ion Effects on Zwitterionic Micelles Are Independent of Interfacial Hydration Change.....	35
1.1 Introduction.....	35
1.2 Material and Methods.....	37
1.3 Results and Discussion.....	41
1.4 Conclusions.....	58
4.2 Dehydration Determines Hydrotropic Ion Affinity for Zwitterionic Micelles.....	59
2.1 Introduction.....	59
2.2 Methods.....	61
2.3 Results and Discussion.....	63
2.4 Conclusions.....	72
4.3 Anion Effect on the Zwitterionic Surfactant Micellization.....	73
3.1 Introduction.....	73
3.2 Material and Methods.....	75
3.3 Results and Discussion.....	77
3.4 Conclusions.....	84
4.4 Anion competition at positively charged dialkyldimethylammonium monolayers.....	84
4.1 Introduction.....	85
4.2 Material and Methods.....	87
4.3 Results and Discussion.....	95
4.4 Conclusions.....	111
4.5 Thermotropic phase behavior of imidazolium-based surfactant vesicles.....	112
5.1 Introduction.....	112
5.2 Material and Methods.....	113
5.3 Results.....	117

5.4 Conclusion.....	127
5 Conclusions.....	128
6 References.....	131
7 Appendix.....	142
8 Attachment 1 – Curricular Summary.....	155

1 Introduction

This thesis focuses on the aggregation of surfactants into micelles or vesicles and the specific anion interactions with the interfaces formed by these surfactants. In the introduction section, we present some concepts underlying this work, and each chapter contains an appropriate introduction for the specific topic. Published papers and unpublished results prepared for publication comprise the structure of this thesis.

Surfactants are amphiphilic molecules consisting of a non-polar, hydrophobic portion and a polar, hydrophilic portion that can be ionic, non-ionic, or zwitterionic. In aqueous solutions, surfactants can form aggregates spontaneously. Several factors, such as the balance between the hydrophobic and the hydrophilic moieties, the geometry of the monomer, temperature, salt nature, and concentration, determine the size and shape of the surfactant aggregate.

These aggregates find a wide range of applications, such as cosmetics, cleaning, and drug delivery, depending on the specific type of aggregate formed. Micelles have a hydrophobic core that can solubilize hydrophobic molecules, while the hydrophilic outer shell allows this aggregate to remain soluble in water and even adsorb hydrophilic compounds. Conversely, vesicles have an aqueous core that can encapsulate hydrophilic molecules, and their bilayer can hold hydrophobic substances. Vesicles are commonly used in drug delivery systems (Herrmann, 1966).

The main driving force for micelle formation is the hydrophobic effect. This term, first proposed by Kauzmann (Kauzmann, 1959) describes the tendency of non-polar groups to adhere to one another and remove themselves from the aqueous environments. At first, the term drew some criticism (Hildebrand, 1979), with some authors arguing that the adhesion

energy measures a favorable interaction energy between water and other alkane liquids. Although (depending on the temperature) the enthalpy of interaction between water and hydrocarbons is favorable, the overall free energy of the mixture is not due to the losses of entropy caused by dissolving neutral molecules in this already highly structured solvent that is water. (Southall et al., 2002)

The hydration entropy and enthalpy of small non-polar molecules are highly temperature-dependent, resulting in a characteristic large positive heat capacity, ΔC_p , while the overall free energy is not and shows a non-monotonic behavior (Chandler, 2005).

These thermodynamics characteristics, namely, the large contribution and the temperature dependence of the entropy for the hydrophobic effect, were interpreted by Frank and Evans in terms of the ordering effect of water around the non-polar solute. These authors proposed that the first water shell around the solute forms a more crystalline structure, with frozen patches or microscopic icebergs. The "freezing" of water causes the entropy to be lost, and with increasing temperatures the structure of water is broken down, diminishing the entropic contribution (Frank and Evans, 1945).

Based on the heat capacity of hydrophobic solvation, Gill and coworkers proposed a two-state model, where water molecules in the first hydration shell of hydrophobic solutes behave in a "non-cooperative mode", different from the bulk water. The heat capacity properties of the solvation shell was quantitatively described due to this difference in behavior (Gill et al., 1985). Supported on Gill's two-states model, Muller suggested that the hydrogen bonds of water are different in bulk and the hydration shell, and the breaking of H-bonds has different enthalpy, entropy, and free energy for both molecule types (Muller, 1990).

These approaches lead to the conclusion that the surface area of hydrophobic compounds in water is sufficient to explain the hydrophobic effect, but experiments have shown

this is not true. The free energy of transfer of small oil molecules from liquid hydrocarbon to water is about 25 cal mol^{-1} per \AA^{-2} of surface. In contrast, the free energy cost to eliminate the hydrocarbon/water interface is about 75 cal mol^{-1} per \AA^{-2} of surface (Tanford, 1979). If the transfer of oil molecules were to be proportional only to the surface area of the hydrocarbon molecule, these values should be the same.

The explanation for this difference in both experiments is that distinct mechanisms are involved in each system: for small molecules, the solute provokes an ordering of water molecules that scales with the occupied volume, where there is no need to break hydrogen bonds, whereas, for large solutes, the free energy cost scales with the area because of the water hydrogen bonds are broken. The crossover from one regime to another is at approximately 1 nm^2 solute volume (Chandler, 2005), indicating that hydrophobicity depends not only on the surface area of a solute but also on its shape and curvature (Southall and Dill, 2000).

This difference between both regimens is precisely what explains the aggregation of oil molecules in water. The free energy gain associated with the aggregate formation comes from the difference between the free energy of solvation of small oil species that are well separated in water, i.e., entropically dominated solvation free energy, and the free energy of solvation of a large cluster of these same species, i.e., the enthalpically dominated solvation free energy of large surfaces (Maibaum et al., 2004).

Southall and Dill explained the difference between hydrating small or large solutes using a two-dimensional water model (Ben-Naim, 1971), reaching similar conclusions to the above (Southall and Dill, 2000). In this model, each water molecule is represented by a 2-dimensional circular disk that can interact through three hydrogen bonds with other molecules, arranged similarly to the Mercedes-Benz logo, hence the name. The authors showed that the free energy of hydrating a small spherical solute increases with the solvent's radius by ex-

panding the cage's structure and lowering enthalpy and entropy. In contrast, for a large solute, free energy increases due to the breakage of hydrogen bonds in the cage.

Because of the amphiphilic nature of surfactants, the hydrophobic effect is crucial to explain the formation of micelles. However, an opposing force to aggregation arises from electrostatic or volume repulsion between the polar head groups (Equation 1.1 (Tanford, 1974)).

$$\Delta G_m^o = \Delta U_m^o + W_m \quad (1.1)$$

,where ΔU_m^o is the free energy associated with the alkyl chain transfer (negative – hydrophobic effect), and W_m is the free energy associated with the head group repulsion (positive).

The free energy can be further divided into several contributions for a more realistic picture. Nagarajan and Ruckenstein split the contributions for the free energy of micelle formation into four components: 1. The transfer of the surfactant tail from water into hydrophobic micelle core (μ_{tr}); 2. The conformational free energy of the tails arising due to the positional constraints (μ_{def}); 3. The free energy of formation of aggregate-water interface (μ_{int}); 4. The head group interactions, as stated by Tanford, are repulsive steric contributions (μ_{steric}). In the case of a zwitterionic micelle, the head groups' dipole interaction must also be considered (μ_{dipole}). For an ionic micelle, another term related to the charged head group at the micelle interface and the ions (μ_{ionic}) is introduced (Nagarajan and Ruckenstein, 1991).

Similarly, Maibaum and coworkers separate the thermodynamics of micellization into three contributions (Figure 1.1): 1. The creation of a cavity in the solvent (Figure 1b); 2. Transferring the hydrophobic chains from the aqueous solution into the cavity (Figure 1c) and 3. Distributing the polar units over the surface of the cavity and reconnecting them to the

hydrophobic groups (Figure 1.1d) (Maibaum et al., 2004). These models help understand the thermodynamics, temperature, and salt effects on the aggregation of surfactants.

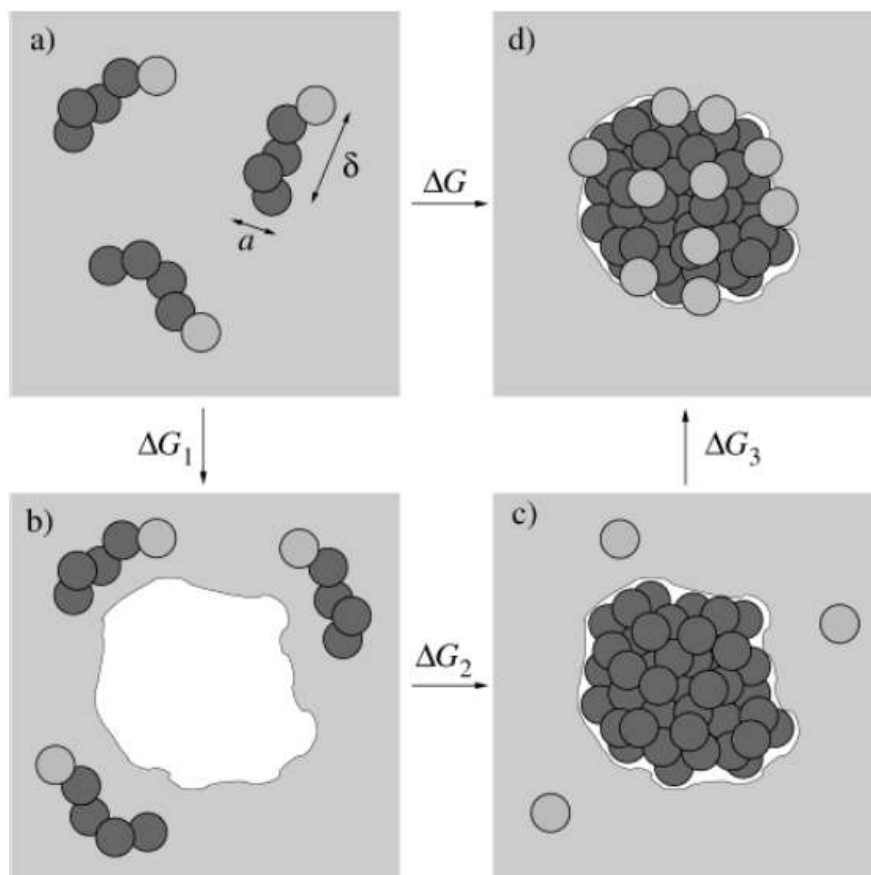


Figure 1.1: Thermodynamic cycle of micelle formation. Reprinted with permission from (Maibaum et al., 2004). Copyright 2004 American Chemical Society.

A micelle can be regarded as a distinct chemical species and treated using a mass action model or a separate phase with a phase separation model. Both models have advantages and disadvantages. Individual micelles are usually not large enough to be considered a different phase, but the ensemble of these aggregates shares properties similar to a separate phase.

The aggregation of a zwitterionic surfactant in water can be described with Equation

1.2



Where n is the number of monomers in an aggregate S (N_{agg}), and S_n represents the aggregate. In this equilibrium representation, monomers can enter or leave the micelle. N_{agg} can be measured experimentally (Alargova et al., 1998). The monomer concentration threshold for micelle formation is known as the critical micelle concentration (cmc). Cmc is a well-defined quantity, measurable by determining several properties of the surfactant system that change abruptly with surfactant concentration (Figure 1.2). These properties include surface tension, osmotic pressure, turbidity, and conductivity. Cmc depends on the temperature, ionic strength, pH, and the nature of the ions or other molecules in the solution.

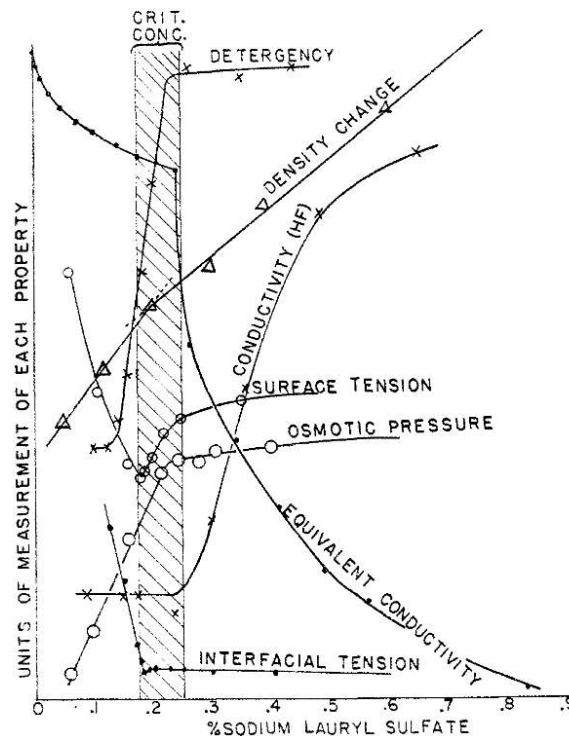


Figure 1.2: Physical property curves for sodium dodecyl sulfate. Reprinted with permission from (Preston, 1948). Copyright 1948 American Chemical Society.

From Equation (1.2), an equilibrium constant (K_m) can be defined as:

$$K_m = \frac{[S_n]}{[S]^n} \quad (1.3)$$

Using the relationship $\Delta G^\circ = -RT \cdot \ln K_m$, the free energy for micelle formation is:

$$\Delta G^\circ = -RT \cdot \ln([S_n] - n \cdot \ln[S]) \quad (1.4)$$

where R is the gas constant, and T is the temperature. Considering the $[S] = cmc$ and dividing both sides by n, one obtains the free energy per monomer:

$$\Delta G_{mic}^\circ = (-RT \cdot \ln[S_n])/n + RT \cdot \ln(cmc) \quad (1.5)$$

As n is typically large ($n > 50$), the first term of Equation 1.5 is much smaller than the second one (Nagarajan and Ruckenstein, 1991). Thus, Equation 1.5 can be simplified:

$$\Delta G^\circ \approx RT \cdot \ln K(cmc) \quad (1.6)$$

For ionic surfactants, the counterions need to be considered:

$$\Delta G^\circ \approx (1 + \alpha)RT \cdot \ln K(cmc) \quad (1.7)$$

where α is the degree of counterion ionization, $\alpha = p/n$, with p = free counterion in solution.

The size of ionic micelles is affected by the presence of salts and the nature of the counterion. As stated above, one of the opposing forces to aggregation is the repulsion of the polar head groups, which can be screened by the presence of ions with opposed charges. For ionic micelles, the counterion condensation at the micelle interface influences both the CMC and the aggregation number (Mukerjee et al., 1966). The effect of counterion depends not

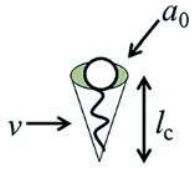
only on the charge but also varies with the nature of the ion, known as the specific ion effect (SIE), which will be discussed later.

The shape of the aggregate formed by the surfactant monomers is also dependent on the monomer structure. Israelachvili, Mitchell, and Ninham introduced geometrical considerations of the monomer that allow for predicting the shape of surfactants aggregates (Israelachvili et al., 1977, 1976). The molecular packing parameter or critical packing parameter (CPP) can be written as (Equation 1.8)

$$CPP = \frac{v}{a_0 \cdot l_0} \quad (1.8)$$

where v = volume of hydrocarbon core, a_0 = effective head group area, and l_0 = hydrocarbon chain length. A representation for surfactant CPP is in Figure 3, together with the predicted shape according to CPP value.

Spherical micelles are expected for surfactants with a CPP of $< 1/3$, whereas closed bilayers are expected with a CPP between $1/2$ and 1.



$CPP = v/a_0 l_c$

Critical Packing Parameter ($v/a_0 l_c$)	Critical Packing Shape	Structures Formed
$< 1/3$	Cone	Spherical micelles
$1/3 - 1/2$	Truncated cone	Cylindrical micelles
$1/2 - 1$	Truncated cone	Flexible bilayers, vesicles
~ 1	Cylinder	Planar bilayers
> 1	Inverted truncated cone or wedge	Inverted micelles

Figure 1.3: Molecular shapes, critical packing parameter (CPP) of surfactants and lipids, and the structures formed. Reproduced from (Dutt et al., 2017) with permission from the Royal Society of Chemistry.

Surfactants with two long-chain hydrophobic tails (usually larger than $(CH_2)_{12}$) have a high CPP because the volume of hydrocarbon chains is large. Above a critical aggregate concentration (CAC) (ca. 10^{-10} M), bilayers are formed, and if allowed by the CCP, the bilayers can close into spherical vesicles.

Vesicles of different sizes can be formed, with one (unilamellar) or more (multilamellar) bilayers. Vesicles containing only one bilayer can be classified according to their size as small unilamellar vesicles (SUV) with 15-30 nm in diameter, large unilamellar vesicles (LUV) with 100-200 nm diameter, or giant unilamellar vesicles (GUV), for diameters above 10000 nm. Multilamellar vesicles (MLV) with concentric shells of closed bilayers are commonly observed and form spontaneously upon adding an aqueous solution to dry double-tailed surfactants (Figure 1.4).

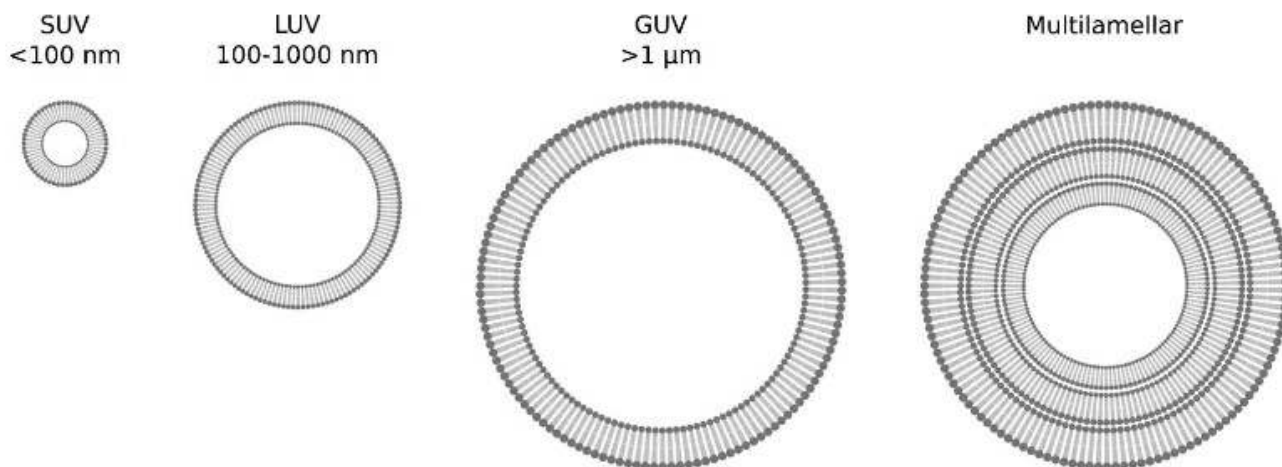


Figure 1.4: Representation of different vesicular aggregates. Modified and reprinted with permission from (Van Swaay and deMello, 2013). Copyright 2013 American Chemical Society.

The formation of aggregates also depends on temperature. Aggregates can be formed in solution above the temperature where the solubility curve intersects with the CMC curve (Figure 1.5). The Krafft point can be interpreted as the temperature at which the solubility of surfactants as monomers becomes high enough for the monomers to start aggregation or micellization (Moroi and Matuura, 1988).

Some authors refer to the Krafft point as the melting point for hydrated solid surfactants (Shinoda, 1987). This interpretation comes from the viewpoint of aggregates being in a different phase than water, i.e., the phase separation model.

At high surfactant concentration (\gg cmc) and above the solubilization temperature, aggregates such as micelles or vesicles begin to interact, and surfactant molecules start to align and orient, forming liquid crystals (Figure 1.5). The most common liquid crystals are: 1. lamellar phase, where a water layers separate bilayers, and the bilayers can extend for microns; 2. hexagonal phase, with rod-shaped micelles of undefined length, packed as hexagonal arrays and separated by a continuous water region; and 3. cubic phase formed by

packing micelles into body-centered cubic or face-centered cubic arrays. Liquid crystal phases can also be considered an intermediate stage between the solid and melt/liquid phases (Tiddy, 1980).

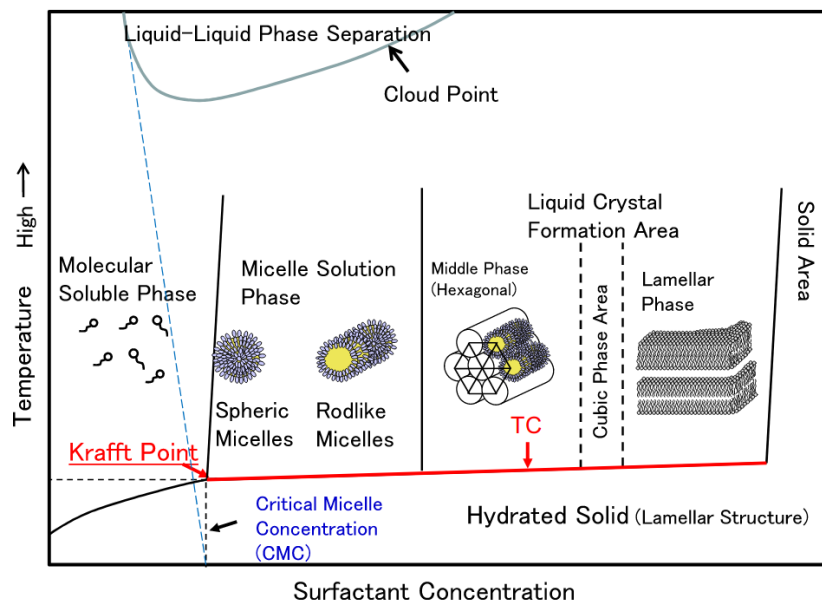


Figure 1.5: Figure 5. Representation of a phase diagram of a mixture of an amphiphile and water. The amphiphile concentration is represented in the horizontal axis, and in the vertical axis, the temperature. Reprinted with permission from (Nakama, 2017). Copyright 2017 Elsevier

One important transition that is observed upon temperature increase of the lamellar phase, is the gel to liquid-crystalline phase. This transition is related to the melting of the hydrocarbon chains, that undergo a shift from an ordered state (referred to as gel) to a more liquid-like conformation (known as liquid-crystalline) as temperature changes (Tardieu et al., 1973). The temperature where this transition occurs can be called melting temperature (T_m), critical temperature (T_c), or main transition temperature. Due to packing constraints of the bilayer, there is a reduced amount of disordering at the phase transition compared to the isotropic melting of alkanes. This transition is also observed at lower surfactant concentrations, for example, in vesicles bilayers (Taylor and Morris, 1995).

The transition temperature depends on the nature of the polar head group and the length and degree of unsaturation of the hydrocarbon chains. For example, the small difference in the headgroups between phosphatidylcholines and phosphatidylethanolamines leads to a difference of almost 30 °C in the T_m (Chapman et al., 1974). This phase transition holds significant biological importance as the fluidity of biological membranes plays a crucial role in various phenomena (Heimburg, 2019).

Other ordered phases are also observed for lipid systems, like the ripple and the subgel phases (Nagle and Tristram-nagle, 2000). Some authors also report the existence of a coagel phase, below T_c . In the coagel phase, the surfactants are in a hydrated-crystalline state separated from the water solution phase (Kodama and Seki, 1991). Krog and Larsson suggest that the gel phase is metastable and may evolve into the crystal and water state (Krog and Larsson, 1968).

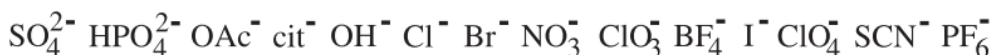
As discussed above, ions generally influence colloids' aggregation and stability. Specific Ion Effects (SIE) have been known since the XIX century (Hofmeister, 1888). Hofmeister observed that anions with the same charge have different effects in several systems: precipitation of blood serum proteins, egg white proteins, colloidal ferric oxide, etc. In his work, he postulated that a salt's colloid precipitating effect depends on its "water withdrawing effect" (Kunz et al., 2004). Salts could absorb the water and "steal" it from the solute, promote the precipitation (Okur et al., 2017). Although Hofmeister studied salts, the ordering known today as the Hofmeister series consists of both anions and cations separately. It is also known as the lyotropic series (Voet, 1937). A typical ordering for the Hofmeister series is in Figure 1.6.

As Kunz and Neueder noted, specific ion effects were first observed by Poiseuille and coworkers and Cox and Wolfenden earlier. These authors observed that some salts increase water viscosity, whereas others decrease it (Kunz and Neueder, 2009) and proposed that the

ions can influence the water structure, thus changing the viscosity. Later, using the relationship between viscosity and entropy of dilution, Frank and Evan proposed that some ions are "water structure-breaker" or "water structure-maker" (Frank and Evans, 1945). Structure breaker anions can also be called chaotropic, whereas structure breakers are kosmotropic.

HOFMEISTER SERIES

Cations



Anions


<p>kosmotropic</p> <p>↑ surface tension</p> <p>harder to make cavity</p> <p>↓ solubility hydrocarbons</p> <p>salt out (aggregate)</p> <p>↓ protein denaturation</p> <p>↑ protein stability</p> <p>weakly hydrated soft cations of low charge density</p> <p>strongly hydrated hard anions of high charge density</p>		<p>chaotropic</p> <p>↓ surface tension</p> <p>easier to make cavity</p> <p>↑ solubility hydrocarbons</p> <p>salt in (solubilize)</p> <p>↑ protein denaturation</p> <p>↓ protein stability</p> <p>strongly hydrated hard cations of high charge density</p> <p>weakly hydrated soft anions of low charge density</p>
--	---	---

Figure 1.6: Typical ordering of cations and anions, from (Kunz and Neueder, 2009).

Salts dissociate in water into solvated ions. Due to the large electric field generated by the ions, especially smaller ones, it is expected that the dipolar water molecules will rearrange in the hydration shells with a structure different from that in bulk water (Marcus, 2009), and as was pointed earlier in this introduction, the insertion of a solute in water will cause an

interfacial water rearrangement. But after analyzing the existing experimental data, Marcus found evidence suggesting that water structure can be modified by the presence of ions beyond their hydration shells. His excellent review also points out that the present data does not prove that this modification is responsible for the specific ion effect.

The ability of an ion to modify the structure and properties of water is a well-accepted mechanism to account partly for SIE. Still, water modification cannot predict many of the observed SIE phenomena. Note that, in the lyotropic series, ions can change order depending, among other factors, on the surface charge of a solute, solvent polarity, temperature, and salt content (Schwierz et al., 2016).

After reviewing specific ion effects theories, Lo Nostro and Ninham suggested that the quantum dispersion forces are ultimately responsible for the specificity and should, therefore, be considered (Lo Nostro and Ninham, 2012). In another fascinating review, Leontidis suggests that "ionic hydrophobicity and complexation capacity" can also be essential to determine ionic behavior (Leontidis, 2017). Thus, it is crucial to consider the specific interaction of the ion with the surface when predicting the ion effect. Here, I will focus the discussion on anion effects on surfactant aggregates. These aggregates have an interesting interface, with the polar head group exposed to the water interface and the hydrophobic portion that is (partially) hidden within the aggregates (Stephenson et al., 2007). It is also important to notice that different geometries of aggregates, like micelles, vesicles, or even monolayers, can play important roles in the specificity due to the difference in packing and hydration (Aroti et al., 2007).

Hydrophobicity is an essential factor for chaotropic ions. The limiting ions of the Hofmeister series are usually SCN^- and ClO_4^- , or guanidinium cation. Although there are studies on more hydrophobic ions, the literature is scattered, and these ions have not been

studied systematically (Leontidis, 2016). It is clear, however, that hydrophobic and hydrotropic (see below) ions cause very strong ion-specific effects in surfactant aggregates (Benrraou et al., 2003; Geng et al., 2006; Lima et al., 2013a)

Mehringer, Kunz, and Neuberg introduced the term hydrotrope to describe molecules that increase the water solubility of organic molecules (Mehringer and Kunz, 2021; Neuberg, 1916). Hydrotropes are amphiphilic molecules with small polar and bulky non-polar moieties (Matero, 2002) but the proportion between polar and non-polar portions is much higher than regular surfactants (Hopkins Hatzopoulos et al., 2011). Because of the amphiphilic character of hydrotropes, some can self-aggregate but at much higher concentrations than surfactants (Hopkins Hatzopoulos et al., 2011). The mechanism behind the solubilization of hydrophobic compounds by hydrotropes is unclear, but the accumulation of hydrotropes around the hydrophobic solute may lead to the observed solubilization increase (Shimizu et al., 2013).

Because of the amphiphilic character, hydrotropes bind to the micellar interface and cause shape transitions and even phase separation, as observed in cationic micelles upon trifluoromethanesulfonate (triflate, Tf) addition (Lima et al., 2015). Hydrotropes with aromatic portions can penetrate the surfactant headgroups region, reduce the charge, and change the packing parameter due to the large size of the ion and induce micellar elongation (Magid et al., 1997). Hydrotropic counterions can also affect the hydration of the micellar surface in cationic micelles, thus leading to phase transition (Geng et al., 2005; Lima et al., 2015) According to Leontidis (Leontidis, 2016), "the hydrophobicity of the aromatic counterions determines the way that they anchor themselves on the micellar interfaces." Still, we do not have enough information to create hydrotropic power sequences or place hydrotropic anions on the anionic Hofmeister series.

All the topics explored above are essential to evaluate the data presented in the thesis. Here, the physical chemistry properties of different surfactant aggregates and specific ion

effects were assessed. In the first chapters, the specific anion effect of chosen hydrotropes on zwitterionic micelles was evaluated on the aggregates and micellization thermodynamics. Cationic surfactants containing two alkyl chains were studied in the following chapters, by characterizing the formed vesicles and specific ion effects in monolayer and vesicles.

2 Objectives

The primary objective of this thesis is to investigate the formation of amphiphilic aggregates and the partitioning of ions in their interfaces. To achieve this, we have outlined three specific objectives:

1. Elucidate the specific ion interaction of hydrotropic anions in zwitterionic interfaces: In the introduction, it is mentioned that the addition of hydrotropic anions to cationic micelle solutions can lead to changes in aggregate size, shape, and even phase separation. However, this effect has not been explored in zwitterionic micelles, except for studies involving perchlorate addition. To gain insights into these specific ion effects, we employed various experimental and theoretical techniques.
2. Quantify and describe the competition between chloride and bromide anions at cationic interfaces using Total-Reflection X-Ray Fluorescence and Molecular Dynamics Simulations: As highlighted in the introduction, it is intriguing to investigate specific ion effects in different aggregate geometries, as the packing and curvature may play crucial roles. Monolayers serve as compelling systems because the area per monomer can be extensively varied, enabling exploration of the ion effect on different lipid phases. Moreover, Total Reflection X-Ray Fluorescence (TRXF) allows for direct quantification of ions at the monolayer interface, a capability not feasible with other techniques.
3. Characterize an imidazolium-based cationic surfactant and compare its properties to a commercially available one: This objective involves describing a novel imidazolium-based surfactant synthesized in our laboratory. The focus of this work was the theoretical exploration of the properties of vesicles based on the headgroup chemistry,

aiming to provide insights into the surfactant's unique characteristics in comparison to a commercially available surfactant.

3 Material and Methods

This thesis comprises articles and manuscripts, with the materials and methods being described in each subsection in results chapter. In this context, I use the material section to present the chemical structures for the surfactant and salts utilized.

In the first 3 subsections, zwitterionic surfactant N-Dodecyl-N,N-dimethyl-3-ammonio-1-propane-sulfonate (DPS) was used, structure is in Figure 3.1. and the hydrotropic salts evaluated are in Figure 3.2.

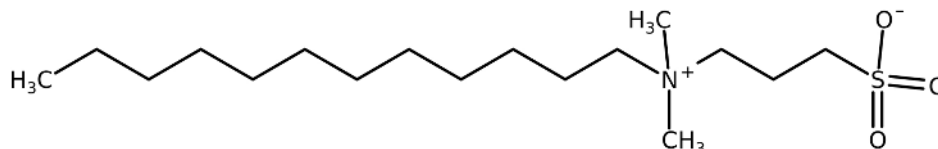


Figure 3.1: Chemical Structure of N-Dodecyl-N,N-dimethyl-3-ammonio-1-propane-sulfonate (DPS)

The hydrotropic salts evaluated here are constituted of two different hydrophilic moieties (Carboxylate or Sulfonate) and three different hydrophobic moieties (Methane, Fluoromethane or Benzene). They are in Figure 3.2.

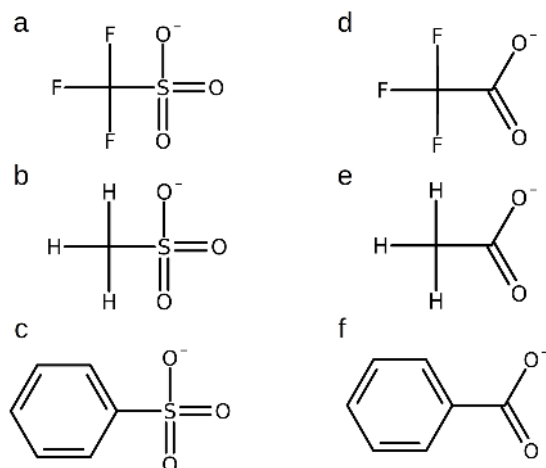


Figure 3.2. Chemical Structures of hydrotropic anions: a) Methanesulfonate (Ms), b) Triflate (Tf), c) Benzenesulfonate (BZS), d) Trifluoroacetate (TFA), e) Acetate (Ac), and f) Benzoate (BZC).

Beside the hydrotropic salts, Bromide (Br⁻), Chloride (Cl⁻) and Perchlorate (ClO₄⁻) were also used.

The cationic surfactants used were Dimethyldioctadecylammonium bromide (DODAB), Dimethylhexadecylammonium chloride (DHDAC) and 1,3-Di-hexadecyl-imidazolium chloride (DHImC). The chemical structures are in the results section of chapter 4.4.

4 Results

4.1 Specific Ion Effects on Zwitterionic Micelles Are Independent of Interfacial Hydration Change

This chapter is a published paper, and was reproduced with permission from *Langmuir* 2018, 34, 37, 11049–11057. Copyright 2018 American Chemical Society.

Abstract

Zwitterionic micelles adsorb anions and several techniques were used to determine the specificity of this interaction. Although at a lower intensity, this adsorption can be compared to those observed in cationic micelles, which showed that interfacial dehydration is a fundamental property for the geometry and size of micelles. Because there is no information on the interfacial hydration of zwitterionic micelles, we used dielectric relaxation spectroscopy (DRS) together with molecular dynamics (MD) simulations to evaluate the importance of surface dehydration promoted by the binding of anions at the micellar interface (sodium bromide, sodium methanesulfonate, sodium trifluoroacetate, and sodium triflate) in N-dodecyl-N,N-dimethyl-3-ammonio-1-propanesulfonate (DPS) micelles. Our results, showing good agreement between DRS and MD simulations, strongly suggest that specificity effects on zwitterionic micelles are unrelated to global changes in the interfacial hydration and depend on specific interactions of the headgroups with selected anions.

1.1 Introduction

Micelles formed by self-association of zwitterionic surfactants adsorb anions preferentially (Baptista et al., 1992; Gerola et al., 2017b). Selective anion binding to the formally neutral interface of N-dodecyl-N,N-dimethyl-3-ammonio-1-propanesulfonate (DPS)

micelles is well-known (Beber et al., 2004; Cuccovia et al., 1990; Okada and Patil, 1998; Priebe et al., 2012; Rodríguez et al., 2001; Santos and Longo, 2016). DPS micelles display negative zeta potentials upon salt addition (Priebe et al., 2012, 2008) with local anion concentrations higher than in bulk (Cuccovia et al., 1990). The interaction of anions with the nitrogen from the polar head of the DPS was determined by measuring the symmetry changes about ^{14}N in NMR measurements (Beber et al., 2004). Anions show specific interaction with sulfobetaine stationary phase (Okada and Patil, 1998) and several reactions using micelle as reaction media display sharp and specificity effects (Priebe et al., 2008; Rodríguez et al., 2001). Molecular dynamics of sulfobetaine micelles also show increased concentration of anions at the interface (Santos and Longo, 2016).

Increase of external salt concentration or binding of hydrotropic anions to positively charged micelles of N-hexadecyltrimethylammonium (CTAX, where X is the anion), a surfactant that has the same positively charged group as DPS monomers, produces severe interfacial dehydration and changes in shape of the micelle (Geng et al., 2005). An extreme case is exemplified by trifluoromethyl sulfonate (triflate, Tfl), a counterion that binds strongly to cationic micelles of N-dodecyltrimethylammonium (DTAX), produces significant dehydration of the interface, and can induce phase separation (Lima et al., 2015, 2011). It is clear, therefore, that for cationic micelles a correlation between specific ion effects in micelles and micellar interfacial hydration is established and even to ion (de)hydration upon adsorption at the micellar interface (Lima et al., 2017).

When comparing the selectivity of anion binding to zwitterionic DPS and cationic ammonium quaternary micelles one would tend to think that as both micelles seem to select anions to a similar degree, changes of interfacial hydration could be equivalent. Despite the amount of information concerning selective ion binding to zwitterionic micelles, the interfacial hydration of these aggregates with salt has been less explored.

Here, we used dielectric relaxation spectroscopy (DRS) as a technique (Rahman et al., 2012; Sonnleitner et al., 2014) to analyze dipole relaxations in systems composed of DPS zwitterionic micelles with or without added salts. We obtained DR spectra of aqueous DPS solutions and of solutions containing NaBr, sodium methanesulfonate (NaMs), sodium trifluoroacetate (NaTfa), and sodium triflate (NaTfl) to investigate the effects of salts on micellar hydration. We also analyzed, using molecular dynamics (MD) simulations, interfacial hydration of the same systems. Our results demonstrated a relative lack of specific salt effects on the various states of bound water and strongly suggest that specific ion effects on zwitterionic micelles are unrelated to overall changes in the interfacial hydration but are dependent on specific interactions of the headgroups with selected anions.

1.2 Material and Methods

1.2.1 Materials. N-Dodecyl-N,N-dimethyl-3-ammonio-1-propane-sulfonate, DPS, (Sigma-Aldrich) was recrystallized twice from methanol/acetone. NaBr (LabSynth, analytical grade) was used as received. Sodium trifluoromethanesulfonate (NaTfI) was prepared by stoichiometric titration of aqueous triflic acid (Sigma-Aldrich) with NaOH (Sigma-Aldrich) and the salt solution was lyophilized. Sodiummethanesulfonate (NaMs) (Aldrich) was recrystallized from water/methanol. Sodium trifluoroacetate (NaTfa) was prepared by the stoichiometric titration of aqueous trifluoroacetic acid (Aldrich) with NaOH (Sigma-Aldrich) and the salt solution was lyophilized. Solutions were prepared with dried salts kept under vacuum. Pyrene (Sigma-Aldrich) was recrystallized from ethanol/water and N-dodecylpyridinium chloride (Aldrich) from methanol/acetone. Salt containing solutions were prepared with dried salt and dried surfactant using Millipore water.

1.2.2 Dielectric Relaxation Spectroscopy. Dielectric spectra were obtained by combining a waveguide interferometer ($60 \leq \nu/\text{GHz} \leq 89$) and an Agilent E8364B vector network analyzer (VNA) operated with an electronic calibration module (Ecal, AgilentN4693A), two commercial open-ended coaxial reflection probes ($0.2 \leq \nu/\text{GHz} \leq 20$ and $1 \leq \nu/\text{GHz} \leq 50$), and a coaxial-line cutoff reflection cell ($0.02 \leq \nu/\text{GHz} \leq 0.5$). The reflection measurements were taken at least two times with independent calibrations, using air, water, and mercury as open, load, and short standards (Sonnleitner et al., 2014). The response of the DRS instrument to the sample submitted to the field of frequency (ν) was recorded as the total complex permittivity, $\hat{\eta}(\nu)$

$$\hat{n}(\nu) = \hat{\epsilon}(\nu) - \frac{i\kappa(c)}{2\pi\nu\epsilon_0} \quad (4.1.1)$$

and the complex permittivity can be described as $\hat{\epsilon}(\nu) = \epsilon'(\nu) - i\epsilon''(\nu)$, where ϵ_0 is the permittivity of vacuum, ϵ' is the relative permittivity, and ϵ'' is the dielectric loss. The complex permittivity spectrum can be described as a sum of n individual relaxation process (modes)

$$\hat{\epsilon}(\nu) = \sum_{i=0}^n S_i \tilde{F}_i(\nu) + \epsilon_\infty \quad (4.1.2)$$

where S_i being the amplitude of the mode i , ϵ_∞ is the “infinite frequency”, and \tilde{F}_i is the band shape function that can be described by the general eq 4.1.3

$$\hat{F}(\nu) = [1 - (i2\pi\nu\tau_i)^{1-\alpha_i}]^{-\beta_i} \quad (4.1.3)$$

If $0 \leq \alpha_i \leq 1$ and $\beta_i = 1$, eq 3 is called Cole–Cole (CC) equation and if $\alpha_i = 0$ and $\beta_i = 1$, eq 3 is called Debye (D) equation. The analysis of the spectra was carried out by simultaneously fitting $\epsilon'(\nu)$ and $\epsilon''(\nu)$ with several models using the selection criteria described in (Rahman et al., 2012).

1.2.3 Conductivity.

Conductivity, κ , was measured for two different samples at 25 ± 0.005 °C using a computer-controlled setup and two-electrode capillary cell, calibrated with aqueous KCl (Nazet et al., 2015). Conductivity values were used in eq 4.1.1.

1.2.4 Density. The densities for two independent solutions for all the samples were measured at 25°C using a vibrating-tube densitometer (Anton PÅr DMA 5000 M) with ± 0.05 kg/m³ uncertainty. Densities of the samples were used to calculate water concentration following eq 4.

$$c_w = \frac{\rho}{MM_w} - C_{DPS} \left(\frac{MM_{DPS}}{MM_w} \right) \quad (4.1.4)$$

where c_w and MM_w are the total water concentration and water molecular mass, respectively; ρ is the sample density, and c_{DPS} and MM_{DPS} are the surfactant concentration and molecular mass, respectively.

1.2.5 Critical Micelle Concentration (cmc). The cmc were determined by measuring surface tension with a Lauda TD3 tensiometer, using a du Noüy ring. Aliquots of a stock surfactant solution were added to 10 mL of water with or without salt, and the cmc was calculated as described previously (Mukerjee and Mysels, 1971). Two independent measures were taken for each salt concentration. Temperature was maintained at $25.00 \pm 0.01^\circ\text{C}$ using a Lauda thermostat.

1.2.6 Aggregation Number (N_{agg}). Micellar N_{agg} 's were measured by time-resolved fluorescence quenching (TRFQ) method as described previously (Lima et al., 2013b). Pyrene, used as fluorophore, was added to the surfactant and salt mixtures. N-Dodecylpyridinium chloride, used as quencher, was added (five times additions) until a final concentration of two quencher molecules per micelle was reached. Fluorescence intensities and decay were determined using an Edinburgh FLS920 spectrometer system with time correlated single photon counting (318.0 ± 0.5 K). Laser pulse was 2 μs . At least two independent measurements for each surfactant and salt mixture were obtained with emission at 383.0 nm and excitation at 335.6 nm with a window of 1 μs and 2,048 channels. N_{agg} was calculated by analyzing the characteristic decay of Pyrene fluorescence in micelles (Lima et al., 2013b).

1.2.7 Molecular Dynamics Simulations. MD simulations were performed for systems containing a micelle of DPS in water and in four salts (NaBr, NaMs, NaTfa, NaTfl) solutions, using GROMACS 5.1.4 (Abraham et al., 2015)) with GAFF for the polar head of the surfactant (Wang et al., 2004), GAFF lipid forcefield was used in the tail of the surfactant (Dickson et al., 2012), and SPC/E forcefield for water (Berendsen et al., 1987). The dihedral parameters of the surfactant polar head were obtained using ab initio calculations with Gaussian ((Frisch et al., 2016) (HF/6-31G*)) for dihedral scans accordingly to the standard procedure in GAFF (Wang et al., 2004). The partial charges of the atoms were also calculated with Gaussian (HF/6-31G*). Dihedral parameters and atomic charges are in Appendix (Tables S1 and S2). An initial structure of a spherical micelle containing 55 DPS molecules, the aggregation number in (Florenzano and Dias, 1997) was built using Packmol (Martínez et al., 2009). Around 30 000 SPCE waters were added in the cubic box with 9 nm edge. For the salt-containing simulations, 60 anions and 60 sodium atoms were added in a box with a previously equilibrated micelle leading to a salt concentration of 0.1 M. Temperature of 298 K was kept using v-scale thermostat, and 1atm pressure was kept using Parrinello–Rahman barostat (Parrinello and Rahman, 1981). Lennard-Jones and Coulomb cut off were set at 1.4 nm. Water angles and bonds were constrained using SETTLE (Miyamoto and Kollman, 1992) and for the other molecules LINCS ((Hess et al., 1997) was used to constrain the bonds. Initially, an energy minimization was performed. Then, two short equilibration steps were performed: one NVT simulation (1 ns) followed by an NpT simulation (200 ns). The preequilibrated system was used as initial configuration for the trajectory production. The equilibrium of the system was assessed by energy fluctuation.

1.3 Results and Discussion

1.3.1 Nagg and cmc. The values for Nagg and cmc of DPS, obtained by TRFQ of pyrene and surface tension, as described in Methods, in the presence of different concentrations of NaBr, sodium triflate, NaTfl, sodium methanesulfonate, NaMs, and sodium trifluoroacetate, NaTfa, are summarized in Table 4.1.1

Table 4.1.1: Average Aggregation Number and Critical Micellar Concentration (cmc) for Salt Containing Solutions of DPS 0.150 M

Salt	Salt Concentration (mol x L ⁻¹)	N _{agg}	cmc (mmol x L ⁻¹)
-	0	65 ± 4	3.3 ± 0.1
NaBr	0.05	64 ± 6	2.9 ± 0.2
NaBr	0.08	61 ± 5	3.1 ± 0.2
NaBr	0.1	60 ± 5	3.0 ± 0.1
NaBr	0.13	58 ± 4	3.0 ± 0.1
NaTfl	0.05	73 ± 6	1.5 ± 0.1
NaTfl	0.08	69 ± 5	1.0 ± 0.1
NaTfl	0.1	67 ± 3	1.0 ± 0.1
NaTfl	0.13	68 ± 5	1.0 ± 0.1
NaTfa	0.05	60 ± 5	2.4 ± 0.1
NaTfa	0.1	58 ± 4	2.1 ± 0.2
NaMs	0.05	61 ± 6	3.1 ± 0.1
NaMs	0.1	58 ± 4	2.7 ± 0.2

Within the range of concentrations studied (0 – 0.125 M), the effects of salts on the DPS aggregation number were minor and showed no clear concentration dependence (Table 4.1.1). Salt addition lowers the cmc of DPS, showing ion specific effects on this property (Florenzano and Dias, 1997).

1.3.2 DR Spectra. The dielectric spectra of aqueous DPS solutions showed several unique features (Figure 4.1.1a and b). In the frequency region around $\nu \approx 10\text{--}20$ GHz, corresponding to the cooperative relaxation of bulk water (mode 4), the relative permittivity, $\epsilon'(\nu)$ (Figure 4.1.1a), and dielectric loss, $\epsilon''(\nu)$ (Figure 4.1.1b), decreased with increasing DPS concentration. In line with previous investigations (Friesen et al., 2017) a small mode at around 8 GHz (mode 3) was assigned as slow water mode that increases with increasing DPS concentration. Simultaneously, a new contribution arose at ~ 0.4 GHz (mode 2).

On addition of salt the bulk-water relaxation at ~ 20 GHz continued to decrease, whereas the DPS-related mode at ~ 0.4 GHz remained fairly unaffected (Figure 4.1.1c and d). Additionally, a further contribution at even lower frequencies (~ 0.05 GHz) emerged (Figure 4.1.1 for all added salts (NaBr, NaTf, NaMs, and NaTfa) (mode 1).

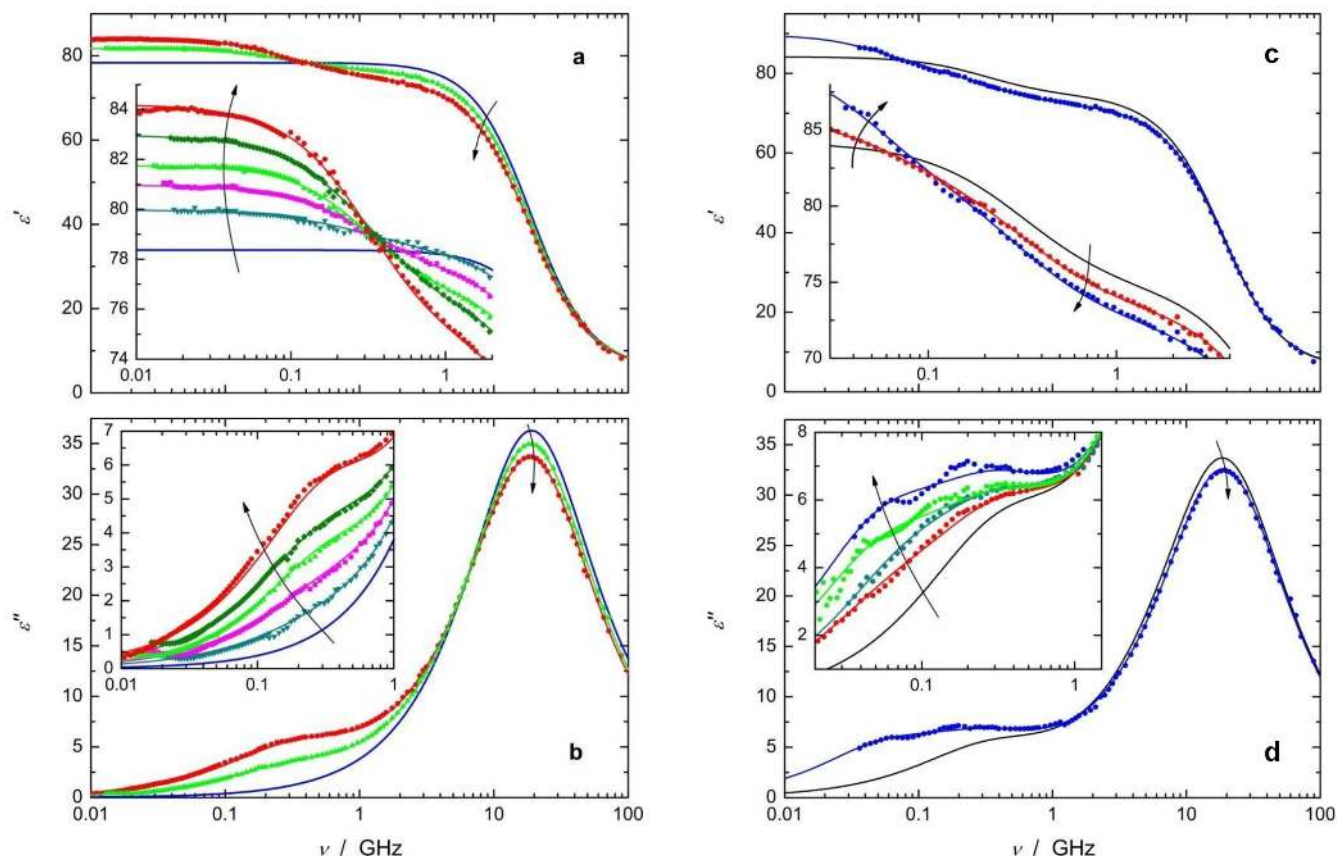


Figure 4.1.1: Spectra of **(a and c)** relative permittivity, $\epsilon'(\nu)$, and **(b and d)** dielectric loss, $\epsilon''(\nu)$, of aqueous solutions of **(a and b)** DPS at 25 °C at the following concentrations: cDPS (M) = 0 (–, blue line), 0.075 (\blacktriangle , light green), and 0.150 (\bullet , red). In the inset, cDPS (M) = 0 (–, blue line), 0.025 (\blacktriangleright , petroleum), 0.050 (\blacksquare , pink), 0.075 (\blacktriangle , light green), 0.100 (\blacksquare , dark green), and 0.150 (\bullet , red) and **(c and d)** DPS 0.150M with NaBr at the following concentrations: cNaBr (M) = 0 (–, black line), and 0.125 (\bullet , dark blue) (additionally shown in inset of (a): cNaBr (M) = 0.050 (\bullet , red)). (b) cNaBr (M) = 0.050 (\bullet , red), 0.075 (\bullet , light blue), and 0.100 (\bullet , green). The symbols show the experimental data and the lines represent fits with a CC + D + D model.

The spectra of all salt-free DPS solutions were best fitted by the superposition of a lower-frequency Cole–Cole equation (mode 2 of Figure 4.1.2a at ~ 0.3 GHz) with two Debye equations centered at ~ 5 GHz (mode 3) and ~ 20 GHz (mode 4). For the spectra of the salt-containing solutions, this CC + D + D model had to be expanded to a D + CC + D + D model with an additional Debye relaxation (mode 1 in Figure 4.1.2b) centered at ~ 0.05 GHz. Mode 4 is at the same position as the dominating dispersion step of pure water (relaxation time $\tau_4 \approx 8.3$ ps) and thus can be unequivocally assigned to the structural relaxation of (bulk) water unaffected by the presence of the solutes. On the basis of previous investigations of

electrolytes and surfactant systems, (Buchner et al., 2005; Buchner and Heffer, 2009; Lima et al., 2013a; Rahman et al., 2013) Mode 3 with a relaxation time of $\tau_3 \approx 30$ ps can be assigned to weakly bound (“slow”) water molecules hydrating the DPS headgroup. The evaluation of the amplitude corroborated this relaxation (see below).

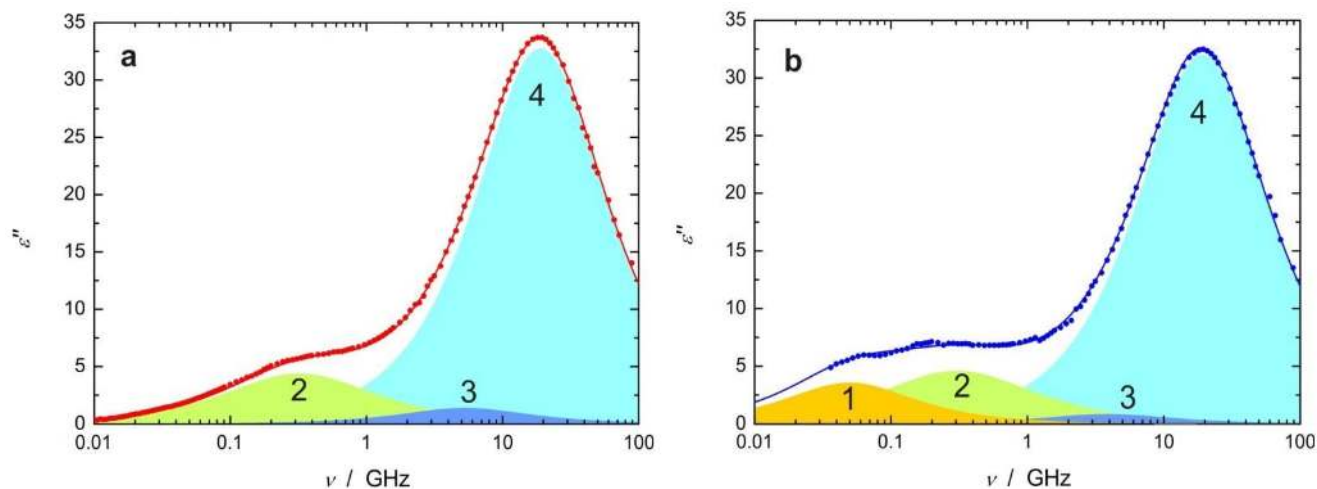


Figure 4.1.2: Dielectric loss spectra, $\epsilon''(\nu)$, of (a) 0.150 M aqueous DPS and (b) 0.150 M aqueous DPS in a solution of 0.125 M NaBr at 25 °C. The symbols show the experimental data, the lines represent fits with a CC + D + D model in (a) and a D + CC + D + D model in (b). The shaded areas indicate the contributions of modes 1–4 (1, yellow; 2, green; 3, dark blue; 4, light blue).

Following Pottel et al., (Pottel et al., 1978) the DPS-related relaxation 2 ($\tau_2 \approx 500$ ps) is assigned to the reorientation of the zwitterionic DPS headgroup (George et al., 2016) and the salt related mode 1 ($\tau_1 \approx 3000$ ps) is probably due to ion–cloud relaxation (Baar et al., 2001; Eiberweiser and Buchner, 2012). Although the fast water mode at ~ 600 GHz (Fukasawa et al., 2005) could not be resolved for the present spectra, as it is outside the covered frequency range, its presence is manifested in the large values obtained for the fitted infinite frequency permittivity of the solutions, $\epsilon_\infty(c) \approx 6$, compared to the value of $\epsilon_\infty(0) = 3.52$ for pure water (Eiberweiser et al., 2015). Accordingly, following the previous work (Buchner et al., 2002) the total amplitude of bulk like water that is not affected by the presence of a solute of concentration c is calculated as

$$S_b(c) = S_4(c) + \varepsilon_\infty(c) - \varepsilon_\infty(0) \quad (4.1.5)$$

The relaxation times, τ_i ($i = 2, 3, 4$), for the salt-free DPS solutions are practically independent of DPS concentration (Appendix, Figure S2). The corresponding amplitudes, S_2 , S_3 , and S_b , are shown in Figure 4.1.3 together with the static permittivity of the solutions, ε . The latter smoothly increased in a nonlinear manner with increasing DPS concentration, c_{DPS} (Figure 4.1.3a), reflecting the growth of the DPS contribution, S_2 (Figure 4.1.3b). The power law equations for S_2 and the linear correlation of S_b and S_3 with surfactant concentration are in the Appendix.

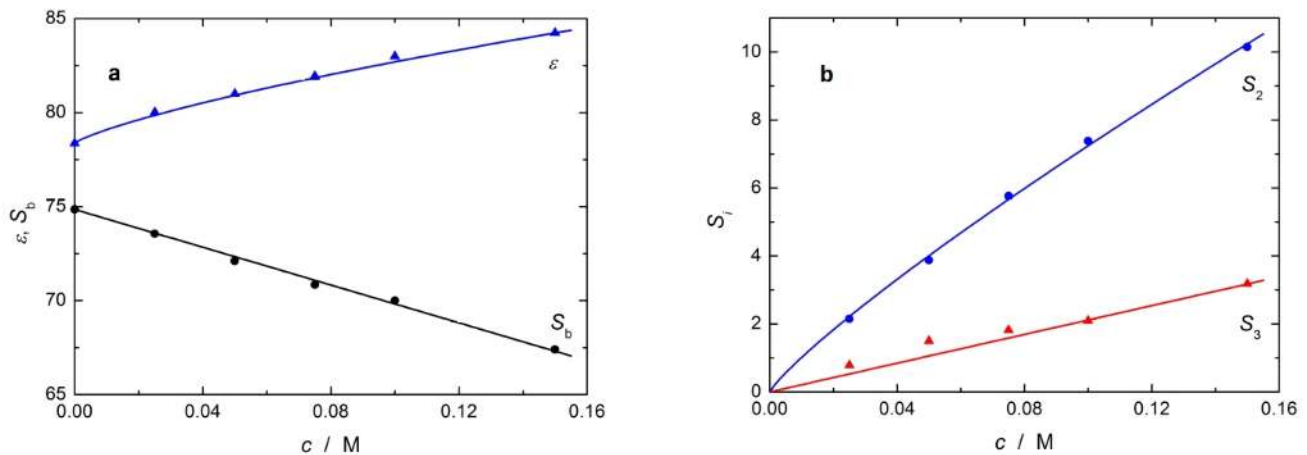


Figure 4.1.3: (a) Static permittivity, ε (▲ blue), and bulk-water amplitude (● black), $S_b(c_{\text{DPS}}) = S_4(c_{\text{DPS}}) + \varepsilon_\infty(c_{\text{DPS}}) - \varepsilon_\infty(0)$, of aqueous DPS solutions at 25 °C. (b) The corresponding amplitudes S_2 (● blue) and S_3 (▲ red). Lines are straight-line (S_b , S_3) or power-law fits (ε , S_2) to the data.

The relaxation times for salt-containing solutions are summarized in Figures 4.1.4. Figure 4.1.5a shows the amplitudes of the lower-frequency modes 1–3 whereas Figure 4.1.5b displays the values for the amplitude of bulk like water, S_b . As expected for conducting samples, the fit parameters obtained with the D + CC + D + D model scatter more than those of the salt-free DPS samples but, as was observed for the salt-free samples, the relaxation times were practically constant (Figure 4.1.4).

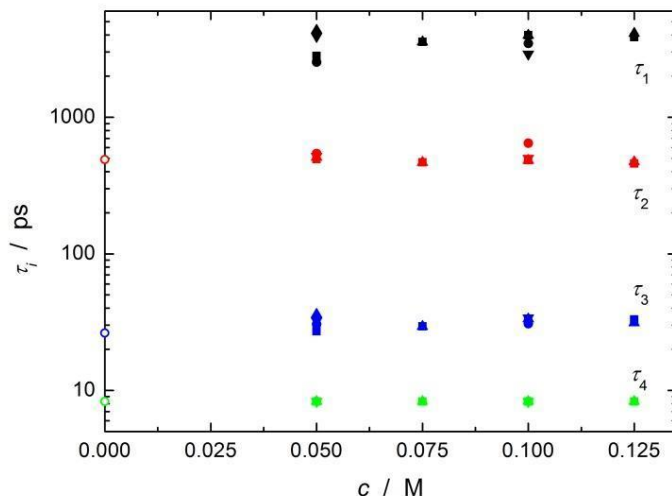


Figure 4.1.4: Relaxation times, τ_i ($i = 1$ black, 2 red, 3 blue, 4 green), of solutions of NaBr (■), NaTfl (▲), NaMs (●), and NaTfa (▼) in 0.150 M aqueous DPS at 25 °C as a function of salt concentration, c . The open symbols are the data for salt-free 0.150 M DPS, except for τ_1 that is only present in salt-containing solutions.

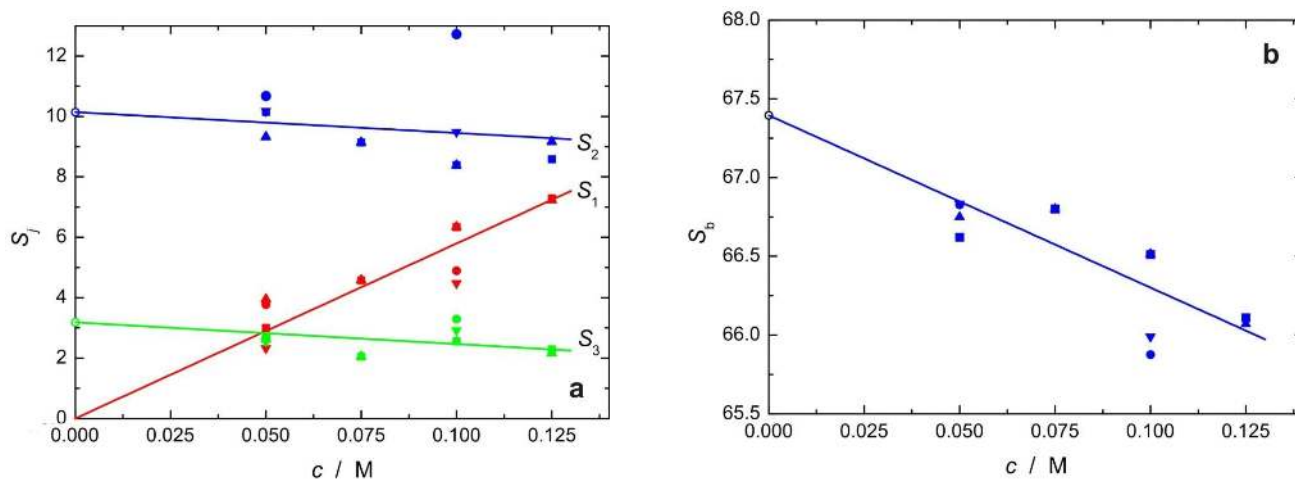


Figure 4.1.5: (a) Amplitudes, S_i , of the salt-related mode ($i = 1$ red), the DPS headgroup rotation (2, blue) and of slow water (3, green) as a function of salt concentration, c , of solutions of NaBr (■), NaTfl (▲), NaMs (●), and NaTfa (▼) in 0.150 M DPS at 25 °C. (b) The corresponding bulk-water amplitudes, $S_b(c)$. Lines are straight-line fits to these data forced through the origin (S_1) or through the values for salt free 0.150 M DPS (S_2 , S_3 , S_b).

Regarding the amplitudes, S_1 increased considerably with increasing salt concentration, c , whereas S_2 and S_3 exhibit a weak decrease (Figure 4.1.5a), as did the amplitude of bulk like water, S_b (Figure 4.1.5b). It is important to note that, within experimental

uncertainty, there is no anion-specific trend in the parameters obtained from the DR spectra, that is, we cannot distinguish between NaBr, NaTfl, NaMs, and NaTfa. In cationic micelles of DTAX, there were clear changes in the lower S_1 mode with different counterions. For NaTfl, for instance, even the relaxation time was severely altered (Lima et al., 2013a). Accordingly, all salt data were pooled, and the amplitudes were fit with straight lines either forced through the origin (S_1) or through the value calculated for salt free 0.150 M DPS for S_2 , S_b , or S_3 (Figure 4.1.5). The linear fitting equations for the amplitude of modes versus salt concentration are in Appendix.

1.3.2.1 Water Relaxation: Mode 3 and 4. Pure DPS. From the water-related amplitudes S_3 and S_b , the corresponding concentrations of slow water, c_s , and bulk like water, c_b , can be calculated with the normalized Cavell equation (Cavell et al., 1971). Both depend linearly on DPS concentration with

$$c_b = 55.361 M - 37.34 \times c_{DPS} \quad (\sigma_{\text{fit}}=0.13) \quad (4.1.6)$$

and

$$c_s = 15.64 \times c_{DPS} \quad (\sigma_{\text{fit}}=0.01) \quad (4.1.7)$$

taking again only the origin and the c_s values at (0.100 and 0.150) M DPS.

From c_b , the total hydration number, $Z_t(C_{DPS}) = [C_w(C_{DPS}) - c_b(C_{DPS})]/C_{DPS}$ (i.e., the amount of water not behaving as bulk water per equivalent of solute), is available, where c_w is the analytical water concentration, computed from eq 4. On the other hand, c_s directly yields the hydration number of weakly bound water, $Z_s(C_{DPS}) = c_s(C_{DPS})/C_{DPS}$. The number of irrotationality bound (“frozen”) H_2O is given by $Z_{ib} = Z_t - Z_s$. The parameters of eqs 1.6 and 1.7 were used to determine the number of irrotational bound water, providing the following effective hydration numbers for DPS

$$Z_t^{DPS} = \frac{(\partial c_w)}{(\partial c_{DPS})} - \frac{(\partial c_b)}{(\partial c_{DPS})} = 19.5 \pm 0.7$$

$$Z_s^{DPS} = \frac{(\partial c_s)}{(\partial c_{DPS})} = 15.6 \pm 0.1$$

$$Z_{ib}^{DPS} = 3.9 \pm 0.8$$

Thus, 4 H₂O molecules were strongly bound (i.e., frozen) by each DPS molecule, presumably by the DPS headgroup. Additionally, ~15–16 weakly bound hydrating water molecules were retarded by a factor of $\tau_3/\tau_4 \approx 2.9$, compared to bulk water. Zwitterionic micelles without salt are less hydrated than cationic micelles with chloride, a weakly binding anion, as counterion with the same chain length (El Seoud et al., 1995; Phukon and Sahu, 2017). Our results are in line with those obtained by Phukon and Sahu (Phukon and Sahu, 2017) because DRS of cationic micelles of N-dodecyl-N,N-trimethylammonium chloride, DTAC, yielded a value of 26 for the Z_t of DTAC micelles, compared to a Z_t of 19 found here for DPS. For other counterions in cationic systems of DTAX, where X is (Cl, Br, Ms, or Tfl), Z_t is lower, and this will be discussed in the next session. For an anionic surfactant with the same tail length and the sulfate group, such as sodium dodecyl sulfate, SDS, a $Z_t = 20 \pm 4$ was determined (Baar et al., 2001). For the zwitterionic dodecylphosphocholine, DPC, micelle around 18 waters per surfactant was proposed (Pottel et al., 1978), also by DRS, very similar to the value for DPS.

1.3.3 Salt-Containing Solutions. From the water-related amplitudes S_3 and S_b again the corresponding concentrations of slow water, c_s , and bulk like water, c_b , were calculated with the normalized Cavell equation (Buchner et al., 2002) The concentration of irrotationally bound H_2O , $c_{ib} = c_w - c_b - c_s$, as well as the corresponding fractions of total bound water, $f_t = (c_w - c_b)/c_w$, of slow water, $f_s = c_s/c_w$, and ib water, $f_{ib} = c_{ib}/c_w$, are displayed in Figure 4.1.6. Within experimental uncertainty linear trends are also observed for f_t , f_s , and f_{ib} and the linear equations are in SI.

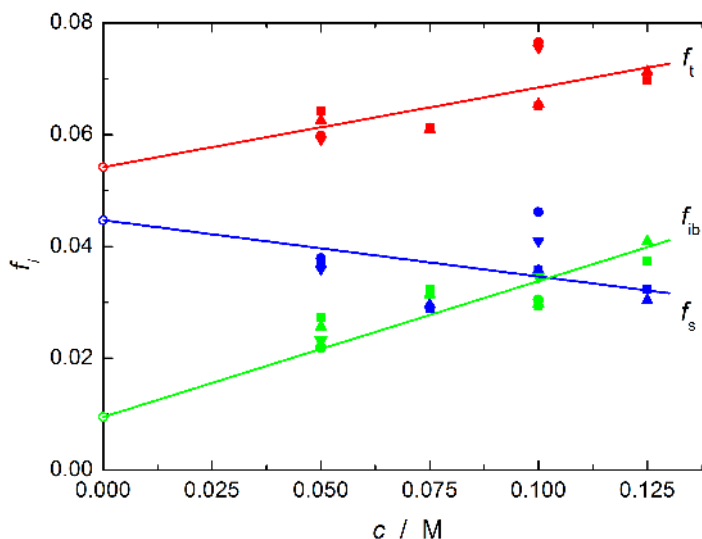


Figure 4.1.6: Fractions of total bound water, f_t (red), slow water, f_s (blue), and irrotationally bound water, f_{ib} (green), as a function of salt concentration in NaBr (■), NaTfl (▲), NaMs (●), and NaTfa (▼) in 0.150 M aqueous DPS at 25 °C

These results are very interesting because the total fraction of bound water increased with salt concentration (Figure 4.1.6). This result may be expected as Na^+ ions are highly hydrated (Eiberweiser et al., 2015). However, this increase is entirely due to the strongly increasing fraction of ib water, because at the same time weakly bound (slow) water was released.

For the salt-containing samples, the calculation of the effective hydration numbers Z_t , Z_s , and Z_{ib} is not straightforward as we have two solutes, namely DPS and the salt. However, due to the linear dependence of c_b and c_s on c_{DPS} and (at $c_{DPS} = 0.150$ M) on c (salt concentration), we can assume additivity of the DPS and salt contributions and derive “salt-related” values for Z_t^{salt} , Z_s^{salt} , and Z_{ib}^{salt} in 0.150 M DPS as

$$Z_s^{salt} = \frac{(\partial c_s)}{(\partial c)} = -6.6 \pm 1.1$$

$$Z_t^{salt} = 6.7 \pm 0.7$$

From the linear fit of

$$c_w - c_b = Z_t^{DPS} \times c_{DPS} + Z_t^{salt} \times c \quad \text{with}$$

and

$$Z_{ib}^{salt} = 11.9 \pm 0.6$$

from the linear fit of

$$c_{ib} = c_w - c_b - c_s = Z_{ib}^{DPS} \times c_{DPS} + Z_{ib}^{salt} \times c \quad \text{with}$$

$$Z_{ib}^{DPS} \times c_{DPS} = 3.9 \times 0.150 \text{ M}$$

where c_{ib} is slow water concentration, c_b is bulk water concentration, c_w is total water concentration, c_s is slow water concentration, c_{DPS} is DPS concentration, and c is salt concentration. In addition to the water bound by DPS ($Z_t^{DPS} \approx 19-20$) one unit of added salt additionally binds ~ 7 further H_2O . Interestingly, this occurs through a strong increase of ib water ($Z_{ib}^{salt} \approx 12$) whereas simultaneously $\sim 6-7$ weakly bound (slow) H_2O molecules “disappear”. Most likely, these are converted to ib water. A part of the additional ib water is hydrating Na^+ where we have $Z_{ib}(Na^+) = 5.2 \pm 0.2$ at $c \rightarrow 0$ (Baar et al., 2001) (and $Z_s(Na^+) = 0$). This would leave $Z_{ib}^{salt} - Z_{ib}(Na^+) \approx 7$ H_2O either as anion or salt-induced additional binding by DPS. For Br^- $Z_{ib}(Br^-) = Z_s(Br^-) = 0$ (Buchner and Hefter, 2009) and for Tfa^- $Z_{ib}(Tfa^-) \approx 1$, Z_s

(Tfa⁻) \approx 20 (among them \sim 5–6 H₂O hydrating –COO⁻) (Rahman and Buchner, 2012) For Ms⁻ (Rahman, 2012) of Z_{ib} (Ms⁻) \approx 0, Z_s (Ms⁻) \approx 10–11. Although there is no data for Tfl⁻, it is possible to assume Z_{ib} (Tfl⁻) \approx 0, due to the low effect of Tfl⁻ on hydrating water (Bergström and Lindgren, 1990). Thus, i_b through anions, or at least free anions, cannot explain this result. Therefore, it is possible to conclude that the additional ($Z_{ib}^{salt} - Z_{ib} (Na^+)$) \approx 7 irrotationally bound H₂O originally were only weakly bound by DPS in the salt-free solutions and are now frozen because they simultaneously interact with the DPS headgroup and the added ions. This implies that also DPS head groups and the added cations and anions interact, as already proposed for DTAX (Lima et al., 2013a) and CTAX micelles (Buchner et al., 2005). There is a correlation between shape transition of cationic micelles and decrease in micellar interface hydration (Geng et al., 2005). Cationic micelles of DTAX with triflate as a counterion have very high aggregation numbers, that is, above 100, and are very dehydrated as seen by DRS (Lima et al., 2013a) leading to phase separation (Lima et al., 2015) For DPS with added salts, there is little change in aggregation number and no change in hydration number as described in the DRS experiments.

1.3.3.1 Ion Cloud: Mode 1. Support for electrostatic ion–DPS interactions comes from the magnitude of the salt-related mode (Figure 4.1.5a). For ion cloud relaxation of the dissolved salt, values of $S_1 < 2$ would be expected (Brandes et al., 2017). However, we have $S_1 \approx 7.3$ at $c = 0.125$ M (Figure 4.1.5a). This probably indicates some sort of ion condensation on the DPS micelles and the associated formation of an ion cloud around these micelles.

1.3.3.2 DPS Relaxation: Mode 2. Mode 2 at 500 ps can be assigned as the DPS polar head relaxation, as seen for DPC (George et al., 2016) at 600 ps. As with hydration numbers, there is also no trend of the amplitude of the mode S_2 , either with salt concentration or with the nature of the added salt. Molecular dynamics simulations (Santos and Longo, 2016) show that the polar head angle is only affected by the binding of perchlorate anion and the effect is still very subtle. This is in line with our result.

1.3.4 Molecular Dynamics Simulation. Molecular dynamics (MD) simulations, were performed, for a DPS micelle in the presence of the different salts to simulate some characteristics presented in the DR spectra of the zwitterionic micelles.

1.3.4.1 Water. The behavior of water molecules around all DPS atoms up to the second hydration shell was studied. The radial distribution functions, $g(r)$, of water oxygen atoms and N or S of the surfactant polar head (Appendix, Figure S3) were used to determine the hydration shell. Only the water molecules that remained for at least 60 ps within the chosen region were considered for the analysis and those were labeled bound water. A snapshot of the MD is in Figure 4.1.7 showing a DPS micelle and its bound water molecules. This time window was chosen since it is long enough for the orientational correlation function of bulk water to decay to zero.

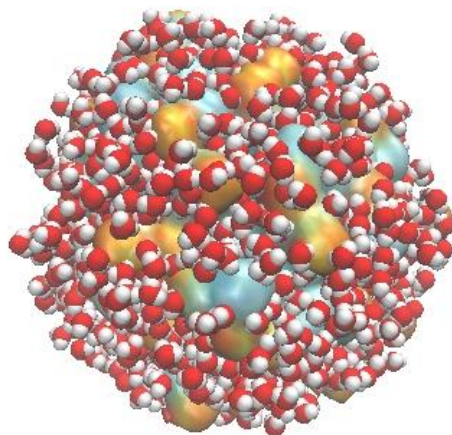


Figure 4.1.7: Snapshot of a DPS micelle with bound water molecules. Gold color shows the sulfur and blue color shows the carbon atoms of DPS.

The orientational autocorrelation functions ($C(t)$) of bound waters were calculated for DPS in water and with added salts and compared with that of bulk (free) water (Figure 4.1.8). The autocorrelation functions were fitted using double exponential decays and the rotational relaxation times (τ) were computed from these functions by integration (Lima et al., 2014). As the bound water molecules were slower than the bulk water, either due to the presence of hydrophobic or hydrophilic groups, (Laage et al., 2009; Laage and Hynes, 2006) the rotational relaxation times of the former (τ_{slow}) were longer than that of bulk water (τ_{free}). The $\tau_{\text{slow}}/\tau_{\text{free}}$ for all the systems (with the different salts and without salt) remained in the range of τ_3/τ_4 determined in DRS experiments (from 3.2 to 2.6). The average numbers of waters molecules in the hydration layer of the DPS are shown in the Table 4.1.2.

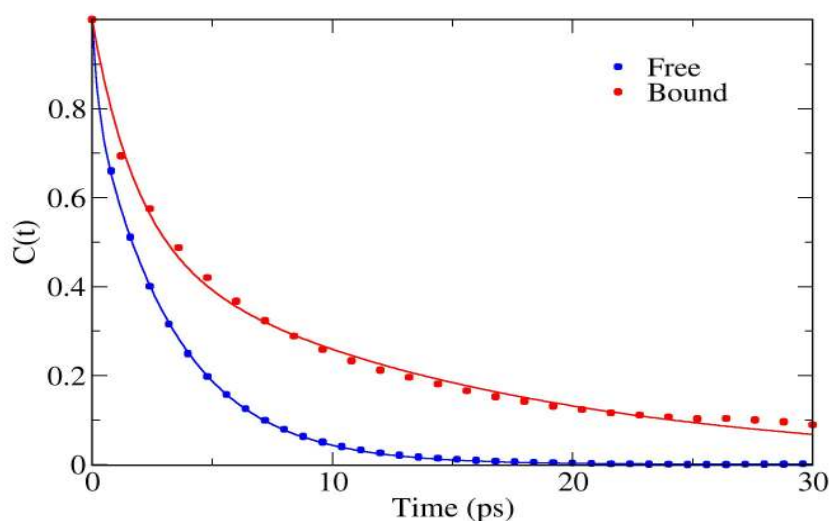


Figure 4.1.8: Autocorrelation function of water molecules bound to the micelle or free in the simulation box

Table 4.1.2: Hydration Number of DPS by Molecular Dynamics Simulation

Salt	Waters
-	17
NaBr	20
NaMs	21
NaTFA	21
NaTf	21

In line with the DRS data, even though salt addition increases the number of water molecules in the vicinity of the micelle, no ion specificity was observed. Upon addition of salt, some slow water molecules became irrotationality bound in DRS experiments, and we proposed that these waters were interacting with both DPS headgroups and salt molecules.

To evaluate our proposal we used molecular dynamics to analyze the rotational correlation function for water molecules that were (a) interacting with both surfactant and ion (choosing triflate as an example); (b) only in contact with DPS; or (c) only in contact with

triflate ions that were not interacting with the micelle. The selection of water molecules followed the same criteria used in the bound water calculation (molecules up to the second hydration layer with residence times longer than 60 ps in both systems, DPS, or DPS and salt), except that for water molecules solvating only triflate ions, the residence time was chosen to be 20 ps as it was the longest time window in which water molecules stayed in the desired region due to their shorter residence times in the solvation shell of this anion. The orientational correlation functions of these molecules are shown in Figure 4.1.9. The orientational correlation function for water molecules bound in DPS and the other salts are in Appendix (Figure S4).

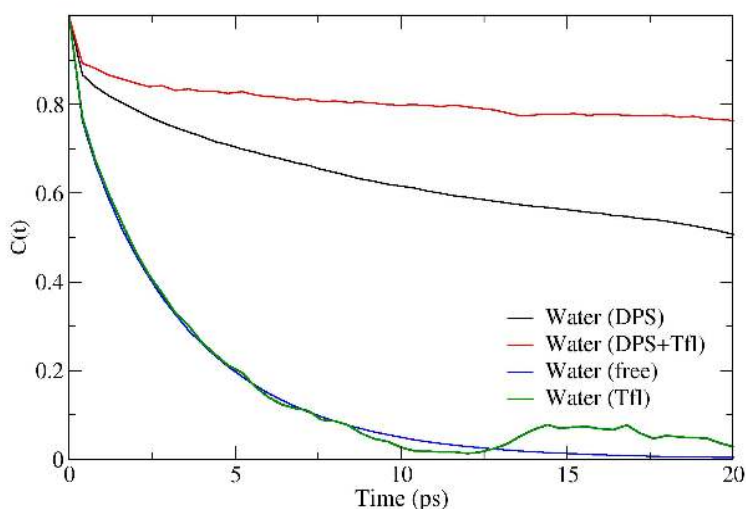


Figure 4.1.9: Autocorrelation function of water molecules bound to DPS, DPS + Tfl, Tfl, or free.

The orientational correlation function for waters “bound” to triflate ions was similar to the free water, agreeing with the assumption that triflate ion has $Z_s = 0$ and $Z_{ib} = 0$. For DPS bound water, the total correlation time was 40 ps, very close to the value for slow water mode (~ 30 ps). For water molecules bound to both DPS and Tf^- , the total fitted correlation time was 209 ps, much longer than the residence time of these water molecules in the hydration layer,

seven times longer than the correlation time of the slow water, and about 20 times the correlation time of free water molecules. We further investigate hydration shell of the anions or cations bound to the micelle during at least 100 ps in MD based in their distance to the surfactant) (Lima et al., 2014). On average, in our simulations we found that half of the anions that were bound to the micelle had about 2–3 waters bound to each anion simultaneously with DPS in the surface of the micelle thus forming water bridges (single solvent-separated ion-pairs). The other half formed contact ion-pairs since we did not detect any hydration water sharing. For the cation, we did not find any water bridges (cation and DPS did not share any hydration water) but rather ion pair formation. Ion pair formation was observed for sodium ions in SDS (Bruce et al., 2002) in MD simulations and in DRS experiments with cationic and anionic micelles (Buchner et al., 2005). Finally, in X-ray experiments with DTAB and CTAB the average number of water molecules in the hydration shell of bromide at the micellar surface (Harada et al., 2007) is about 3–4.

1.3.4.2 DPS Relaxation. The mobility of the headgroup of the DPS was also analyzed with first-order Legendre polynomial autocorrelation functions of the vector pointing from the N atom of DPS to the S atom of the surfactant for the pure and salt-containing DPS systems (Appendix, Figure S5). The first Legendre rotation correlation function of DPS for all the simulations were fitted with a double-exponential decay. A longer correlation of around 4 ns was observed for all systems, as described by Lima et al (Lima et al., 2013a) as the very long component of reorientation because of surfactant confinement in the micelle, and a short correlation around 500 ± 40 ps was observed for all the systems. This value matches those determined by DRS in this work. Added salts did not alter significantly the DPS mode in MD or in the DRS determinations.

1.4 Conclusions

The properties of cationic micelles are severely affected by the nature of the counterion, for example, its interfacial hydration, a property related to shape transitions. Despite the structural resemblance between cationic and zwitterionic micelles, and the specificity of anion effects upon such micelles, our DRS data showed no ion specificity in DPS micelles with added sodium salts. Salt effects, however, were observed and our results showed that while the hydration number of the surfactants did not change upon the salt addition, salt addition slowed the water molecules in the vicinity of the surfactant, by a simultaneous interaction between water and surfactant/ions. In DR spectra, there was also the appearance of a salt-related mode (mode 1) suggesting some sort of ion-cloud formation around the DPS head groups of these micelles. Molecular dynamics simulation, used to complement the findings from DRS experiments, support our interpretation of the data, especially the changes in the rotational correlation times of water when interacting with both ion and surfactant, supporting the proposed changes from slow to irrotationally bound water upon salt addition.

Our results, obtained both experimentally and from molecular dynamic calculations, strongly suggest that the specific effects of salts on zwitterionic micelles are related to detailed interactions between ions and headgroups and do not reflect a specific effect on the global hydration of the headgroup region. Although no ion specific effect is seen in the hydration of micelles, our cmc results show that there is anion specificity in the micellization of this surfactant. We are currently developing experimental and theoretical work to investigate the relationship between interfacial hydration and thermodynamics of micelle formation.

4.2 Dehydration Determines Hydrotropic Ion Affinity for Zwitterionic Micelles

This chapter is a published paper, and was reproduced with permission from *Journal of Chemical Information and Modeling*, 60 (2), 604-610. Copyright 2020 American Chemical Society."

Abstract

Specific ion effects in zwitterionic micelles, especially for anions, are evident in reaction kinetics, zeta potential, and critical micelle concentration measurements. However, anion binding to zwitterionic micelles does not produce significant changes in shape, aggregation number, or interfacial hydration. Here we used molecular dynamics simulation of systems containing sulfobetaine zwitterionic micelles of N-Dodecyl-N,N-dimethyl-3-ammonio-1-propanesulfonate (DPS) and nine different salts to explore ion binding in terms of group dehydration. Our results, in line with those obtained for cationic micelles, showed that the binding degree of anions containing both hydrophobic and hydrophilic portions, i.e., hydrotropes, were correlated with the ion dehydration, and were governed mainly by the hydrophobic portion dehydration upon binding.

2.1 Introduction

Specific ion effects (SIEs) in ionic micelles can determine changes in aggregation number, shape and in the thermodynamics of aggregation, i.e., critical micelle concentration (cmc). The origins of SIEs are still unclear, especially for those complex polyatomic ions that produce greater changes in the aggregation behavior of micelles. Ion effects are common in

cationic or anionic micelles (Bostrom et al., 2002; Evans et al., 1984; Perger and Bešter-Rogač, 2007; Tapia et al., 2002), being the effects of monoatomic ions less dramatic than those observed with hydrotropic ions. (Abezgauz et al., 2010; Geng et al., 2005; Lima et al., 2017, 2014, 2011; Magid et al., 1997; Sarac et al., 2013). Although the magnitudes are different, for monoatomic or polyatomic ions the higher is the ion adsorption upon the micellar interface, the larger are the ion effects. We have shown recently that the degrees of hydrotropic ion binding to cationic micelles is correlated with the dehydration of the hydrophobic portion of the counterion (Lima et al., 2017)

Zwitterionic micelles are formally neutral but can selectively adsorb ions at the interface (Baptista et al., 1992; Beber et al., 2004; Gerola et al., 2017b; Iso and Okada, 2001; Souza et al., 2015; Wu et al., 2019). Several experimental techniques have been used to evaluate specific anion adsorption at the interface of sulfobetaine micelles, a very studied zwitterionic model system, and the degree of anion adsorption is usually associated with its hydration free energy (Drinkel et al., 2013; Wu et al., 2019). The studied anions usually belong in the Hofmeister series and the degree of binding follow this series. Thus, perchlorate anion adsorbs in the interface a larger degree than bromide, as seen by zeta potential measurements, but still does not produces changes in aggregation number or micelar shape (Mortara et al., 2018; Priebe et al., 2012).

Our studies with polyatomic anions in zwitterionic micelles show that there are no specific changes in micelle interfacial hydration induced by greater ion association (Mortara et al., 2018) mostly because the anion association in zwitterionic micelles does not produce changes in shape or aggregation number (Abezgauz et al., 2010; Lima et al., 2017; Magid et al., 1997). Specific ion effects for polyatomic anions are observed, for example, in the critical micelle concentration for sulfobetaine micelles, and also in the aggregation behavior of zwitterionic imidazolium micelles (such as 3-(1-alkyl-3-imidazolium) propanesulfonate) (Wu et al., 2019).

Which are the factors that controls polyatomic hydrotropic ion adsorption? Here we used molecular dynamics simulations to evaluate the adsorption of anions in zwitterionic N-dodecyl-N,N-dimethyl-3-ammonio-1-propanesulfonate (DPS) micelles and the role of group dehydration in the ion adsorption of hydrotropic anions. The chosen anions were chloride, Cl^- , bromide, Br^- and perchlorate, ClO_4^- , from the Hofmeister series and a combination of three different hydrophobic portions (CH_3 , CF_3 and C_6H_5) with two hydrophilic portions (CO_2 and SO_3), i.e., acetate, Ac (CH_3CO_2^-), trifluoroacetate, TFA (CF_3CO_2^-), benzenecarboxylate, BZC ($\text{C}_6\text{H}_5\text{CO}_2^-$), methanesulfonate, Ms (CH_3SO_3^-), triflate, Tf (CF_3SO_3^-) and benzenesulfonate, BZS ($\text{C}_6\text{H}_5\text{SO}_3^-$). We used sodium as the counterion in all salts. Our results showed that the adsorption degree of hydrotropes to zwitterionic micelles was governed mainly by the dehydration of the hydrophobic portion upon adsorption.

2.2 Methods

A spherical N-dodecyl-N,N-dimethyl-3-ammonio-1-propane-sulfonate (DPS) micelle composed of 55 monomers was built using Packmol (Martínez et al., 2009) in a cubic box of 10 nm edge. The micelle was hydrated using GROMACS 5.1.4. (Van Der Spoel et al., 2005), with approximately 30,000 SPCE water molecules and a 200 ns NpT simulation was performed also using GROMACS, after a short energy minimization and a 1 ns NVT equilibration simulation. The equilibrated micelle was used as initial configuration in the salt containing simulations. Nine salt containing simulations were performed, randomly adding to the box 60 sodium ions and 60 anions (NaBr, NaCl, NaClO_4 , NaAc, NaTFA, NaBZC, NaMs, NaTf or NaBZS), also using Packmol (Martínez et al., 2009). The system was also hydrated and after minimization steps, a 200 ns NpT simulation was performed. A temperature of 298 K was kept using v-scale thermostat, and 1 atm pressure was kept using Parrinello–Rahman

barostat (Parrinello and Rahman, 1981). Lennard-Jones and Coulomb cut off were set at 1.4 nm. Water angles and bonds were constrained using SETTLE (Miyamoto and Kollman, 1992) and for the other molecules LINCS (Hess et al., 1997) was used to constrain the bonds. The GAFF force field (Wang et al., 2004) was used for all salts and DPS, with the dihedral parameters obtained as already described (Mortara et al., 2018). The partial charges of the atoms were calculated with Gaussian 09 (Frisch et al., 2016)(HF/6-31G*). During the micelle simulation at most 1 monomer exited the micelle, and only micellized DPS molecules were considered in the calculations. MD simulations were also performed for a single salt molecule and a single DPS monomer or a hydrotropic anion in water (c.a. 6,500 water molecules) in a 4 nm-edge cubic box, using a uniform neutralizing background charge when required.

From the MD trajectories, lifetime functions for the sodium and the anions in the micellar interface were calculated to determine a cutoff distance for “free” and “bound” ions (Lima et al., 2017, 2014). The lifetimes profile of the ions as a function of the distance from the micellar interface were computed as follows: a binary residence function of individual ions inside spherical shells equally spaced from the mCOM was determined for each frame of the simulation, being 1 if the ion was inside a given shell and 0 otherwise. Then, a normalized autocorrelation function of the residence function was constructed. For each ions and shell, the integral of the autocorrelation function (τ) was computed, and the profile of τ versus the distance from the micellar interface was averaged over all ions, providing the lifetime profile. The cutoff distance criteria for labeling an ion “bound” or “free” was defined from the lifetime profiles. However, as the lifetime profiles were similar among the anions, we used 0.55 nm as a cutoff for anions and 0.52 nm as a cutoff for sodium, distances at which the lifetime profiles kept nearly constant.

The fraction of hydration, FH, (Lima et al., 2017, 2014) was calculated using the number of water molecules in the first hydration shell (fhsw),

determined by the first minimum in the RDF between the group of interest and water oxygen, in “bound” ions or micellized monomers (bound fhs_w) and the fhs_w in single ions or monomer simulations (free fhs_w), using the single salt and single monomer simulation (number of “free” water molecules). The FH was computed as $FH = \text{bound fhs}_w / \text{free fhs}_w$.

2.3 Results and Discussion

Zwitterionic micelles, with and without added sodium salts, were modeled with MD simulations. The number of monomers in the present simulations (55), was the same for all systems and close to the reported values (Florenzano and Dias, 1997) We note that salt addition has minimal effects on the aggregation number of micelles of this surfactant (Mortara et al., 2018). Maintaining the same aggregation number allows direct comparison of specific ion effects (SIEs) on micelles.

The radial distribution functions (RDF) between the center of mass of the micelle (mCOM) and the nitrogen and sulfur atoms of DPS with or without added salts are in Figure 4.2.1. The peak positions of the RDF between the mCOM and the N atom of DPS were very similar for all MD simulations, with a maximum at c.a. 1.8 nm (Figure 4.2.1a-c). This value is close to the expected micellar radius of an aggregate composed of surfactants with 12 carbons in its hydrophobic chain (Tanford, 1980) and close to the values obtained from MD simulations of DTA-based micelles (Lima et al., 2017, 2014). Small differences were observed for ClO₄⁻, which shifted the peak towards the mCOM (Fig. 4.2.1a). Compared with the DPS without added salt, no significant differences were found for the carboxyl (Fig. 4.2.1b) or sulfonated hydrotropes (Fig. 4.2.1c). The peak position of the RDF between the mCOM and the S atom also was c.a. 1.8 nm DPS micelles with no added salt. This result was expected on the basis of the calculated average angle of the hydrophobic tail and the headgroup dipole of a

micellized surfactant similar to the DPS (Santos and Longo, 2016) Differently from the mCOM-N RDF, clear SIEs were observed for the RDF between the mCOM and the S atom. Compared with the DPS micelle without added salt, no salt effects were detectable for NaCl and NaBr additions, while the NaClO₄ increased the distance between the mCOM and the S atoms (Fig. 4.2.1d). Small salt effects were observed for the carboxylated hydrotropes (Fig. 4.2.1e). TFA increased the mCOM-S distance, although to a lesser extent than the BZC (Fig. 1f). The sulfonated hydrotropes changed the peak position but more significantly than the carboxylated anions. Tf shifted the RDF peak farther from mCOM, and the addition of BZS, not only resulted in a RDF displacement to larger distances but also broadened the distribution peak. Besides the ClO₄, the greater effects were induced by the hydrotropic ions, excluding the Ms and the Ac, similar to the reported MD results for DTA micelles with these anions as counterions (Lima et al., 2017) .

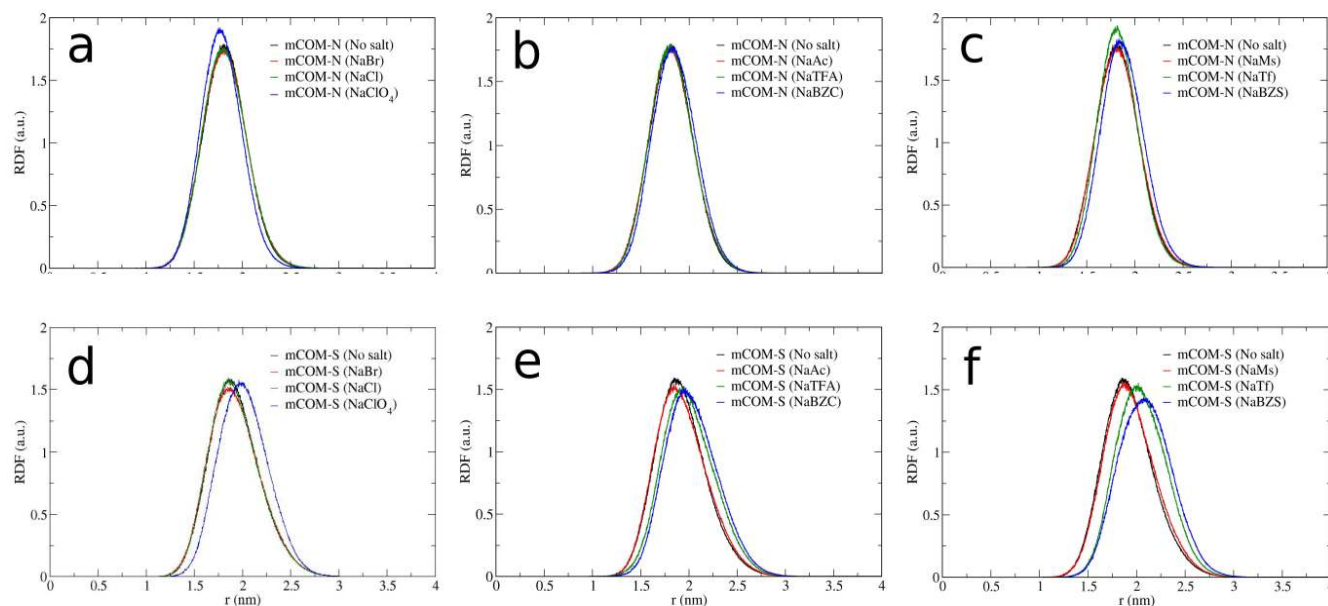
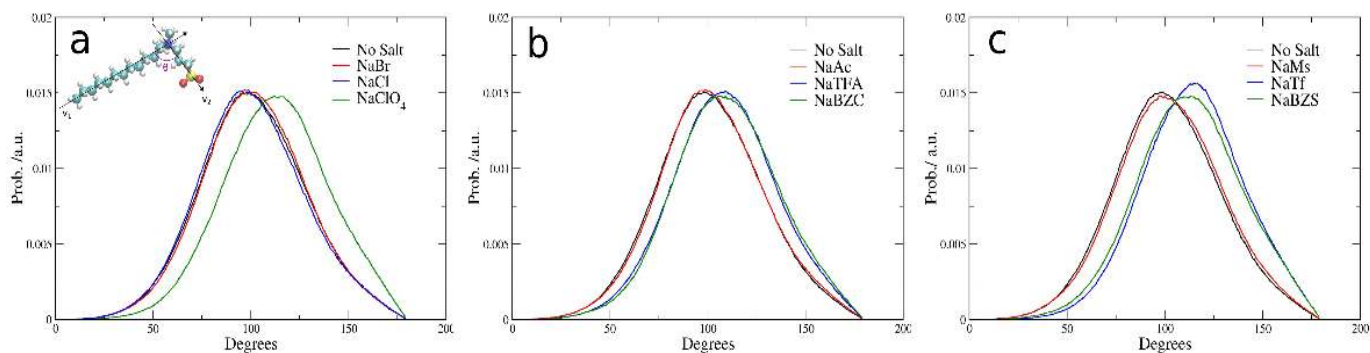


Figure 4.2.1: RDF between the center of mass of the DPS micelle (mCOM), N (top) and S (bottom) atoms of the surfactant. Parts a and d) – no salt, – (red) NaBr, – (green) NaCl, – (blue) NaClO₄; b and e) – no salt, – (red) NaAc, – (green) NaTFA, – (blue) NaBZC; c and f) – no salt, – (red) NaMs, – (green) NaTf, – (blue) NaBZS.

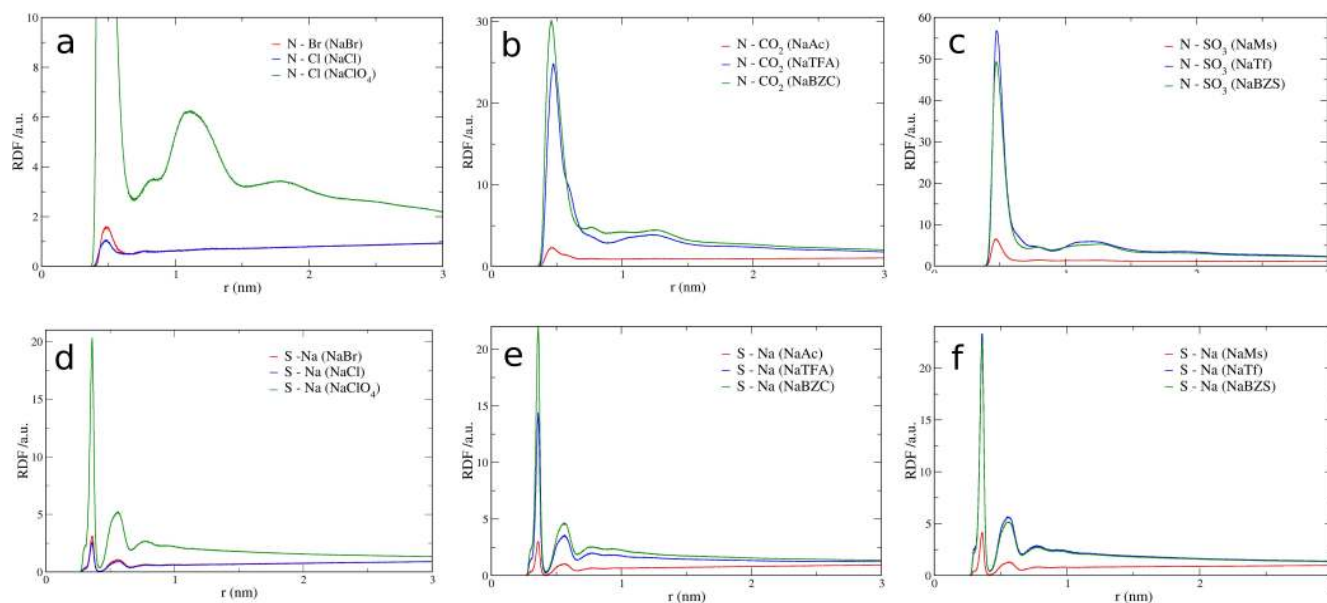
The differences in the relative position of the nitrogen and sulfur atoms of DPS upon addition of added salts were also evident from the values of captured by the probability distributions of the angle (θ), defined by the vector pointing from the CH₃ terminal in the hydrophobic chain to the nitrogen atom of DPS and the vector pointing from nitrogen to sulfur (Fig. 4.2.2). The probability value of θ was bell-shaped for all systems. The most probable average angle for the DPS without added salt was 102 degrees, a orientation with the N-S vector almost perpendicular to the normal of the interface, as previously reported for similar systems (Santos and Longo, 2016) and close to the orientation of headgroups in membrane composed of zwitterionic headgroups (Hauser et al., 1981). This result is also consistent with the dipolar moment determined experimentally (Mortara et al., 2018). Addition of Cl⁻, Br⁻ and acetate did not change the distribution, with average angles of 101 and 102 degrees, respectively. Addition of ClO₄⁻ displaced the peak position of the θ angle distribution to a more stretched surfactant, with an average angle of 113 degrees (Fig. 4.2.2a). TFA and BZC ions also shifted the peak position (Fig. 4.2.2b), with average angles of 109 and 110 degrees, respectively. No effect on angle distribution was observed upon addition of methanesulfonate to the DPS micelle (average angle of 103 degrees), whereas benzenesulfonate and Tf also distended the surfactant (Fig. 4.2.2c), leading to average angles of 113 and 114 degrees, respectively. Additionally, Tf also showed a narrower angle distribution (Fig. 4.2.2c).

Figure 4.2.2: Probability distribution of the angle θ , formed by the vector pointing from the terminal CH₃ of the hydrophobic tail to the N atom of the DPS (vector v₁) and the vector pointing from the N atom to the S atom of the DPS (vector v₂). Inset: representation of the angle θ . a) – no salt, – (red) NaBr, – (blue) NaCl, – (green) NaClO₄; b) – no salt, – (red) NaAc, – (blue) NaTFA, – (green) NaBZC; c) – no salt, – (red) NaMs, – (blue) NaTf, – (green) NaBZS.



We also evaluated the ion distribution at the micellar interface by computing the RDF between the N and S atoms of the micellized DPS and atoms of the ions (Fig. 4.2.3). We chose the N of DPS, the central atom of the most positively charged group of the surfactant ($\text{N}^+(\text{CH}_3)_2$), to be the reference for computing the RDF with the atoms of the added salt. For Br^- or Cl^- , the RDF between the N of DPS and the halides showed a small peak, at c.a. 0.45 nm, while a pronounced maximum was observed in the RDF between the N atom and the Cl of ClO_4^- ion at a similar distance (Fig. 4.2.3a). The difference between the RDF distributions of the halides and perchlorate indicates that there is a significant excess of perchlorate ions at the micellar interface. A significant excess of ions at the interface was also observed for TFA and BZC (Fig. 4.2.3b) and Tf and BZS (Fig. 4.2.3c), but lower RDF peak values for Ac (Fig. 4.2.3b) and Ms (Fig. 4.2.3c). These results are in line with those reported for simulations of cationic micelles with these ions as counterions (Lima et al., 2017), even though there is a negative barrier at the micellar interface, composed of the $-\text{SO}_3$ group of the DPS, which prevents the adsorption of the anions at the more buried positively charged layer of the $\text{N}(\text{CH}_3)_2$ groups. For the ions with high affinity to the interface, the RDF did not converge at larger distances (not shown).

Figure 4.2.3: RDF between the N (top) and S (bottom) atoms of the DPS and the counterions (or groups of atoms of the counterions). a) – (red) N-Br (NaBr), – (blue) N-Cl (NaCl), – (green) N-Cl (NaClO_4); b) – (red) N- CO_2 (NaAc), – (blue) N- CO_2 (NaTFA), – (green) N- CO_2 (NaBZC); c) – (red) N- SO_3 (NaMs), – (blue) N- SO_3 (NaTf), – (green) N- SO_3 (NaBZS); d) – (red) S-Na (NaBr), – (blue) S-Na



(NaCl), – (green) S-Na (NaClO₄); e) – (red) S-Na (NaAc), – (blue) S-Na (NaTFA), – (green) S-Na (NaBZC); f) – (red) S-Na (NaMs), – (blue) S-Na (NaTf), – (green) S-Na (NaBZS).

As anions adsorb, the micellar interface acquires a negative net charge and generates an electrostatic potential at the interface, which is proportional to the amount of adsorbed anions. Na⁺, in this case, the counterion of the added salt, interact with the electrostatic field, adsorbing at the micellar interface establishing balance of charges. The increase in the interfacial anion concentration, therefore, should lead to an increase in the interfacial concentration of Na⁺. We also evaluated the adsorption of Na⁺ at the micellar interface. We chose S, the central atom of the most negatively charged group of the surfactant ($-\text{SO}_3^-$), as reference for computing the RDF with Na⁺ in the salt-containing systems. As expected, in the systems in which the anion adsorption was the highest, larger Na⁺ adsorption was also observed. As Cl⁻, Br⁻, Ac⁻ and Ms⁻ showed a poor tendency to be concentrated at the micellar interface (Fig. 4.2.3a-c), the Na⁺ adsorption at the interface was low, (Fig. 4.2.3d-f). In contradistinction, the local distribution of Na⁺ at the micellar interface with ClO₄, TFA, BZC, Tf and BZC was significant (Fig 4.2.3d – f). Cation binding was seen experimentally using zeta potential measurements (Priebe et al., 2012).

We analyzed the orientation of the hydrotropic ions at the micellar interface by computing the angle formed by the vector pointing from the mCOM to the carbon atom bound to the S atom in the SO_3 group or the C atom of the CO_2 group in the anions and the vector pointing from this carbon atom to the S atom or the C atom of the SO_3 and CO_2 groups, respectively. Only the anions closer to the mCOM than the first minimum in the RDF between mCOM and the anion were taken into consideration for this computation. The angle distributions (not shown) were similar to those obtained for cationic aggregates with the anions analyzed here as counterions (Lima et al., 2017). The average angle for Ac was c.a. 68° , while those for TFA and BZC were 45° and 39° , respectively. These values showed that the hydrophobic moiety of the anions was inserted in the hydrophobic core of the micelle, while the hydrophilic group was exposed to the aqueous environment. For the sulfonated hydrotropes, the average angles obtained were equal to 79° , 42° and 43° for Ms, Tf and BZS, respectively. Thus, both the $-\text{CF}_3$ group and the benzene group were effective in localizing the anions at the interface, by inserting into the micellar core.

In cationic micelles, the adsorption of hydrotropic ions at the micellar interface is also followed by a sizable reduction in the exposition of the hydrophobic tail of the surfactant to water (Lima et al., 2017, 2014, 2013b, 2013a; Mortara et al., 2018). The fractional hydration (FH), i.e., the ratio of water molecules in contact with each (group of) atom(s) of the micellized and infinitely diluted surfactant, was computed for the present systems and the results are in Figure 4.2.4. In all cases, the FH was closer to 1 for the atoms at the polar groups of the surfactant and decayed significantly for the atoms at the hydrophobic chain, a result similar to those obtained for a zwitterionic surfactant (Stephenson et al., 2007). Although the overall profiles were similar, differences were evident. Perchlorate induced a more drastic reduction in chain hydration than the chloride or bromide (Fig. 4.2.4a) and slightly increased the hydration of the SO_3 group. Likewise, compared with the DPS with no added salt, the NaAc

did not change the surfactant hydration, but TFA and BZC induced similar changes to those observed for perchlorate. Finally, while we observed no effect of Ms, Tf and BZS increased the SO_3 group hydration and decreased the hydration of the other groups of the surfactant.

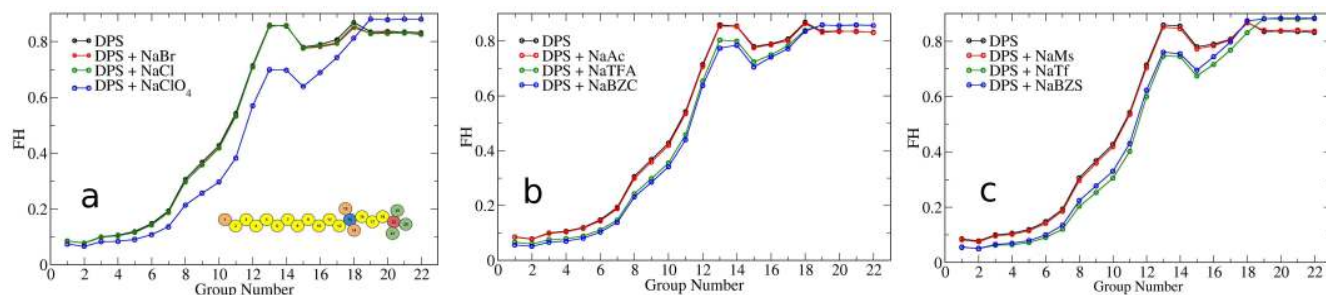


Figure 4.2.4: Figure 4. FH of DPS with different salts. a) – no added salt, – (red) NaBr, – (green) NaCl, – (blue) NaClO₄; b) – no added salt, – (red) NaAc, – (green) NaTFA, – (blue) NaBZC; c) – no added salt, – (red) NaMs, – (green) NaTf, – (blue) NaBZS. Inset: group numbering in DPS, light orange spheres are CH₃ groups, yellow spheres are CH₂ groups, green spheres are O atoms, the blue sphere is the N atom and the red sphere is the S atom.

In cationic micelles, the nature of the salt greatly affect the hydration of the aggregates, and shape transitions are accompanied by micellar interfacial dehydration (Bijma and Engberts, 1997; Geng et al., 2005; Lima et al., 2015; Magid et al., 1997). This effect is partially explained by the anchoring of ions at the micellar interface, promoting packing of the surfactant chains and lowering the exposure of the micellized surfactant to the neighboring water. In zwitterionic micelles, however, no interfacial hydration changes are observed with the addition of salts in DPS aggregates in dielectric relaxation experiments (Mortara et al., 2018). While our simulations also showed only subtle ion effects upon the interfacial hydration of the aggregates, more evident effects were observed in the core of the micelles, suggesting that although the reported values of aggregation number are insensitive to the nature of the added ions, the ionic adsorption at the micellar interface led to a denser packing of the surfactants in the aggregates.

Besides the micellar hydration, ion hydration may also change upon adsorption at the micellar interface. Lanthanide ions dehydrates on adsorption at the interface of dodecylsulfate micelles (Tapia et al., 2002). This ion dehydration upon adsorption occurs in dodecyltrimethylammonium halide micelles (Harada et al., 2007) where halides form contact ion pairs with the headgroup of the surfactant (Buchner et al., 2005). In cationic micelles with hydrotropic ions as counterions, ion dehydration occurs, but due to the anchoring of the ions at the micellar interface, the dehydration of the more hydrophobic regions of the ion is more severe than those of the hydrophilic regions and that the amount of ion adsorption at the micellar interface is related to the ion dehydration (Lima et al., 2017). The hydration of the hydrotropic ions in the present simulations was analyzed, by calculating the FH of the hydrophobic and hydrophilic groups, using single-ion simulations and defining water as “bound” to the group of the ion if the distance between the molecules was smaller than the first minimum in the RDF between them (not show). The cutoff distance (defining the “bound” and “free” for each group) was based on the probability distribution of the distance between the ions and the micellar interface (not show). Then, α was computed as the ratio of the number of “free” ions and the total number of ions at the simulation. The results are presented in Figure 4.2.5

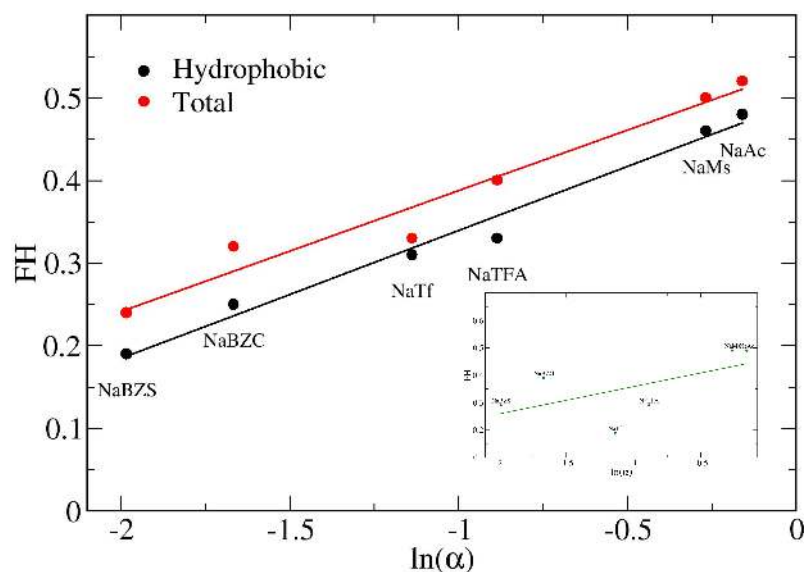


Figure 4.2.5: FH of hydrotropic ions as a function of $\ln(\alpha)$. a) ● (red) full ions, ● hydrophobic region. Inset: FH of the hydrophilic region of the ions. Solid lines are linear fits to the data (R = correlation coefficient): – (red) $FH = 0.146 \cdot \ln(\alpha) + 0.533$, $R=0.97$; – (black) $FH = 0.154 \cdot \ln(\alpha) + 0.4941$, $R=0.99$; – (green) $FH = 0.099 \cdot \ln(\alpha) + 0.458$, $R=0.6$.

As expected from the RDF between ions and the N atom of the DPS, Ac and Ms showed the lowest affinity to the micellar interface, leading to higher α values than those observed for the other hydrotropic ions. The ion effect in DPS cmc upon NaMs addition is very small (Mortara et al., 2018). The α values are consistent with those determined for perchlorate, showing that the anion coverage is 0.2 at most (Drinkel et al., 2013), considering the increase of negative charge measured by zeta potential. If we consider the difference between the anions and cations in the same simulation, close to 0.3 negative charges were added to the interface.

FH increased linearly with $\ln(\alpha)$ for both the full ions and their apolar moieties, but the correlation was very weak for the hydrophilic region of the ions. These results are very similar to those reported for cationic micelles with these ions, showing the high tendency of benzene and $-CF_3$ groups to insert into the hydrophobic core of the micelles. Also in the present simulations, the apolar region of the ions rather than the nature of the hydrophilic regions was

pivotal for controlling ion adsorption and, hence, the properties of ions and surfactants in the micellar aggregates. Thus, although the carboxyl group has less tendency of forming ion pairs with quaternary ammonium groups than the sulfonate group, BZC has almost the same interfacial concentration than the BZS and higher interfacial concentration than Tf. Note that the hydrophilic region of the hydrotropic ions was considerably more dehydrated in the present simulations than the reported results for cationic micelles. Still, no correlation was found for α and FH of the hydrophilic region, showing that ion adsorption depends on the dehydration of the hydrophobic region of the ions and less on specific interactions of the ionic groups.

2.4 Conclusions

Salt effects upon zwitterionic micelles (Baptista et al., 1992; Beber et al., 2004; Gerola et al., 2017b; Iso and Okada, 2001; Mortara et al., 2018; Priebe et al., 2012; Souza et al., 2015; Wu et al., 2019) are less pronounced than those observed in cationic or anionic micelles (Corrin and Harkins, 1947; Gamboa and Sepúlveda, 1986; Jackson et al., 2002; Lima et al., 2014; Rehage and Hoffmann, 1983; Sarac et al., 2013) Although smaller, SIEs are still observed in these systems. As expected, bromide showed higher interfacial affinity than chloride, but both anions did not disturb the DPS micelle. Hydrotropic ions affected the micellar properties of zwitterionic aggregates at higher extension than the monoatomic ions, and with similar magnitude as the effects promoted by perchlorate, an anion known for altering the properties of zwitterionic micelles. The behavior of such ions at the interface of zwitterionic micelles was similar to that observed in cationic micelles. Although no micellar increase or shape change occurs upon addition of TFA, Tf, BZC or BZS are observed in DPS aggregates (Mortara et al., 2018) an excess of those ions was found at the micellar interface, a preferential orientation of those ions at the interface was also observed, with the apolar

moieties inserted into the micellar core, and micellar dehydration throughout the hydrophobic chain of the surfactant was observed in our simulations. Additionally, dehydration of the hydrophobic region of the ions determined the extension of anionic adsorption at the micellar interface. In general, these results are very similar to the ones reported for these ions at the interface of dodecyltrimethylammonium micelles (Lima et al., 2017). However, the cationic micelle undergoes shape and even phase transitions upon the addition of TFA or Tf, depending on the conditions (Geng et al., 2006; Rehage and Hoffmann, 1983). Thus, although the behavior of the hydrotropic ions at the cationic and zwitterionic interfaces is very similar, the SIEs on the structure of the micelles is quite distinct. Additionally, our MD simulations suggest that the driving force that leads hydrotropic ions to micellar interfaces, regardless the nature of the interface, is the same: it is the dehydration of the apolar region of the ions.

4.3 Anion Effect on the Zwitterionic Surfactant Micellization

3.1 Introduction

Zwitterionic surfactants (zws) contain both positive and negative charges in their headgroup, but are formally neutral. These amphiphiles are usually highly water-soluble, exhibit low toxicity (Cheng et al., 2012) and are less irritating to the skin and eyes than ionic ones (Rosen, 2004). Due to these properties zwitterionic surfactants are suitable to be used in cosmetics, and medical applications, such as nanoemulsion-based vaccines (Bhattacharjee et al., 2019). They can also be used as a model system for biological membranes as the main component of these structures are zwitterionic phospholipids (Eeman and Deleu, 2010).

Ions can partition between bulk solutions and micellar interfaces formed by ZwS aggregates, and the specific ion effects are known to follow the Hofmeister or lyotropic series (Aroti et al., 2007; Gerola et al., 2017b). Ion hydration, size, and charge are some factors responsible for the ion-specific effects, but the nature of the interface also needs to be taken into consideration. For instance, to assess the specific interaction of ions with soft matter, other properties such as ion-pairing, complexation capacity, and ion hydrophobicity are also important (Leontidis, 2017). Anions containing hydrophobic portions, like hydrotropic anions have a strong partition in cationic micelles interfaces (Geng et al., 2005; Lima et al., 2017) but the effects are not so strong in zwitterionic interface (Mortara et al., 2018).

Specific ion effects can be seen, for example, in surfactant micellization. Above the critical micelle concentration (cmc), surfactants aggregate in aqueous solutions with the transfer of hydrophobic tails from water to the interior of micelle being a favorable energy towards aggregate formation and the repulsion arising from the surfactant polar heads due to geometric constraints being an unfavorable energy (Tanford, 1974).

For ionic micelles, the counterion interaction with the headgroup will cause lowering the interfacial electrostatic repulsion and, consequently, the cmc. As the partition between bulk and interface depends on specific ion effects, cmc is also affected on the same degree, with bigger, less hydrated ions like Cs^+ or Br^- lower the CMC to a higher degree than small hydrated ions like Li^+ and F^- (Paredes et al., 1984; Ropers et al., 2003) and hydrotropic anions, having a very strong interaction with the micellar interface, causing a significant lowering of cmc (Lima et al., 2017; Sarac et al., 2017).

For uncharged nonionic surfactants, the salt effect on micellization is interpreted as a salting-in and salting-out phenomenon in the aqueous solution (Mukerjee, 1965). The role of salt-headgroup interaction is considered minor in this case.

For ZwS, both mechanisms have been proposed for the lowering of cmc upon salt addition (Gerola et al., 2017a; Tori and Nakagawa, 1963). Even though the formal charge in ZwS aggregates is zero, ion adsorption into the dipolar region can screen the charges and decrease the cmc (Florenzano and Dias, 1997). Both anions and cations can affect the cmc, but the effect is milder compared to ionic surfactants (Kroflič et al., 2012).

We have previously observed a significant lowering of the cmc in sulfobetaine surfactant upon hydrotropic anion addition (Mortara et al., 2018), but as far as we know, there are no more studies on hydrotropic anions affecting zwitterionic micellization. Since cmc and enthalpy of micellization can be easily determined, they are adequate tools to study ion-specific effects. Here we evaluated the effect of several sodium salts on the micellization of DPS. Our results show a significant decrease in cmc with hydrotropic anions, following the same trend as cationic ones.

3.2 Material and Methods

3.2.1 Materials. N-Dodecyl-N,N-dimethyl-3-ammonio-1-propanesulfonate (Sigma 97%) (DPS) was recrystallized 2x from Acetone/Methanol. Sodium Bromide (Synth 99%) (NaBr), Chloride (Synth 99%) (NaCl), Perchlorate (Merck) (NaClO₄), Benzoate (Sigma-Aldrich > 99%) (NaBZSC) and Acetate (Baker 99.5%) (NaAc) were used without further purification. Sodium Methanesulfonate (Sigma 98%) (NaMs) was washed 2x with acetone. Sodium Trifluoroacetate (NaTFA), Trifluoromethanesulfonate (NaTf) and Benzenesulfonate (NaBZS) were synthesized by the neutralization (NaOH) of respective acids (Trifluoroacetic Acid – Sigma-Aldrich 98%; Trifluoromethanesulfonic Acid – Sigma-Aldrich 98%; Benzenesulfonic Acid – Sigma-Aldrich 98%).

3.2.2 Isothermal Titration Calorimeter. Isothermal Titration Calorimetry (ITC) experiments were performed at a VP-ITC (Microcal Inc). Solid DPS was dissolved in aqueous solutions containing 100 mM of either NaAc, NaBr, NaCl, NaMs, NaTFA, NaBzs, NaBzo, NaTf or NaClO₄. The final surfactant concentration was ca. 40 mM, i.e., 12 times the critical micellar concentration (cmc). Saline solution without DPS was placed in the calorimeter cell, and the saline solution with DPS was injected stepwise (x 32; 8 mL each) into this solution using the ITC syringe, in. Time between injections was usually 300 seconds, enough for the signal to return to baseline values. Upon each injection, a peak was produced (Fig. 4.3.1 – A), and the integration of each heat peak allowed the construction of a heat exchange as a function of DPS concentration lead the a sigmoidal type curve with DPS concentration (Fig 4.3.1 – B, dots). A modified sigmoidal expression was used to model the data (Király and Dekány, 2001) (Equation 4.3.1)

$$\Delta H_{dil} = \frac{a1[Surf] + a2}{1 + \exp((([Surf] - a3)/dx))} + a4[Surf] + a5 \quad (4.3.1)$$

where a_i 's are fitting parameters. The critical micelle concentration (cmc) was taken as the maximum (or minimum) of the first derivative of the adjusted equation and the demicelization enthalpy was taken as the difference between the two baselines at the cmc, one at the beginning and the other one at the end of the titration. In the results section we report micellization enthalpy, i.e., $(-1) \times \Delta H_{\text{demicelization}}$.

The Gibbs free energy can be determined from the cmc. For non-ionic or zwitterionic surfactants, cmc can be approximated as (Equation 4.3.2).

$$\Delta G^o \approx RT \cdot \ln(\text{cmc}) \quad (4.3.2)$$

where R is the gas constant, T is the temperature and cmc is the critical micelle concentration.

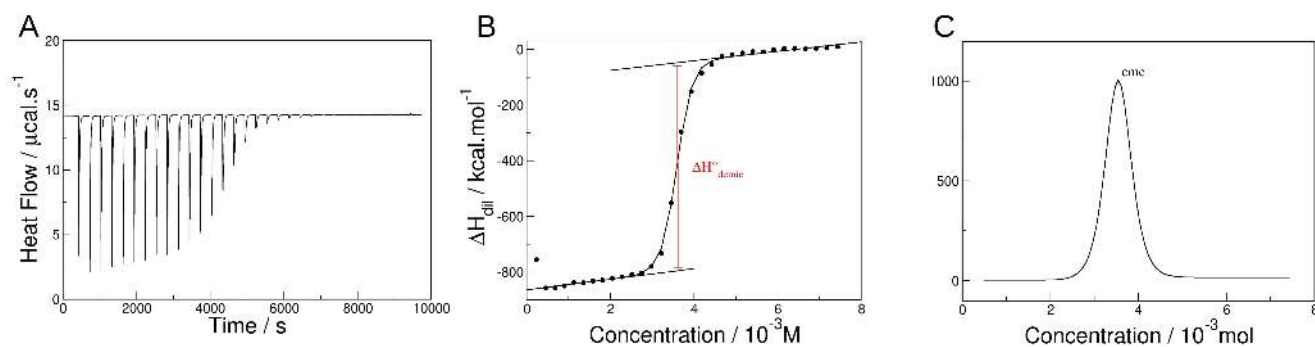


Figure 4.3.1: Titration calorimetry experiment for DPS in water at 25°C. (A) Heat flow versus time caused by 32 injections of 8 μL of DPS into 1.4 mL of water at 25 °C. (B) integration of peak area (points), fitting with Eq. 1 and determination of $\Delta H_{\text{demicelization}}$. (C) First derivative of first derivative of the adjusted equation (B), cmc is determined at the peak maximum.

3.3 Results and Discussion

The effects of anions on the micellization thermodynamics of DPS was determined using ITC. Figure 4.3.2 shows the cmc and the enthalpy of micelization for DPS at three

different temperatures in 100 mM salt solution of NaAc, NaMs, NaCl, NaBr, NaTFA, NaBzo, NaBzs, NaTf and NaClO₄. The raw data is in Appendix (Table S8).

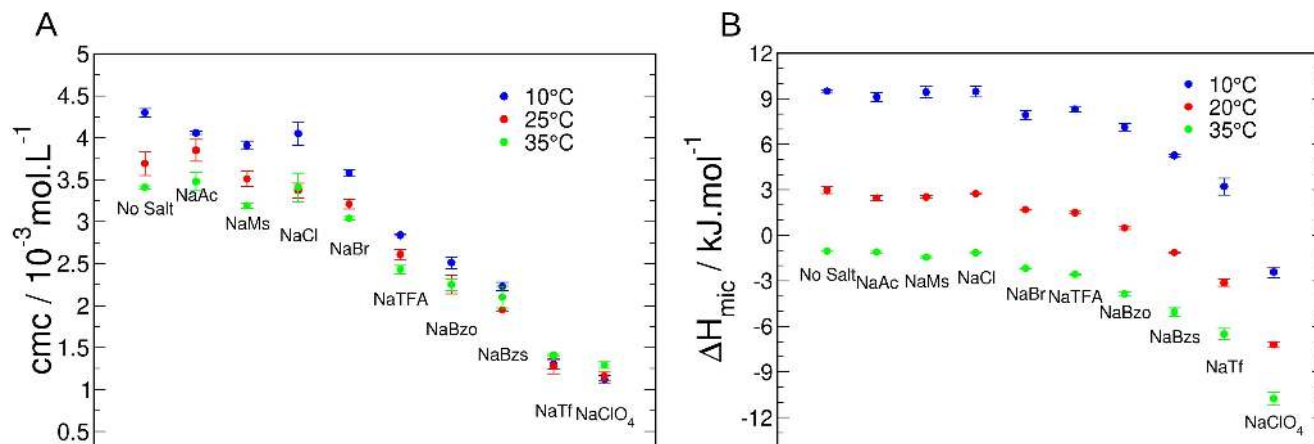


Figure 4.3.2: (A) cmc and (B) Enthalpy of Micelization for DPS at 10°C, 25°C and 35°C in different solutions containing 0.01 M of the salts.

The cmc for DPS in water was 3.6 mM at 25°C, in line previous data (Brinatti et al., 2014) and with the cmc determined by surface tension (Mortara et al., 2018). The salt-dependent cmc decrease was small upon addition of NaAc, NaMs or NaCl, but NaTf and (NaClO₄) caused significant cmc decrease. The value of cmc followed the order NaAc ~ NaMs ~ NaCl > NaBr > NaTFA > NaBzo > NaBzs > NaTf > NaClO₄.

Because zwitterionic surfactants are formally neutral, it was proposed that the ion effect is similar to the non-ionic ones (Tori and Nakagawa, 1963), where the cmc lowering is attributed to the salting-out of the hydrocarbon moiety of the monomeric detergent molecule (Mukerjee, 1965; Ray and Némethy, 1971; Zhang et al., 1996). For these non-ionic surfactants, the decrease of cmc typically follows the order F⁻ > Cl⁻ > Br⁻ > ClO₄⁻ (Krescheck, 2009; Ray and Némethy, 1971; Zhang et al., 1996) the opposite of what was observed for DPS, where the larger decrease was obtained with (NaClO₄).

These results indicate that the effect of salts on zwitterionic detergent aggregation must be compared with ionic, rather than non ionic surfactants, where the head group repulsive interactions are shielded by electrolyte, leading to a decrease in the cmc (Florenzano and Dias, 1997).

Although the same trend of salt effects on zwitterionic and ionic surfactants is expected, the effect of anions on zwitterionic micellization is not as pronounced. The cmc of 3-[(3-Cholamidopropyl)-dimethylammonium]-1-propanesulfonate, CHAPS (Kroflič et al., 2012) or of Dodecylphosphocholine, DPC (Aroti et al., 2007) does not change significantly in the presence of different anions, Cl^- , Br^- , and I^- or even ClO_4^- in DPC. Here, for DPS, the salt effect is not negligible even at low salt concentrations (100 mM).

The order of salt effect on cmc observed here is very similar to the counterion effect on the micellization of 1-dodecyl-3-methylimidazolium ($[\text{C12mim}]^+$), a cationic surfactant (Sarac et al., 2017), and didodecyldimethylammonium (DTA^+) (Lima et al., 2017) but in a much lower degree. Thus it is safe to assume a low degree of counterion condensation for DPS. For example, even at high salt concentrations, the maximum coverage of ClO_4^- in a similar propanesulfonate surfactant but with 14 carbons in the hydrophobic chain is 0.2 (Beber et al., 2004). Because of the low degree of counterion condensation, Equation 4.3.2 was used to extract the free energy of micellization. Entropy was calculated from the micellization enthalpy and the free energy. In Figure 3 the energies are plotted for the three temperatures analyzed.

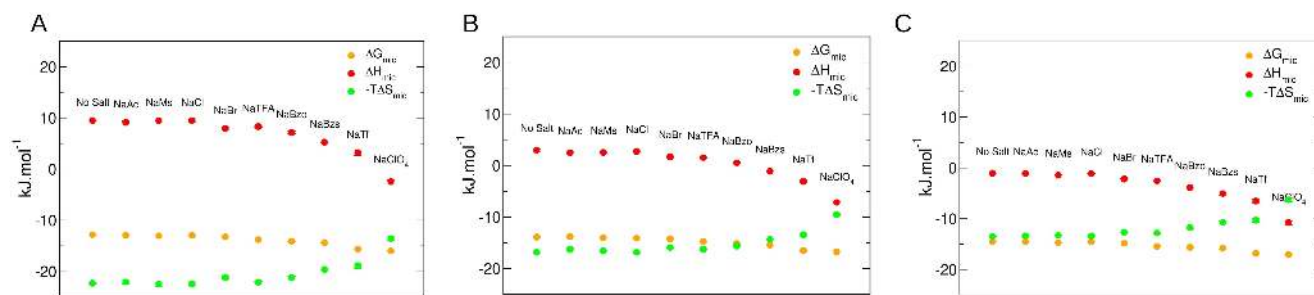


Figure 4.3.3: Free energy (ΔG_{mic}), enthalpy (ΔH_{mic}) and $-T\Delta S_{mic}$ for DPS at 100 mM of NaX salts, in (A) 10°C, (B) 25°C and (C) 35°C.

The micellization process is endothermic at low temperatures and becomes exothermic at high temperatures, reflecting the negative heat capacity $\Delta C_{p,mic}$ of this process. This is characteristic of hydrophobic effect (Gallagher and Sharp, 2003). At lower temperatures, the aggregation free energy is negative is mainly due to the entropy and at higher temperatures, it is mainly due to enthalpy (Southall et al., 2002). For DPS in salt solutions, at 10°C, enthalpy is positive for most of the salts evaluated here (except for NaClO_4), showing that the contribution for the negative free energy comes mainly from the entropy. With increasing temperature, the enthalpy becomes negative and at 35°C all of the salts have enthalpy contribution for the free energy. It is interesting to note that for DPS in NaClO_4 the enthalpy contribution is very significant in all temperatures.

As stated above, the change in heat capacity $\Delta C_{p,mic}$ is observed in upon hydrophobic solvation, and can be correlated with molecular surface area of the non-polar molecule (Gill et al., 1985). In a parallel, for surfactant aggregation, $\Delta C_{p,mic}$ is usually correlated with change of water accessible non-polar surface areas upon micelization (Király and Dekány, 2001). In the narrow range of temperature evaluated here, it can be assumed that the enthalpy of micelization scales linearly with temperature (fits are in Appendix, Figure S6), and from that the heat capacity ($\Delta C_{p,mic}$) ($\Delta C_{p,mic} = (\partial\Delta H_{mic})/(\partial T)_P$) can be extracted. The temperature where

enthalpy is zero (T_0) can be extracted from the intercept of the fitting. Both $\Delta C_{p,mic}$ and T_0 are in Table 4.3.1.

Table 4.3.1: Heat capacity and temperature with zero enthalpy for the micellization of DPS with 100 mM salt.

Salt	$-\Delta C_{p,mic} / \text{J.mol}^{-1}.\text{K}^{-1}$	T_0 / K
-	422.6 +/- 8.9	305
NaAc	411.7 +/- 24	305
NaMs	437.2 +/- 17.4	304
NaCl	426.7 +/- 16.4	305
NaBr	404.9 +/- 7.5	302
NaTFA	437.7 +/- 12.7	302
NaBzo	440.1 +/- 2.5	300
NaBzs	413.9 +/- 9.5	295
NaTf	391.6 +/- 22.4	291
NaClO ₄	331.8 +/- 10	276

Heat capacity is very similar for all systems, with the exception of (NaClO₄). This is in line with our early work that showed that hydration of the DPS micelles interfaces are very similar when either of the salts are added (NaBr, NaMs, NaTFA and NaTf) (Mortara et al., 2018). Interestingly, the heat capacity for (NaClO₄) shows a less dehydrated system. This might be explained by the cation binding promoted upon (ClO₄⁻) uptake (Priebe et al., 2012).

For small non polar solutes like neopentane, the temperature at which enthalpy of solvation is zero (T_0) is approximately 25°C (Southall et al., 2002). For ionic surfactants, is observed that T_0 depends on the counterion and chain length. For

didodecyldimethylammonium chloride, for example, T_0 is approximately 33°C, and lowers to 28°C upon 1 M NaCl addition (Šarac and Bešter-Rogač, 2009). For cationic surfactant 1-dodecyl-3-methylimidazolium the lowest T_0 is observed for hydrophobic counterions like iodide or salicylate (Sarac et al., 2017). It can be observed here that T_0 for DPS in NaClO_4 is much lower than the other salts, with NaTf and NaBzs also being lower than 25°C.

The anion effect on micellization was also investigated at higher salt concentrations. The enthalpy and cmc for some of the salts (NaBr, NaTFA, NaBzo, NaBzs, NaTf and NaClO_4) are in Figure 4.3.4 and raw data in Appendix (Table S9).

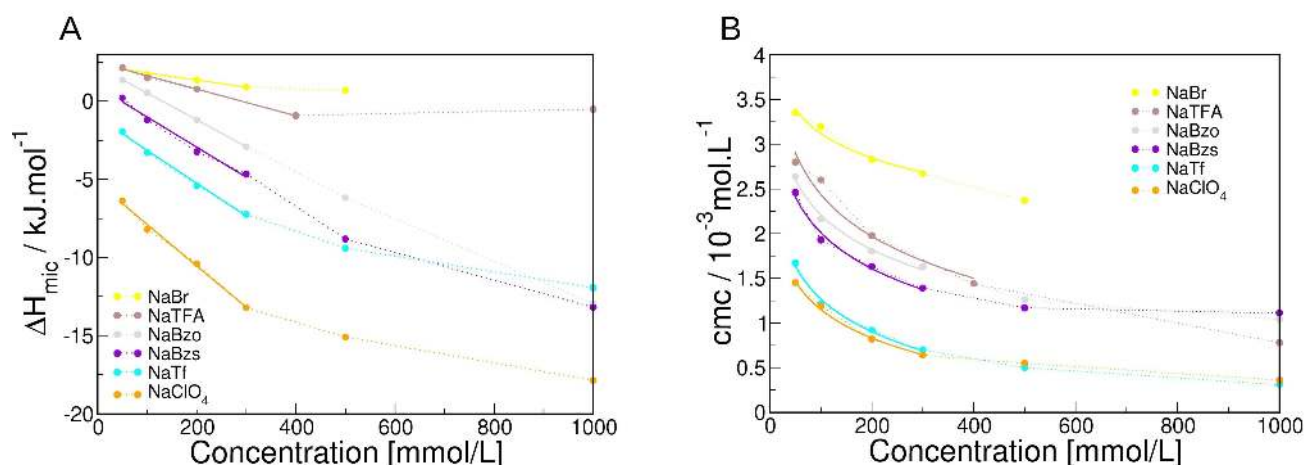


Figure 4.3.4: (A) Enthalpy of micellization and (B) cmc for DPS in increasing salt concentration. Full lines are linear regressions and dashed lines are guide for the eye.

Up to 300 mM the effect on enthalpy of micellization appears to vary linearly with the salt concentration. For neutral surfactants, the salt effect on cmc can be correlated with the salt concentration by the simple empirical law (Mukerjee, 1965) (Equation 4.3.3).

$$\log(\text{cmc}) = \text{const.} - K_s \cdot (C_{\text{sal}}) \quad (4.3.3)$$

where K_s is salt-effect parameter, and C_{salt} is the salt concentration.

This correlation was applied for a range of non-ionic (Ray and Némethy, 1971) and zwitterionic (Kroflič et al., 2012; Tori and Nakagawa, 1963) and even some ionic surfactants (Kroflič et al., 2011). For a series of alkyltrimethylammonium chloride, Equation 3 could only be fitted for addition of NaCl, on the shorter chain surfactant DeTAC (Kroflič et al., 2011). For the salts evaluated here, only NaBr appears to follow this relationship, with $K_s = 0.33$. This value is comparable to the one determined for NaCl in CHAPS, which was 0.21, and far from the cationic surfactant DeTAC, which was 0.66. This difference in K between ionic and zwitterionic is expected, since the dependence on cmc of ionic surfactants is significant higher than for zwitterionic ones. For the other salts, the linear relationship holds until 300 mM, giving the K_s in table 4.3.2.

Table 4.3.2: K_s values

Salt	K_s
NaBr	0.33
NaTFA	0.84
NaBzo	0.8
NaBzs	0.93
NaTf	1.43
NaClO ₄	1.43

It is interesting to note that the salt effect of (NaClO₄) and NaTf on cmc is very similar, but not on enthalpy of micellization. This points to the fact that the entropy of micellization plays an important role in the free energy of micellization when NaTf is present in the system.

3.4 Conclusions

Anion effect on the micellization of zwitterionic DPS was evaluated from the change in cmc and enthalpy of micellization when NaX added in solution. Both cmc and enthalpy followed the order NaAc ~ NaMs ~ NaCl > NaBr > NaTFA > NaBzo > NaBzs > NaTf > (NaClO₄), showing that anion effect in zwitterionic micelle follows the same order as the anion effect in cationic micelles, although in a lower degree. From the heat capacity changes it was can be argued that the micelles formed in salt solution are similar to the micelles formed in water, except for (NaClO₄). Linear change of enthalpy with salt concentration is only observed up to 300 mM salt.

4.4 Anion competition at positively charged dialkyldimethylammonium monolayers

Abstract

Specific ion effects have long been associated with the ion capacity of modifying the water properties around it, but this is not enough to describe this phenomena. Direct quantification preferential anions interaction can give important information regarding the factor behind specific ion effect. In this work we quantified the preferential anion binding between chloride and bromide in cationic monolayers of dioctadecyldimethylammonium and dihexadecyldimethylammonium was determined using Total Reflection X-Ray Fluorescence. Monolayers in subphases containing these anions were characterized using Grazing-incidence X-ray Scattering and Brewster Angle Microscopy. Molecular Dynamics simulations of monolayers were also performed, where the Lennard-Jones potential of the pair head-group

anion was rescaled to reproduce osmotic coefficient measurements. For both monolayers, the proportion of anions at the interface was 80 Br⁻/20 Cl⁻, independent of the area per molecule and the monolayer phase. There was good agreement between simulations and experiments, showing that for this system, the pair head-group anion interaction plays an important role in preferential anion interaction.

4.1 Introduction

More than 100 years ago Hofmeister described the effect of different salts in several colloidal systems and postulated that colloid precipitating effect of a salt is dependent on its water absorbing capability (Kunz et al., 2004). The ion ability to modify the structure and properties of water was a well accepted mechanism for SIE, however there is no consensus whether ions can affect water outside its solvation shell (Tielrooij et al., 2010; Wachter et al., 2005). Recent reviews have argued that not only ionic size and hydration are essential components of SIE but it is also important to consider ionic hydrophobicity and complexation capacity with the interface (Leontidis, 2017) and the "local" interactions between ion and interface (Lo Nostro and Ninham, 2012).

Micelles have long been used as convenient systems to analyse SIE (Fendler, 1982). Several studies have described the effect of different counterions on surfactants containing methyl ammonium quaternary head groups such as dioctadecyldimethylammonium DODA⁺ or hexadecyltrimethylammonium (CTA⁺) (De Neve et al., 2017; Feitosa and Alves, 2008; Nascimento et al., 1998; Paredes et al., 1984). Phase transition temperatures from gel phase to liquid crystalline are different for vesicles of DODAC or DODAB (Feitosa and Alves, 2008) and the choice of counterion has practical effects such as efficiency in RNA delivery using cationic: monoolein liposomes (Oliveira et al., 2014). The critical micelle concentration (cmc)

of hexadecyltrimethylammonium decreases with counterion size (i.e., CTAF > CTACl > CTABr > CTAI). The nature of the counterion also affects the enthalpy of micellization of (CTA⁺) (Paredes et al., 1984).

Langmuir monolayers at the air-water interface of cationic surfactants also show SIE (Ahuja et al., 1994; Cavalli et al., 2001; Nihonyanagi et al., 2014; Wojciechowski et al., 2012). For example, the surface pressure of dioctadecyldimethylammonium bromide (DODAB) monolayers increases (for the same area per molecule) with the electronegativity of the anion in the subphase (Ahuja et al., 1994; Cavalli et al., 2001), following the Hofmeister series.

Bromide ion binds preferentially to chloride ions in cationic interfaces (Fabre et al., 1980). However, only some methods can directly quantify the interaction. The amount of counterion bound to the interface can be inferred from conductivity measurements (Cuccovia et al., 1990; Sepúlveda and Cortés, 1985). Selectivity coefficients or ion exchange constants demonstrated the preferential interaction of anions in interfaces. A selectivity constant for Br/Cl exchange at the interface of DODAB vesicles is ~ 2 (Scarpa et al., 2002).

Molecular dynamics simulations, a complementary tool for the experimental investigations, demonstrated that the hydrotropic counterion interaction with cationic and zwitterionic micelles directly correlates to the anion dehydration upon binding (Lima et al., 2017; Mortara et al., 2020).

Because specific ion effects cannot be described only by electrostatics interaction, aggregate geometry is an essential factor to consider. Using experimental methods and molecular dynamics simulations, we quantitatively determine the competitive interaction between Chloride and Bromide anions at cationic monolayers of DHDA⁺ or DODA⁺ in monolayers at different points of surface pressure-area isotherm.

4.2 Material and Methods

4.2.1 Materials. Dihexadecyldimethylammonium chloride (DHDAC) was prepared by passing Dihexadecyldimethylammonium bromide (DHDAB, Sigma Aldrich), dissolved in methanol, through a Dowex 21K anion-exchange resin. Dioctadecyldimethylammonium bromide (DODAB) was from Merck ($\leq 98\%$) and used as received. The methanol was evaporated and the powder was recrystallized in a methanol/acetone mixture. NaCl (99.0%) and NaBr (99.5%) were purchased from Sigma Aldrich, and used as received. Double-deionized ultrapure water (resistivity: 18.2 M Ω .cm), obtained from a Milli-Q purification system, was used to prepare the salt solutions. The surfactant stock solutions were prepared by weighing the appropriate amount of solid surfactant in an analytical balance and subsequently dissolving in chloroform to a concentration of 1 mg/mL. Monolayers of DHDA⁺ or DODA⁺ were formed by depositing ~ 30 μ L of the chloroform solutions onto aqueous subphases containing either 2 mM NaBr ("NaBr subphase"), or 2 mM NaCl ("NaCl subphase"), or 1 mM NaBr + 1 mM NaCl ("mixed subphase") and waiting 10 minutes for the solvent to evaporate.

4.2.2 Pressure-area isotherms and Brewster-angle microscopy. Pressure-area isotherms of DHDA⁺ and DODA⁺ monolayers were measured with a Langmuir trough by KSV Nima (Accurion, KSV NIMA, Biolin Scientific, Espoo, Finland) and the pressure was measured with a Wilhelmy paper plate. The monolayer were laterally compressed with a movable barrier at a constant compression rate of $dA_{\text{mol}}^{\text{a}}/dt \approx 5 \text{ }^2/\text{min}$, where $A_{\text{mol}}^{\text{a}}$ is the available area per molecule.

Brewster-angle microscopy (BAM) experiments were carried out with an Ultrabam system by Accurion (Göttingen, Germany) at a laser wavelength of $\lambda = 658 \text{ nm}$, combined with the Langmuir trough described above. The size of the focal region is enhanced with the help of suitable optics, due to the non-perpendicular observation. The optical distortion was corrected using the software AccurrionImage, and contrast enhancement was done using the software ImageJ (Schneider et al., 2012). Further details are described elsewhere (Mukhina et al., 2022a).

4.2.3 Synchrotron-based grazing-incidence x-ray scattering techniques. Grazing-incidence X-ray scattering experiments were carried out at the beamline P08 at storage ring PETRA III of Deutsches Elektronen-Synchrotron (DESY, Hamburg, Germany). The Langmuir trough (Riegler & Kirstein, Potsdam, Germany) was located in a hermetically sealed helium-filled container with Kapton windows, and the temperature was kept at 25°C with the help of a thermostat. The x-ray beam was monochromatized to a photon energy of 15 keV, corresponding to a wavelength of $\lambda = 0.826 \text{ \AA}$. The incident angle was adjusted to $\theta_i = 0.07^\circ$, about 85% of the critical angle of total reflection, $\theta_c = 0.082^\circ$. A ground glass plate was placed approximately 0.3 – 1 mm beneath the illuminated area of the monolayer in order to damp the vibration of the water surface. Under the imposed total-reflection conditions, an x-ray standing wave (SW) is formed at the air/water interface. At the given incident angle, the penetration depth of its evanescent tail into the aqueous hemisphere is $\Lambda \approx 7\text{nm}$.

4.2.4 Grazing incidence x-ray diffraction (GIXD). The diffraction signal was collected with a one-dimensional position sensitive detector (PSD) (MYTHEN, PSI, Villigen, Switzerland) by scanning the azimuth angle 2θ and, with that, the in-plane component $Q_{xy} = (4\pi/\lambda) \sin(\theta)$ of the scattering vector $Q=(Q_{xy}, Q_z)^T$. The out-of-plane component, $Q_z = (2\pi/\lambda) [\sin(\alpha) + \sin(\alpha_i)]$, is encoded in the vertical position of the PSD channels, where α denotes the angle between the scattered direction and the sample plane. The in-plane beam divergence was collimated with a Soller collimator placed in front of the PSD providing $\Delta_{2\theta} \approx 0.09^\circ$ (full-width-at-half-maximum, FWHM), corresponding to $w_{xy}^{\text{res}} = (4\pi/\lambda)\sin((\Delta_{2\theta}/2)) \approx 0.012 \text{ \AA}^{-1}$. To reconstruct the 2D crystalline structure of the monolayers in terms of lattice parameters and chain tilt, the diffraction peaks on the resulting intensity maps, $I(Q_{xy}, Q_z)$, were fitted with a self-written python macro yielding their Q_{xy} and Q_z positions and the peak widths in both directions. Further details of this analysis are described elsewhere (Mukhina et al., 2022b).

4.2.5 Grazing incidence x-ray off-specular scattering (GIXOS). The interfacial electron density profile (i.e., the laterally-averaged structure of the surfactant layer in the direction perpendicular to the surface) was determined by GIXOS. The details of this technique are described elsewhere (Mora et al., 2004; O’Flaherty et al., 2005; Pusterla et al., 2022), from where the following paragraph is largely reproduced. In brief, the Q_z -dependence of the diffuse scattering intensity $I(Q_{xy} \neq 0, Q_z)$ recorded at low-enough yet finite Q_{xy} (“out of the specular plane”) with the help of a narrow slit contains information equivalent to that of the conventional reflectivity $R(Q_z)$ and can be transformed as $I(Q_{xy} \neq 0, Q_z) = V(Q_z)R(Q_z)/R_F(Q_z)$ to good approximation, where $V(Q_z)$ is the Vineyard function and $R_F(Q_z)$ the Fresnel reflectivity of an ideal interface between the two bulk media. The approximation is based on the assumption of conformal topographic roughness of all interfaces, which is justified for mono-molecular surface layers subject to capillary wave roughness. In the present work, the GIXOS signal was measured at $Q_{xy} = 0.04 \text{ \AA}^{-1}$. The experimental data were analyzed with slab models where the reflectivities $R(Q_z)$ were multiplied with $V(Q_z)/R_F(Q_z)$ to obtain the theoretical GIXOS signal.

4.2.6 Total-reflection x-ray fluorescence (TRXF). The x-ray fluorescence spectra were recorded using an Amptek X-1235DD detector. The detector was placed almost parallel to the water surface and perpendicular to the X-ray beam axis, in order to keep elastic and Compton scattering into the detector as weak as possible. A detailed description of the method can be found elsewhere (Brezesinski and Schneck, 2019; Klockenkamper et al., 1992). The fluorescence intensity (I_j) from an element or ion species j is determined by the concentration profile along the direction normal to the interface $c_j(z)$:

$$I_j = b_j \int_{-\infty}^{\infty} \Phi(z) c_j(z) dz \quad (4.4.1)$$

, where $\phi(z)$ is the SW intensity at distance z from the surface and b_j is a constant determined by the fluorescence yield and detection efficiency, but independent of the structure and composition of monolayer. The counterions adsorbed to a charged monolayer are known to be confined to a thin region with an extension of less than 5 Å, such that ϕ can be assumed to be constant along this region (Shapovalov et al., 2007).

The spectra were analyzed by fitting the element-characteristic fluorescence peaks with Gaussian functions. Peak positions were restrained based on the tabulated line energies (X-ray data booklet, 2001). The integrated peak area for the bare subphases were subtracted from the integrated peak area from the monolayer containing spectra.

4.2.7 Molecular dynamics simulations. All simulations were performed with the GROMACS simulation package (Abraham et al., 2015)(Abraham et al., 2015) on the Lichtenberg II cluster from of TU Darmstadt (Project ID 1544). The SPCE water model (Berendsen et al., 1987) was combined with the GAFF (Wang et al., 2004) parameters for surfactant headgroups or free tetramethylammonium (Tet^+) and Slipids (Jämbeck and Lyubartsev, 2012) parameters for the surfactant tails. Ions (Na^+ , Cl^- , and Br^-) were modeled according to Joung and Cheatham (Joung and Cheatham, 2008) with full charges. The partial charges for atoms in molecules were calculated using Restrained electrostatic potential (RESP) (Bayly et al., 1993) at HF6-31G*, as the default charge approach for Amber, using the software packages Gaussian (Frisch et al., 2016) and AmberTools21 (Case et al., 2021). All bonds were constrained with the LINCS algorithm (Hess et al., 1997) up to the fourth order expansion. A van der Waals cutoff of 1.2 nm was used without any long range corrections. The particle-mesh-Ewald (PME) method (Darden et al., 1993) was used to treat long-range electrostatic interactions. Periodic boundary conditions were applied in all three directions. For all simulations the temperature was kept at 298 K with the velocity-rescale thermostat (Bussi et al., 2007) with 0.1 ps coupling time.

For bulk simulations we used version 2019.4 of GROMACS. Osmotic coefficients were calculated for chloride and bromide tetramethyl ammonium salts (TetCl and TetBr , respectively) at 1 *m* and 25°C. Tet^+ and the respective anion were added randomly distributed in a 5 nm x 5 nm x 5 nm simulation box using Packmol (Martínez et al., 2009) and then water was added to a 5 nm x 5 nm x 10 nm box with the ions kept in the center of the box. Osmotic coefficient was determined using OPAS method (Kohns et al., 2016). A flat-bottom potential is applied to the ions in order to keep them inside a central box with $z = \pm 2.5\text{nm}$. Water is not affected by this potential. The simulation and analyses were done as described elsewhere

(Bernhardt et al., 2022). Briefly, after system minimization, a pre-run of NpT simulation was performed, where the osmotic pressure was first estimated. From this osmotic pressure value a new total pressure for the simulation box is chosen such that the pressure of the water slab is approximately 1 bar in the production simulation. The NpT production run was performed for 40 ns, of which the first 20 ns were excluded from the analysis. Parrinello-Rahman barostat was used. The osmotic pressure (π) is then simply given by the time-averaged force acting on the walls, $\langle F_{\text{wall}} \rangle / A$, where A is the cross-sectional area of the wall. The F_{wall} was calculated using the code (Bernhardt et al., 2022). The osmotic coefficient is then determined as $\phi = \pi / (i c R T)$, with $i = 2$ considering full dissociation. In order to correctly reproduce the experimental osmotic coefficients of TetCl and TetBr, scaling factors for the Lennard-Jones pair potentials between anions and Tet⁺ had to be adjusted along the lines described earlier (Fyta and Netz, 2012), see Results text.

For monolayer simulations we used version 2021.1 of GROMACS. Initial structures were built with a 9 nm x 9 nm x 20 nm water layer contacting vacuum boxes of 9 nm x 9 nm x 40 nm on both sides in the z direction. Two monolayers with 100 surfactants each were placed at the water-vacuum interfaces, leading to an initial area per surfactant of 81 Å². Subsequently, 400 water molecules were replaced by anions, either 400 Br⁻, or 400 Cl⁻, or 200 Br⁻ + 200 Cl⁻. In addition, 200 water molecules were replaced with Na⁺ counterions in order to achieve charge neutrality when also accounting for the positive charge of each surfactant. This effectively corresponds to a background salt concentration of approximately 90 mM.

Production simulations of 100 ns were run using constant-volume (NVT) ensemble. After minimization runs, NpT simulation with lateral pressure was run until it reached an area per molecule correspondent to a surface tension of approximately 20 mN/m. For the production run, surface tension is calculated from the diagonal pressure tensor (Nijmeijer et

al., 1990). The surface pressure is obtained $\pi = \gamma_0 - \gamma$, where γ is the surface tension of the monolayer simulation and γ_0 is the bare water surface tension, calculated from a NVT water simulation using the same parameter used for the monolayer simulations. Trajectory analyses were made using the GROMACS tools, where the first 20 ns of each simulations were excluded in order to assure proper equilibration.

4.3 Results and Discussion

Fig. 4.4.1 shows the chemical structures of the two dialkyl-dimethylammonium types investigated, dihexadecyl-dimethylammonium DHDA⁺ with two C16 chains and dioctadecyl-dimethylammonium DODA⁺ with two C18 chains. Although both form insoluble (Langmuir-type) monolayers at the air/water interface, their structural arrangement in densely packed monolayers is different. DHDA⁺ generally exhibits a fluid *liquid-expanded* (LE) phase, while DODA⁺ has the tendency to form a chain-crystalline *liquid-condensed* (LC) phase with significantly smaller area per molecule. In this way, positively charged dialkyldimethylammonium monolayers with different headgroup densities are formed by the two molecules. To evaluate preferential anion interactions with these monolayers, we focused on chloride Cl⁻ and bromide Br⁻. For this purpose, three different aqueous subphases were used, containing either 2 mM NaBr ("NaBr subphase"), or 2 mM NaCl ("NaCl subphase"), or 1 mM NaBr + 1 mM NaCl ("mixed subphase"). These low bulk concentrations facilitate TRXF experiments and were therefore chosen for all experiments. For practical reasons, complementary MD simulations were performed at higher ion concentrations, but this difference does not prevent comparisons with regard to ion-specific effects (see further below).

In the following, we will first describe the experimental results obtained in pressure-area isotherms and with grazing-incidence x-ray scattering techniques. And afterwards we describe the results of the MD simulations, where we will make comparison with the experimental results wherever possible.

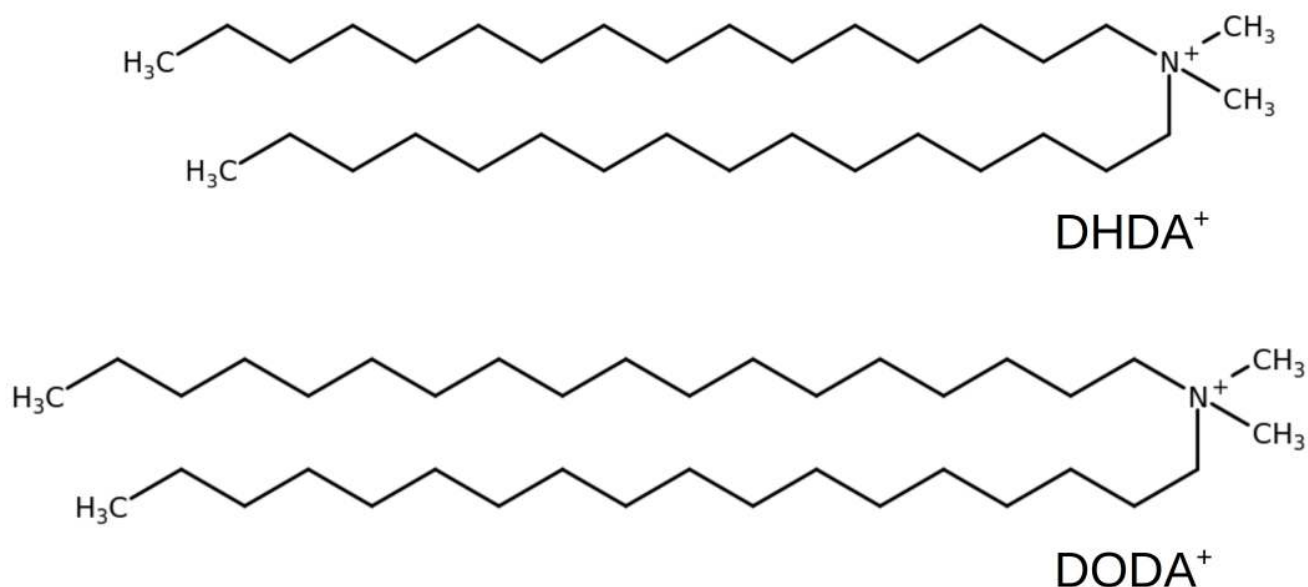


Figure 4.4.1: Chemical structures of dihexadecyldimethylammonium (DHDA⁺) and dioctadecyldimethylammonium (DODA⁺).

4.3.1 Pressure-area isotherms. Fig. 4.4.2 shows pressure-area isotherms recorded with DHDA⁺ (A) and DODA⁺ (B) on NaCl, NaBr, and mixed subphases. $A_{\text{mol}}^{\text{a}}$ is the available area per molecule in the monolayer. As mentioned before, DHDA⁺ exhibits a fluid LE phase at all pressures, which follows from the gradual pressure increase upon compression and the absence of a transition plateau (Fig. 4.4.2A). At a given surface pressure, $A_{\text{mol}}^{\text{a}}$ is largest on the NaCl subphase and smallest on the NaBr subphase, reflecting that Br⁻ ions have a laterally condensing effect on the monolayer in comparison to Cl⁻ ions. On the mixed subphase, $A_{\text{mol}}^{\text{a}}$ is almost as small as on the NaBr, which provides a first indication that Br⁻ ions dominate over Cl⁻ ions at the interface. The isotherms of DODA⁺ (Fig. 4.4.2B) yield a consistent picture. This molecules transitions from the LE phase into the chain-crystalline LC phase when sufficiently compressed laterally. In the isotherms, this transition manifests as a plateau with a characteristic transition pressure π_{tr} . Phase coexistence occurs for $A_{\text{mol}}^{\text{a}}$ values in the plateau. This coexistence is evidenced in the BAM image provided as inset, where roundish LC domains can be clearly identified in a continuous LE phase surrounding them (Honig and Mobius, 1991). Strikingly, π_{tr} is much lower on the NaBr subphase than on the NaCl subphase, demonstrating that the presence of Br⁻ ions stabilizes laterally condensed phases more strongly than that of Cl⁻ ions, in line with earlier reports (Ahuja et al., 1994; Cavalli et al., 2001; Shapovalov et al., 2010). Again, the isotherm on the mixed subphase resembles the one on the NaBr subphase much more than the one on the NaCl subphase, reflecting once more the dominance of Br⁻ over Cl⁻ at the interface.

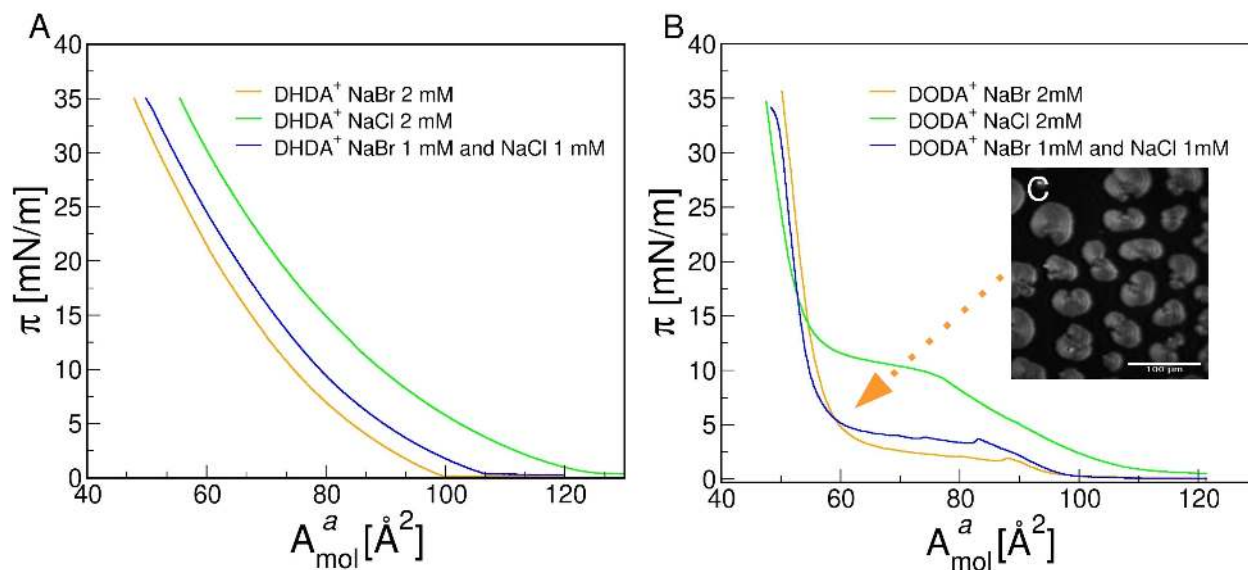


Figure 4.4.2: Pressure--area isotherms recorded with DHDA⁺ (A) and DODA⁺ (B) on NaCl, NaBr, and mixed subphases. Inset panel B: BAM image of a DODA⁺ monolayer on a NaBr subphase at $A_{\text{mol}}^a = 57 \text{ \AA}^2$.

4.3.2 Electron density profiles and in-plane ordering (GIXOS and GIXD). Fig. 4.4.3A shows GIXOS curves measured with DHDA⁺ and DODA⁺ monolayers on NaBr subphases at $\pi = 20 \text{ mN/m}$ and $\pi = 35 \text{ mN/m}$, respectively. The period of the intensity oscillations on the Q_z -axis is seen to be significantly shorter for DODA⁺ than for DHDA⁺, which reflects that DODA⁺ forms a significantly thicker monolayer at the interface because it has longer tails and is in the LC phase. For both surfactant types the data were analyzed by describing the monolayer film with two homogeneous layers of adjustable thickness d and electron density ρ , which represent different portions of the monolayers, namely hydrocarbon chains (hc) and headgroups (hg). The interfaces between the layers are subject to interfacial roughness to an adjustable extent encoded in the roughness parameters σ .

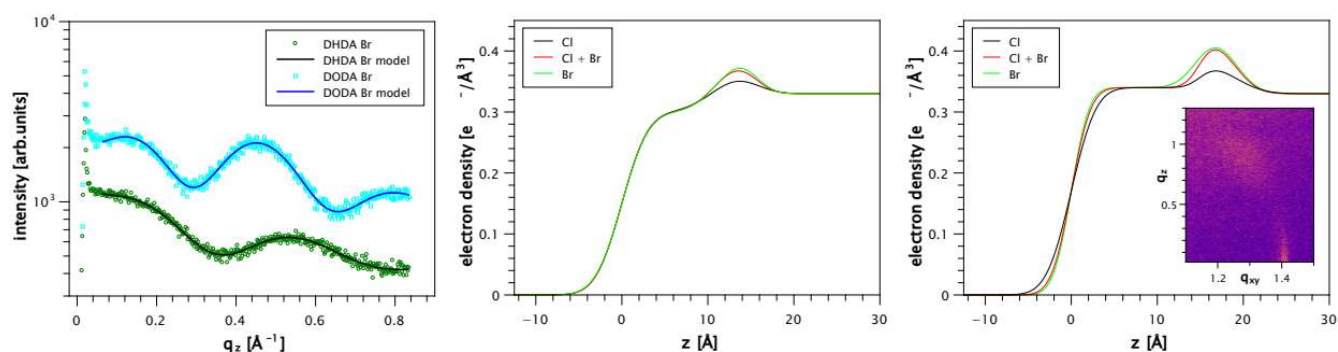


Figure 4.4.3: (A) GIXOS signals for DHDA⁺ and DODA⁺ monolayer at $\pi = 20$ mN/m and $\pi = 35$ mN/m, respectively, on a NaBr subphase. For clarity, the curves are vertically offset in the semi-logarithmic plot through multiplication with a suitable factor. (B and C) Corresponding electron density profiles for all three subphases.

The solid line superimposed to the experimental data points in Fig. 4.4.3A are modeled GIXOS signals based on such a two-layer description after optimization of the parameters d and ρ of the layers and of the σ parameters of all layer interfaces. The associated best-matching electron density profiles of the DHDA⁺ and DODA⁺ monolayers on all subphases are shown in Fig. 4.4.3B and C, respectively. The electron density of the hg layer is comparatively higher than that of the hc layer and the adjacent aqueous medium, because it also accommodates heavy (electron-rich) elements in the form of the counterions Cl⁻ and Br⁻. The best-matching layer parameters for DHDA⁺ and DODA⁺ on all subphases are summarized in Table 1. In order to reduce the number of free fitting parameters, ρ_{hc} was fixed at $0.30 \text{ e}^-/\text{\AA}^3$ for monolayers in the LE phase and to $0.34 \text{ e}^-/\text{\AA}^3$ for monolayers in the LC phase, according to our previous studies (Pusterla et al., 2022; Stefaniu et al., 2019). Moreover, d_{hc} was fixed at a chemically plausible value of 4 \AA because thickness and roughness parameters are highly covariant for such thin layers. A first observation is that the experimental GIXOS curves are well reproduced by the two-layer model. The hc layer thickness is virtually independent of the subphase type and about 4 \AA higher for DODA⁺ than for DHDA⁺. Importantly, ρ_{hc} is highest on the NaBr subphase but nearly as high on the mixed subphase. Since Br⁻, with its 36 electrons,

contributes much more to the electron density of the hg layer, this observation corroborates the picture that the adsorption of Br⁻ is preferred over the adsorption of Cl⁻.

Table 4.4.1: Layer parameters for DHDA⁺ at $\pi = 20$ mN/m and for DODA⁺ at $\pi = 35$ mN/m as obtained by GIXOS.

parameter	DHDA ⁺			DODA ⁺		
	NaBr	NaCl	mixed	NaBr	NaCl	mixed
$\sigma_{\text{air/hc}}$ [Å]	2.5	2.4	2.4	1.6	2.3	1.8
d_{hc} [Å]	11.4	11.1	11.2	14.8	15.1	15.0
ρ_{hc} [e ⁻ /Å ³] (fixed)	0.3	0.3	0.3	0.34	0.34	0.34
$\sigma_{\text{hc/hg}}$ [Å]	2.5	2.8	2.6	2.0	1.4	1.4
d_{hc} [Å]	4.0	4.0	4.0	4.0	4.0	4.0
ρ_{hg} [e ⁻ /Å ³]	0.40	0.38	0.40	0.44	0.38	0.42
$\sigma_{\text{hg/wat}}$ [Å]	1.8	2.2	1.8	2.0	2.6	2.1

The inset of Fig. 4.4.3C shows the GIXD pattern obtained with a DODA⁺ monolayer on NaBr subphase at $\pi = 35$ mN/m, corresponding to the electron density profile shown in the main panel. The pattern features two diffraction peaks, a sharp one at $(Q_{xy}; Q_z) \approx (1.41; 0)$ Å⁻¹ and a broader one at $(Q_{xy}; Q_z) \approx (1.29; 0.85)$ Å⁻¹, which correspond to a chain lattice with the parameters summarized in Table 4.4.2 and confirm that the DODA⁺ monolayer is in the LC phase under these conditions.. Table 4.4.2 also contains the chain lattice parameters obtained at $\pi = 25$ mN/m, which serves for comparison with the MD results presented further below.

Table 4.4.2: Lattice parameters (unit cell vector lengths b and c , their relative angle α , chain tilt t , in-plane area A_{xy} , and chain-cross-sectional area A_0) of DODA⁺ monolayers on NaBr subphase at $\pi = 25$ mN/m and $\pi = 35$ mN/m as obtained by GIXD.

Parameter	$\pi = 25$ mN/m	$\pi = 35$ mN/m
b [Å]	5.6	5.5
c [Å]	6.3	5.9
α [°]	127.3	125.7
t [°]	43	42
A_{xy} [Å ²]	28.1	26.5
A_0 [Å ²]	20.7	19.8

4.3.3 Ion densities at the interface (TRXF). In order to precisely quantify the ion-specific preferential adsorption to the cationic monolayer, TRXF measurements were carried out with DHDA⁺ monolayers and DODA⁺ monolayers on all three subphases and at various surface pressures, $\pi = 10$ mN/m, $\pi = 20$ mN/m and $\pi = 30$ mN/m for DHDA⁺ and $\pi = 15$ mN/m, $\pi = 25$ mN/m and $\pi = 35$ mN/m for DODA⁺. Fig. 4.4.4A exemplifies the resulting x-ray fluorescence spectra in a narrow energy range covering the $K\alpha$) line of chlorine (2.62 keV) and the $L\beta$) line of bromine (1.52 keV) (Bearden, 1967; X-ray data booklet, 2001). The more intense $K\alpha$) line of bromine at 11.92 keV is shown in Fig. 4.4.4B.

As described in the Methods section, the intensities of the peaks associated with these lines are proportional to the interfacial densities of the ions in terms of their surface excesses Γ_{Cl} and Γ_{Br} . It is seen that the Cl peak is intense only for the NaCl subphase but not so much for the mixed subphase, while the two Br peaks are intense for the NaBr subphase and nearly as intense for the mixed subphase. On a qualitative level this observation already demonstrates the pronounced preferential adsorption of Br⁻ in the competition with Cl⁻. As reported earlier (Sung et al., 2015) for another cationic two-chain surfactant, 1,2-dipalmitoyl-3-trimethylammonium-propane (DPTAP), simple charge compensation occurs when only one

anion type is available, such that the surface excesses of different anions measured on two different subphases coincide.

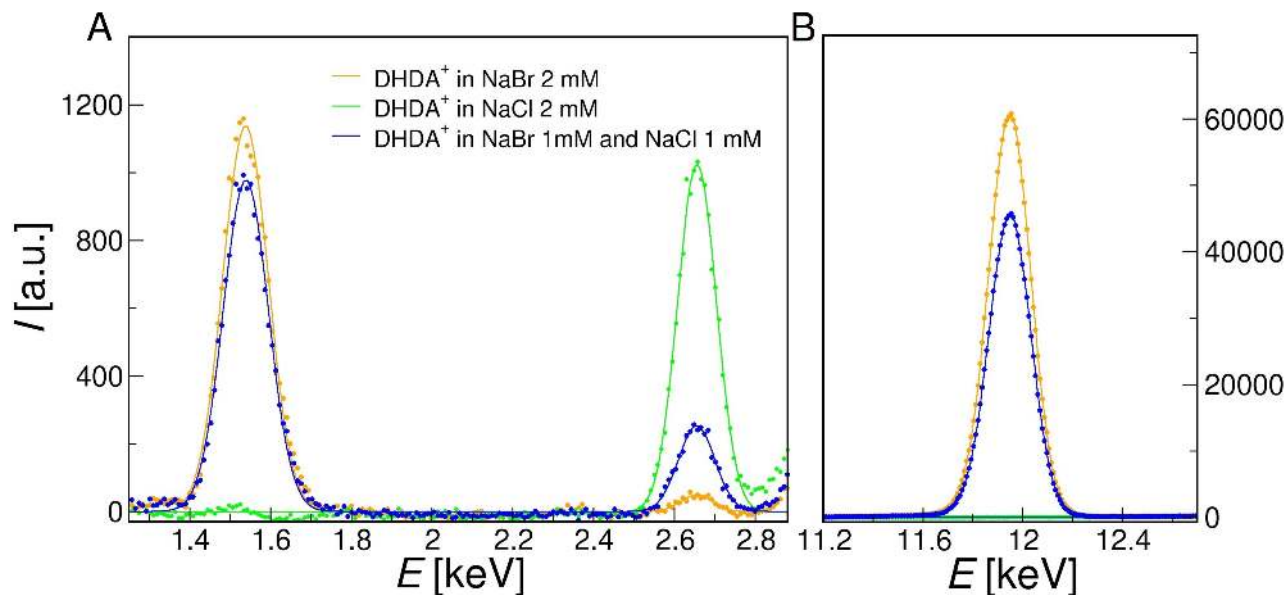


Figure 4.4.4: X-ray fluorescence spectra of DHDA⁺ at 20 mN/m on different subphases (NaBr 2 mM – Orange line; NaCl 2 mM – Green line and equimolar mixture NaCl/NaBr 1 mM each – blue line). Dots are data points and lines are Gaussian fitting.

The ratio between the intensity of the peaks I_j (with $j \in \{\text{Cl}, \text{Br}\}$), calculated from the integral, between the bare monolayer and mixed monolayer were determined, as follow:

$$x_{\text{Cl}} = \frac{I_{\text{Cl}}(\text{mixture})}{I_{\text{Cl}}(\text{NaCl})} \quad \text{and} \quad x_{\text{Br}} = \frac{I_{\text{Br}}(\text{mixture})}{I_{\text{Br}}(\text{NaBr})}$$

The obtained values of x_{Cl} and x_{Br} are summarized in Tables 4.4.3 and 4.4.4 for DHDA⁺ and DODA⁺, respectively. Note that, in the measurements with DODA⁺, some variations in the absolute intensity of the spectra had to be compensated via normalization on the elastic/Compton intensity, while this was not necessary for the measurements with DHDA⁺. It is seen that the contribution of Br⁻ in the competition is of the order of 0.8 for all surface pressures and both surfactant molecules. Reassuringly, this result is also robust with respect

to the choice of the transition line ($K\alpha$ vs. $L\beta$) of bromine. The contribution of Cl^- is always of the order of 0.2. As an independent validation we consider the sum of the two contributions, $x = x_{\text{Cl}} + x_{\text{Br}}$ (see Tables 4.4.3 and 4.4.4), which, by construction, should amount to unity within the experimental uncertainty. Indeed, the obtained values deviate from unity only by few percent, where the deviation must be attributed to the cumulative effect of all experimental error sources.

We recall that DHDA^+ monolayers are in the fluid LE phase at all subphases and all surface pressures (see Fig. 4.4.2). In contrast, DODA^+ monolayers are in the ordered LC phase under all conditions where TRXF was measured. Even though the area per positively charged surfactant headgroup is thus significantly different for DHDA^+ and DODA^+ , the preferential adsorption of Br^- in competition with Cl^- is robust on a quantitative level. This results indicates that the dominating factor in the competition is the pair-wise interaction between the headgroups and the anion, quite independently from headgroup correlation or "bridging" effects. This picture is consistent with an earlier report regarding the anion competition at the surfaces of DODA^+ vesicles, where temperature changes that affect the bilayer phase had no significant effect (Scarpa et al., 2002).

Table 4.4.3: Percentage of the peak intensity in the mixed subphase system of DHDAC compared to the 100 % intensity of pure bromide or chloride system.

Π [mN/m]	$x_{\text{Br}} (L\beta)$	$x_{\text{Br}} (K\alpha)$	x_{Cl}	sum ($K\alpha$)	sum ($K\beta$)
10	0.82	0.78	0.28	1.10	1.06
20	0.82	0.81	0.24	1.06	1.05
30	0.84	0.79	0.21	1.05	1.00

Table 4.4.4: Percentage of the peak intensity in the mixed subphase system of DODAB compared to the 100 % intensity of pure bromide or chloride system.

Π [mN/m]	$x_{\text{Br}} (\text{L}\beta)$	$x_{\text{Br}} (\text{K}\alpha)$	x_{Cl}	sum (K α)	sum (K β)
15	0.76	0.78	0.19	0.95	0.97
25	0.85	0.82	0.19	1.04	1.01
35	0.85	0.90	0.25	1.10	1.15

MD Simulations

4.3.4 Osmotic Coefficient. To validate the force fields applied in this work, we calculated the osmotic coefficients of TetBr and TetCl tetramethyl ammonium salt solutions based on the OPAS method (Kohns et al., 2016). Osmotic coefficients were considered because they are sensitive to subtle changes in ion-ion interactions. The osmotic coefficients calculated for 1 *m* TetBr and TetCl salt solutions were, respectively, 1.15 ± 0.2 and 1.11 ± 0.2 . These values are higher than the experimental ones (Lindenbaum and Boyd, 1964) and indicate that the attractive and repulsive interactions between the cations and anions in solution are not optimally balanced. Therefore, the Lennard-Jones (LJ) diameter, σ_{\pm} , used to describe the cation-anion interaction, was scaled using a scaling factor λ_{σ} according to $\sigma_{\pm} = \lambda_{\sigma}(\sigma_{++} + \sigma_{--})/2$ (Fyta and Netz, 2012). Some scaling factors were tested, and the values λ_{σ} 0.93 for TetBr and λ_{σ} 0.92 for TetCl led to an osmotic coefficient very similar to the one experimentally determined: 0.81 ± 0.04 (0.790) for TetBr and 0.88 ± 0.07 (0.862) for TetCl (Lindenbaum and Boyd, 1964). The satisfactory agreement achieved with the refined models suggests that they suitably describe the ion-specific electrostatic interactions in these systems.

4.3.5 Monolayer Simulations. The surface pressure for SPCE water was $58.1 \text{ mN/m} \pm 2.4 \text{ mN/m}$, similar to previous calculations (Vega and De Miguel, 2007). The surface pressure in the NVT simulations was approximately 18 mN/m for DHDA⁺ monolayers in all subphases and 26 mN/m for DODA⁺, sufficiently close to the surface pressures at which the experimental data were collected (20 mN/m and 25 mN/m). The final pressure for the NVT simulations was approximately 18 mN/m for DHDA⁺ monolayers in all subphases and 26 mN/m for DODA⁺. A snapshot of the simulations setup for DHDA⁺ is Figure 4.4.5. The available area per surfactant $A_{\text{mol}}^{\text{a}}$ in the for the DHDA⁺ was 82 \AA^2 for NaCl, 77 \AA^2 for NaBr and 80 \AA^2 for the equimolar mixture. Because the final surface pressure for all simulations were the same, this result is in line with the experimentally determined isotherms (Fig. 4.4.2), where the monolayer in the bromide subphase has a smaller area per molecule than chloride, and the mixture has an intermediate value. For DODA⁺ the area per surfactant was 57 \AA^2 , in line with an ordered state. It is not possible to directly compare the simulation value with the experimental area per molecule because the simulation salt concentration is not the same as the experimental. For DHDA⁺, the hydrocarbon chain extension in z-direction (average z-projection of the distance vector between the first and last carbon in the alkyl tail) was $11.5 \pm 0.4 \text{ \AA}$ (NaBr subphase), $11.0 \pm 0.4 \text{ \AA}$ (NaCl subphase) and $11.3 \pm 0.3 \text{ \AA}$ (mixed subphase). For DODA⁺ the hydrocarbon chain length was $14.7 \pm 1.5 \text{ \AA}$ for all simulations. These values are similar to the hydrocarbon chain layer thicknesses d_{hc} determined by GIXOS for both systems at similar.

The normalized particle number density distributions for atoms and groups of atoms along the z-axis for the mixed subphase for DHDA⁺ and DODA⁺ are shown in Fig. 4.4.5 B.1 and B.2, respectively. The corresponding electron density profiles are shown in panels C.1 and C.2. The agreement with the experimental data in Fig. 4.4.3 (B and C) is striking. As explained in the experimental section, the peaks observed in the electron density profiles

correspond to the headgroup region, with the electron-rich counterions Cl^- and Br^- , while the shoulder (DHDA^+) and plateau region (DODA^+) at $z \approx 0$ originate from surfactant atoms in the hc layer. In these regions the experimental electron densities (Fig. 4.4.3 B and C) are slightly larger as compared to the simulations which may be because of a lack of ions in this region due to polarization effects not accounted for in the force field. The peak heights for bromide (orange lines) in Fig. 4.4.5 B.1 and B.2 exceed the peak heights for chloride (green lines), in agreement with the experimental data. We however note that the interfacial accumulation of these ions, observed in the simulations, led to a depletion in the "bulk" solution (confined by the two monolayers), where the chloride concentration was somewhat higher than the bromide concentration. This occurred due to the finite size of the simulated system. We therefore corrected the chloride and bromide ion density distributions to achieve equal values in bulk prior to calculating the interfacial bromide/chloride proportion. This proportion was obtained considering only the ions present at the interface up to the Gibbs dividing surface obtained from the water distribution. For DODA^+ , the calculated interfacial Br^-/Cl^- proportion was 78%/22%, while for DHDA^+ it was 82%/18%. These values are very close to the experimental ones determined by TRXF discussed above. The density distributions for some groups along the z axis for the mixed subphase for DHDA^+ and DODA^+ are in Figure 4.4.5 A.1 and B.1, respectively.

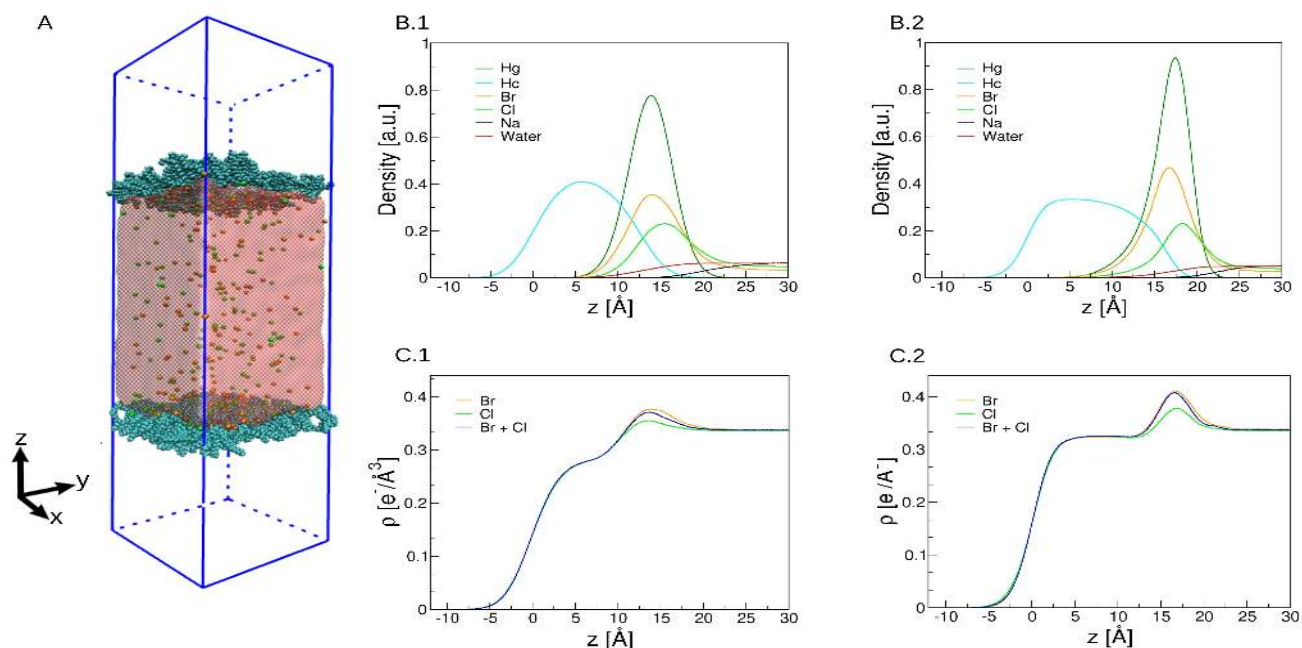


Figure 4.4.5: Snapshot of the simulation box for DHDA⁺ monolayer in mixed subphase (A), normalized particle number density distributions of monolayer components, surfactant head-group (dark green) and surfactant hydrocarbon chain (light blue), ions Br⁻ (orange), Cl⁻ (green) and Na⁺ (black) and water (red) along the z-axis for the mixed subphase for DHDA⁺ (B.1) and DODA⁺ (B.2) and electron density profile of surfactant, ions and water in the all subphases: pure bromide (orange), pure chloride (green) and mixture (blue) for DHDA⁺ (C.1) and for DODA⁺ (C.2).

The preferential interfacial accumulation of Br⁻ over Cl⁻ occurs due to ion specific interactions with the quaternary ammonium head groups. Fig. 4.4.6 shows the anion-nitrogen (quaternary ammonium in DHDA⁺) radial distribution functions for the subphases containing NaCl or NaBr (panel A.1) and for the mixed salt subphase (panel A.2). The peak height (panel A.1) is larger for Br⁻ than for Cl⁻. Therefore, Br⁻ interacts more tightly with the quaternary ammonium head group than Cl⁻. This observation hints at a competitive, or nonadditive, ion effect in the mixed salt system (Bruce et al., 2019; Leontidis et al., 2007; Zhao et al., 2022). It should further be noted that Br⁻ and Cl⁻ both form contact ion pairs with the charged heads groups, i.e. the first peaks of the anion-nitrogen and water-nitrogen radial distribution functions in panels A.1 and A.2 overlap. This direct contact was proposed for micelles

containing alkyl trimethylammonium head groups and bound halide (Br^- and Cl^-) anions (Buchner et al., 2005).

If ranked according to an ion specific (Hofmeister) series, the quaternary ammonium cationic head group classifies as a weakly hydrated cation with a low charge density. As such, it tends to form contact ion pairs with weakly hydrated, low charge-density, anions such as Br^- (but, e.g., also NO_3^- and ClO_4^- : "like seeks like"). The preferred interaction of Br^- over Cl^- with the charged head groups observed herein thus follows this well-established picture (Collins, 2004). The data in panels C.1 and C.2 of Fig. 4.4.6 shows that, upon approaching the charged head group, the weakly hydrated Br^- ion more readily sheds its hydration shell in comparison with Cl^- . Accordingly, Br^- ions approach the plane of the charged headgroups closer. This is shown in Fig. 4.4.6 B.1, which presents the anion number density as a function of the z-component of the anion-nitrogen (quaternary ammonium) distance vector for the subphases containing NaCl or NaBr. Fig. 4.4.6 B.2 shows the corresponding data for the mixed salt subphase. Note that $z > 0$ corresponds to the subphase region; $z < 0$ to the region on the aliphatic-tail side of the surfactant monolayer. Consistent with our observations, it has been experimentally observed that, at the surface of alkyl trimethylammonium micelles, hydration shells of Br^- ions are more perturbed than those of Cl^- ions (Hedin et al., 2000). Furthermore, it has been reported that micelles with Cl^- as counterion are more hydrated than those having Br^- as counterion (Buchner et al., 2005).

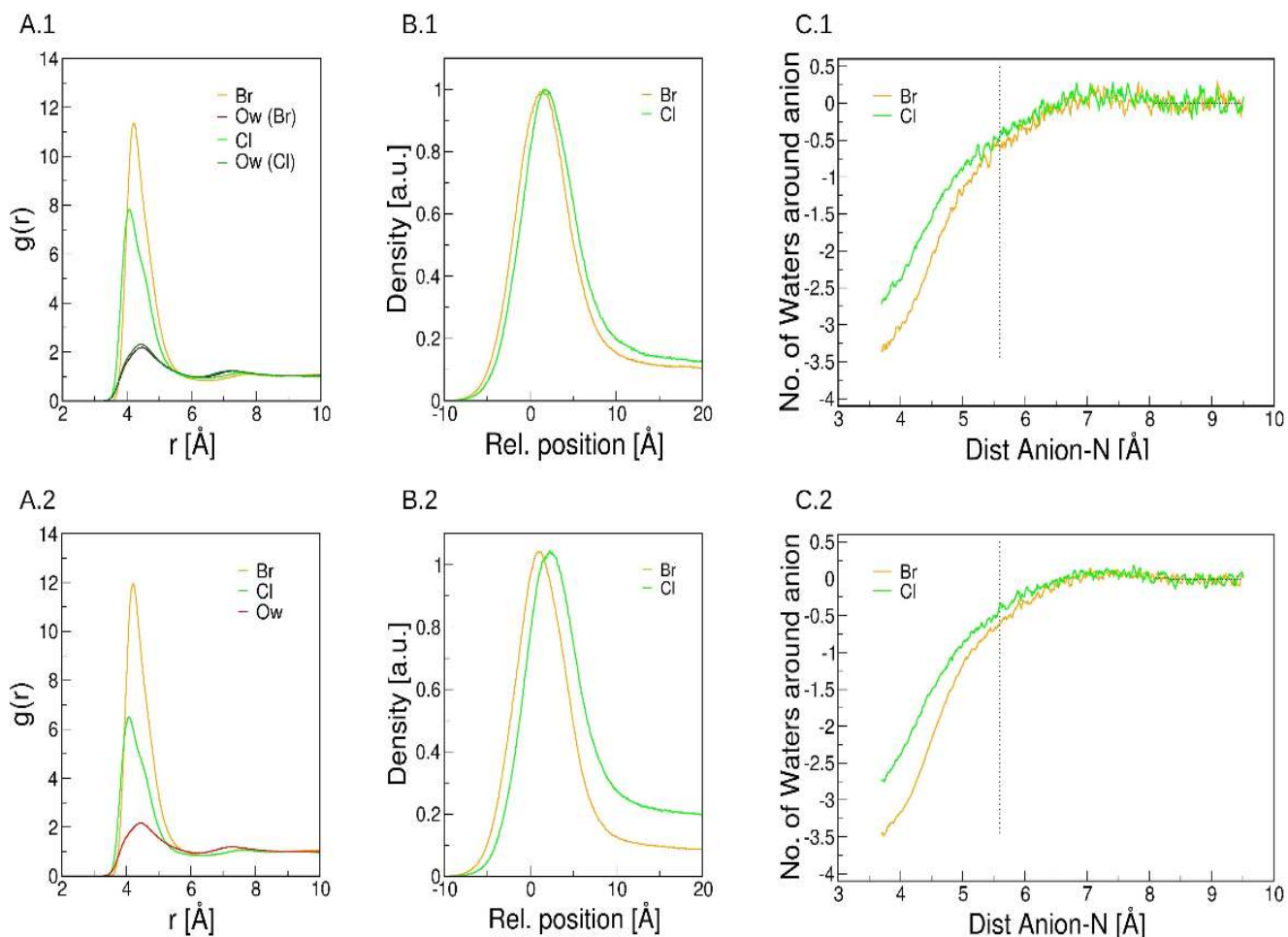


Figure 4.4.6: Interfacial counterion and water distribution for the DHDA⁺ monolayer in contact with pure NaBr or NaCl subphases (1) and the mixed salt subphase (2): Radial distribution function of Cl⁻, Br⁻ and the water oxygen (Ow) relative to the nitrogen atom of the headgroup (A), number density of Br⁻ and Cl⁻ ions in z-direction relative to the headgroup nitrogen atom position (B) and average number of water molecules in the first hydration shell of Br⁻ and Cl⁻ anions as a function of the distance from the nitrogen atom of the surfactant headgroup (C) (the dashed vertical line corresponds to the distance of the first minimum in the anion-N radial distribution function.)

Fig. 4.4.7 shows the cumulative number of positive and negative charges as a function of the z-coordinate perpendicular to the monolayer-solution interface. Comparison of the data for DHDA⁺ (panel A) and DODA⁺ (panel B) shows that the counter ion double layer extends slightly further out into the aqueous sublayer for the monolayer (DHDA⁺) with the lower surface fixed-charge density (higher area per head group). It can also be observed (most notably for the DODA⁺ monolayer) that the diffusive double layer is slightly more contracted

for the system with NaBr compared with NaCl, corroborating the previous analyses which indicated that bromide interacts stronger than chloride with the surfactant head groups).

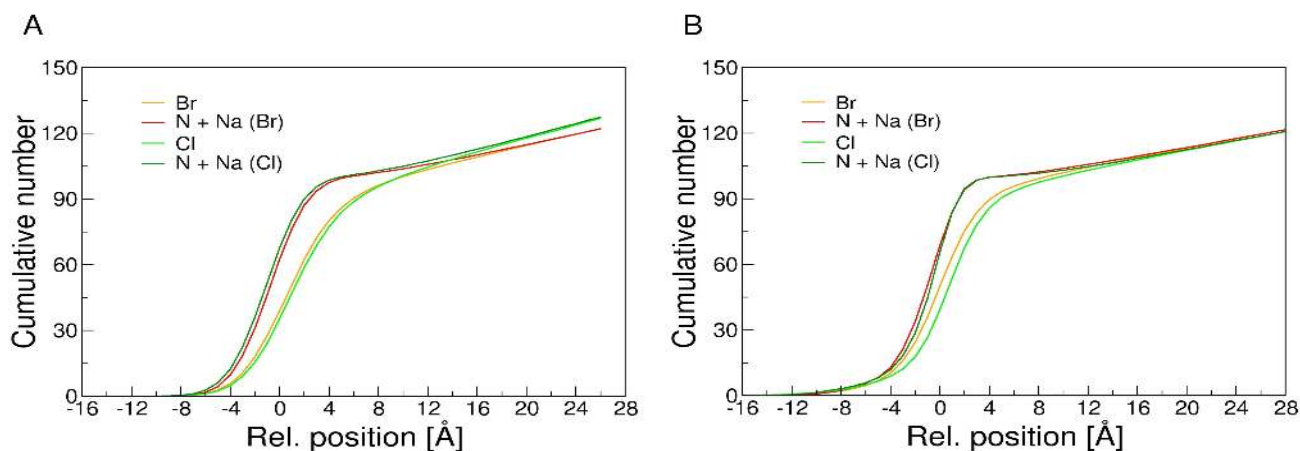


Figure 4.4.7: Cumulative number of charged groups as a function of the z-coordinate: cations (nitrogen of headgroup (N) and Na^+) and anions (Br^- or Cl^-) for (A) DHDA⁺ and (B) DODA⁺, where $z = 0$ corresponds to the plane position at which the surfactant headgroup (nitrogen) density is maximal.

Fig. 4.4.8 shows the lateral organization of charged moieties in the plane of the surfactant head groups for DHDA⁺ (upper panel) and DODA⁺ (lower panel). For DODA⁺, the intermediate-range ($> 5 \text{ \AA}$) lateral correlations between Br^- ions are significantly stronger than between Cl^- ions and are approximately in phase with the oscillations in the in-plane radial distribution of the quaternary ammonium groups. Furthermore, the bromide-bromide lateral correlations are slightly more pronounced for the DODA⁺ monolayer on the mixed salt subphase (panel B.2) compared to the single-salt subphase (panel A.2). For DHDA⁺, these correlations are weaker. Snapshots of a section of the simulation box are shown in panel C.1 for DHDA⁺ and in panel C.2 for DODA⁺. The structures shown in these snapshots represent the experimental situation where, for the chosen pressure, DODA⁺ is in an ordered LC phase whereas DHDA⁺ is in a fluid LE phase. The chain tilt (t) for the DODA⁺ monolayer in the ordered phase was experimentally determined by GIXD (see above) and was also calculated from the MD simulations. On the mixed-salt subphase, the angle formed

between the z-axis and the vector pointing from the surfactant tail to the surfactant head was $40^\circ \pm 5$. This value is very similar to the experimentally determined value (42° for 25 mN/m in pure NaBr).

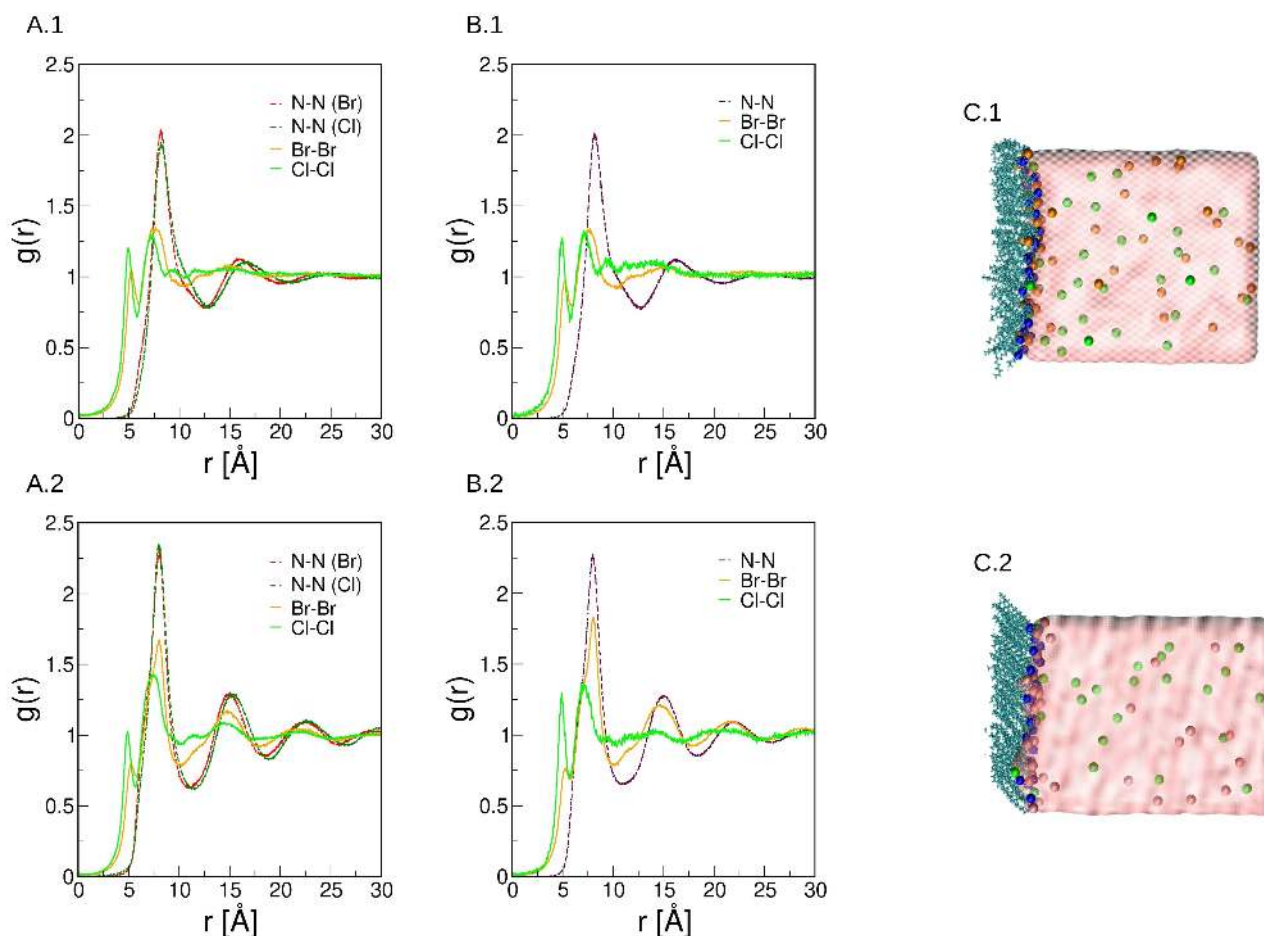


Figure 4.4.8: In plane radial distribution function for the nitrogen of surfactant headgroup (N-N) and anion (Br-Br or Cl-Cl) for simulations of DHDA⁺ (1) and DODA⁺ (2) monolayers in pure NaBr or NaCl subphases (A), or mixed salt subphases (B). Snapshots of box section are in C.

4.4 Conclusions

We successfully determined the preferential interaction of bromide over chloride anions at cationic monolayer interfaces. The monolayers composed of the shorter chain surfactant DHDA⁺ are in liquid expanded phase in all analyzed subphases while the long chain DODA⁺

shows phase transitions LE-LC that is dependent on the subphase. BAM images confirmed the presence of both phases. Analyzing the same area per molecule, the surface pressure for the equimolar subphase isotherms are similar to the surface pressure for bare NaBr in both surfactants, showing already preferential bromide interaction. Using total Reflection X-ray fluoresce we could determine a 80%/20% Br/Cl proportion at the interface of both surfactants, showing that the phase of the surfactant did not matter. This points towards the importance of anion-headgroup specific interaction to determine the preferential adsorption at this system. Scalling the anion force field to reproduce properties like osmotic pressure for the pair anion-head-group led to a good agreements between experiments and molecular dynamics simulations, showing again the importance of specific interaction anion-headgroup in this case. Finally, anion dehydration upon binding to the interface must be considered when interpreting preferential adsorption of ions at soft interfaces.

4.5 Thermotropic phase behavior of imidazolium-based surfactant vesicles

5.1 Introduction

Ionic liquids (IL) are composed of ions with a melting point below 100°C. IL are beneficial as “green solvents” (Lei et al., 2017) and the type of anion and cation of the ionic liquid can be changed to get the desired physical properties such as viscosity, density, melting points (Kaur et al., 2022).

New types of IL have been explored varying the chemical structure of the components. In surface-active ionic liquids (SAILS) ions with long alkyl chains display self-assembling properties (Kaur et al., 2022). SAILS containing imidazolium-based cations as headgroups

(Im-SAIL) exhibit the highest thermal stability and best surface activity (Cao et al., 2020). Compared to the conventional quaternary ammonium surfactants with the same hydrocarbon chain, Im-SAILS show lower Kraft temperatures, lower critical micelle concentrations (cmc), and higher efficiency in reducing the surface tension (Cao et al., 2020). These molecules form micelles in aqueous solutions and can produce unilamellar vesicles at higher concentrations (Wang et al., 2013). Interaction, at room temperature, of ionic liquids (RTIL) with bio-membranes has been explored, and although these molecules can kill bacteria or cancer cells, they also show cytotoxicity (Benedetto, 2017).

Here we synthesized and characterized 1,3-Dihexadecylimidazolium chloride and compared the aggregates formed with the commercially available quaternary ammonium surfactant with the same number of carbons in the hydrocarbon chain. We showed the formation of vesicles in water and low salt concentration. We demonstrated that the gel-liquid crystalline phase transition temperature of the imidazolium surfactant bilayer is higher than that of the comparable quaternary ammonium surfactant.

5.2 Material and Methods

5.2.1 Materials and sample preparation. 1,3-Dihexadecylimidazolium Chloride (DHImC) was synthesized in our laboratory (synthesis, mass spectra and RMN are in Appendix). Dihexadecyldimethylammonium chloride (DHDAC) was prepared by exchanging Br⁻ from Dihexadecyldimethylammonium bromide, DHDAB, (Aldrich) dissolved in methanol through a Dowex 21K anion-exchange resin previously saturated with Cl⁻. The solvent was evaporated at reduced pressure, and DHDAC recrystallized (x2) in methanol/ acetone (90/10; v/v).

Solutions were prepared by weighing the appropriate amount of solid surfactant and adding water or salt until the desired concentration. The suspensions were heated at 60°C in

a water bath, alternated with ultrasonic mixing until obtaining a transparent solution. Some samples were extruded after this procedure, using a heat plate at 55°C and an Avanti Polar Lipids extruder (x21) equipped with a Whatman nucleopore track-etch 100 nm membrane. For EPR experiments, the solid surfactant was dissolved in chloroform, and the EPR labels were also added from a chloroform stock solution to the surfactant. After evaporation of the solvent under N₂, the films were dried under vacuum for at least 2h. These films were resuspended in NaCl 5mM solution and were heated in a 60°C bath. The final concentration of the surfactant was determined by measuring Cl⁻ concentration (Schales and Schales, 1941).

5.2.2 Dynamic Light Scattering (DLS). A Zeta Sizer Nano (Malvern) series was used to determine the size and zeta potential at 25°C for extruded vesicles.

5.2.3 Electron Paramagnetic Resonance (EPR). Measurements were made in a Bruker EMX-200 spectrometer, measured at a frequency of approximately 9.4 GHz, with a sweep width of 100 G, a modulation amplitude of 1.0 G, and a time constant of 0.163 s. Samples were added to flat quartz cells. Spectra were analyzed with WINEPR software (Bruker). Two types of measurements were made. 1. **Encapsulation:** 4-trimethylammonium-2,2,6,6-tetramethylpiperidine-1-oxyl iodide (CAT- Fig. 4.5.1 A) 1.25 and 5 mM NaCl solution were used to hydrate the surfactant solid. Suspensions were extruded as described above. The EPR spectra were measured before and after ascorbic acid (AA) was added to the solution. AA reduces nitroxide (Paleos and Dais, 1977), suppressing the EPR signal. The total intensity of CAT was determined by integrating both spectra, and the residual signal was attributed to the CAT probe encapsulated into the vesicles. Four surfactant concentrations were used (0 mM, 10 mM, 15 mM, and 20 mM). Encapsulated percentages ($\%_{\text{enc}}$) were determined from the ratio $I_{\text{afterAA}}/I_{\text{beforeAA}}$. The volume of the internal aqueous compartments was estimated from the slope of $\%_{\text{enc}}$ vs. surfactant concentration curve. Samples after AA addition were remeasured after 1h at room temperature and then were heated above the main transition temperature and measured a third time. 2. **Spin label:** Methyl X-Doxyl-stearate (X=5 or 16 – Fig. 4.5.1 B and C) were added from chloroform into the lipid films as described above. Spectra were measured at different temperatures using a liquid and gaseous nitrogen temperature control.

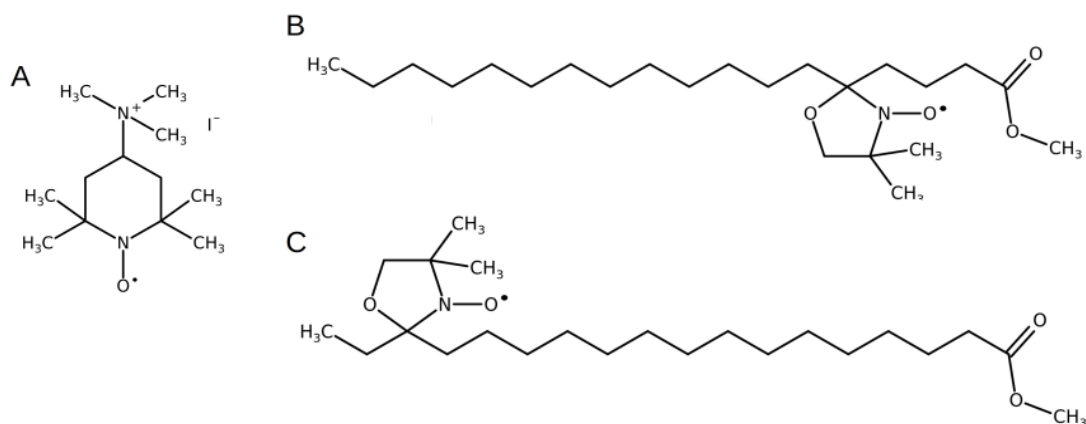


Figure 4.5.1: EPR labels (A) 4-trimethylammonium-2,2,6,6-tetramethylpiperidine-1-oxyl iodide (CAT); (B) Methyl 5-Doxyl-stearate (C) Methyl 16-Doxyl-stearate.

5.2.4 Optical microscopy. Surfactants were diluted in Tris/HCl 10 mM pH 8, and the suspensions were observed with a Zeiss Axiovert 200 inverted microscope equipped with a Zeiss AxioCam Hsm digital camera and a 63 objective. The sample was filmed while being heated using a water-circulating bath system. Silane-coated slides were used.

5.2.5 Differential Scanning Calorimetry (DSC). A VP-DSC, Microcal Inc, was used to collect DSC data for solutions of DHDAC and DHImC at 10 mM from 10°C to 60°C, at a 12°C/h scan rate.

5.2.6 Pressure x area isotherms. Stock solutions prepared at approximately 1mg/mL of surfactant in chloroform. All glass used in the preparation was previously washed with NOCHROMIX. Water with at least 18 M Ω /cm² was used to prepare the NaCl 5 mM solution, which was used as a subphase for the monolayer. A KSV NMA LB (Nima) system with a medium trough size was used in a clean room. The surface tension was measured using a platinum Wilhelmy plate. The temperature was kept at 23°C using a Lauda Thermostat. The surfactant solution (10 μ L) was added at the solution interface (~180 mL), and the solvent was evaporated for at least 10 minutes. The monolayer was compressed at 10mm/min.

5.2.7 Conductivity. The counterion dissociation (α) was measured for extruded vesicles from conductivity data (Carpena et al., 2002). The pre-aggregation inclination was taken from a similar system, cetyltrimethylammonium chloride (CTAC) surfactant, see results section.

5.3 Results

We characterized aggregates formed by 1,3-dihexadecylimidazolium chloride (DHImC) and compared our results with the commercially available dihexadecyldimethylammonium chloride (DHDAC). DHImC and DHDAC contain two alkyl chains of sixteen carbons and are expected to form vesicles in aqueous solutions (Israelachvili et al., 1977). The properties of DHDAC have not been widely explored, but the correspondent bromide salt, DHDAB, forms bilamellar vesicles in water (Tucker et al., 2008). The structures of the two surfactants used in this work are in Figure 4.5.2.

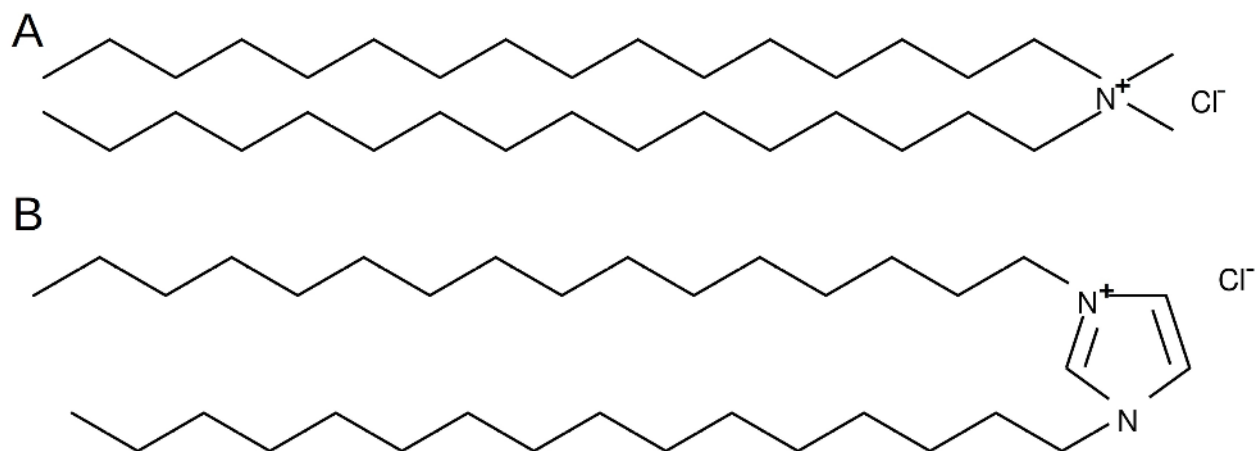


Figure 4.5.2: Structures of (A) dihexadecyldimethylammonium chloride (DHDAC) and (B) 1,3-dihexadecylimidazolium chloride (DHImC).

5.3.1 Aggregate size and surface charge. Following extrusion (see Methods), DHImC and DHDAC formed stable structures of low poly-dispersity (Pdl) and similar Zeta potential (Table 4.5.1). The values of the diameters and Zeta potentials (Table 4.5.1) suggested that the aggregates formed with DHImC and DHDAC were Large Unilamellar Vesicles (LUVs).

Table 4.5.1: Diameter, polydispersity, and zeta potential of DHDAC and DHImC LUVs in water

Sample	Diameter (nm)	Pdl	Zeta (mV)
DHImC	106.5 ± 1.2	0.186 ± 0.010	43.6 ± 4.2
DHDAC	103.2 ± 1.2	0.138 ± 0.011	41.3 ± 4.5

Both surfactants showed a similar Zeta potential value, with a slightly larger value for DHDAC. Zeta potential reflects the degree of counterion ionization, which is known to depend on the aggregate size (Cuccovia et al., 1990).

5.3.2 Monolayer formation by DHDAC and DHImC. DHDAC and DHImC formed Langmuir films in a NaCl 5 mM subphase at the air/water interface, where the isotherms show the variation of pressure (Π) vs. the available area per molecule (A_m^a) (Figure 4.5.3).

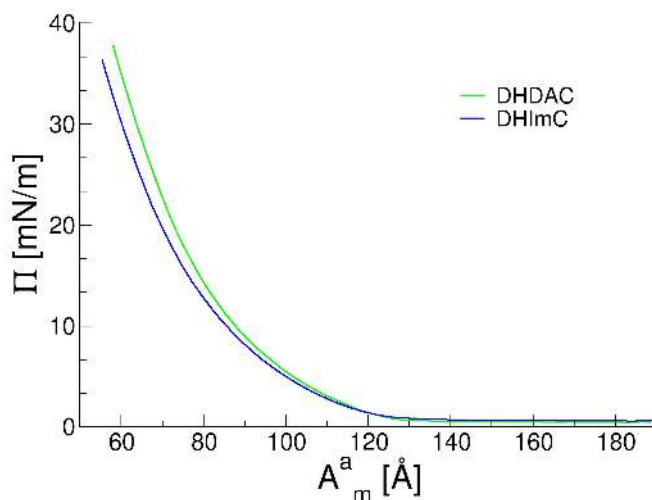


Figure 4.5.3: Pressure-area isotherm for DHDAC and DHImC in 5 mM NaCl

Both surfactants showed a continuous increase of pressure upon compression, with no observable phase transitions. This result is similarly to $C_{15}Ime.HI$ (Wang et al., 2016). The area per monomer at the collapse pressure was ca. 58 \AA^2 for both surfactants.

5.3.3 Demonstration of the formation of closed vesicles. The LUVs were prepared with CAT in solution (see Methods), a percentage of CAT could be encapsulated into the aqueous vesicle compartment if closed LUVs were formed in our preparation. EPR spectra were measured before (Fig. 4.5.4 black lines) and after ascorbic acid addition (Fig. 4.5.4 red lines) to investigate whether closed LUVs formed. As ascorbate reacts rapidly with CAT in solution but penetrates LUVs very slowly (Schreier-Muccillo et al., 1976) any remaining EPR signal after ascorbate addition is related to a closed LUV inner compartment.

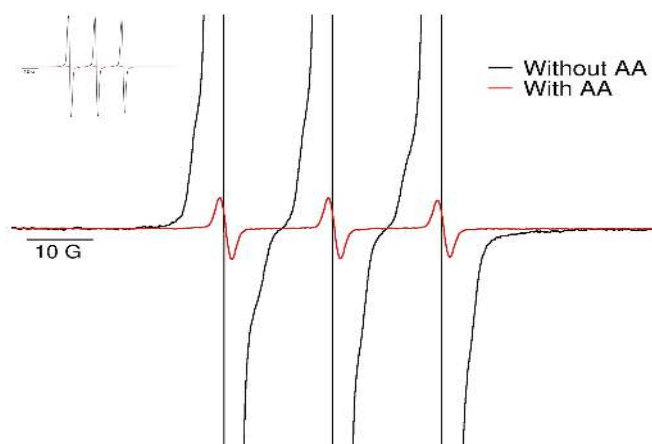


Figure 4.5.4: EPR signal for CAT in SUVs solutions before (black) and after (red) the addition of Ascorbic Acid. In the inset is the full spectra.

After ascorbate addition, a small but evident EPR signal was obtained (Figure 4.5.4). Peak integration permitted calculating the volume encapsulated in the inner aqueous compartment of the LUVs. Linear correlation for encapsulated percentage vs. surfactant concentration was 0.99 for DHDAC and DHImC (plots are Appendix, Figure S11). Assuming an area per molecule of 58 \AA , from the monolayer measurements (see Section 5.3.2) and a diameter of 100 nm (Table 4.5.1) for the extruded vesicles, the encapsulated volume corresponding to

the aqueous inner compartment of the LUVs were 0.13 L/mol for DHDAC and 0.19 L/mol for DHImC. These values lead to an inner radius of 38 and 43 nm, respectively.

One hour after ascorbate addition (Appendix, Fig. S11), the total intensity of CAT diminished, probably due to the slow penetration of ascorbate. As DHDAC and DHImC vesicles were in the gel state at room temperature (see below) heating above the transition temperature led to leakage of CAT (or ascorbate penetration) because of the fluid membrane state and the EPR signals were lost.

5.3.4 Vesicles change shape with increasing temperature. After hydrating the solid surfactant with Tris/HCl 10 mM pH 8 solution, and heating at 60 °C (see Methods), giant vesicles were formed. The sample was filmed while increasing the temperature, and snapshots of vesicles of DHDAC and DHImC are shown in Figure 4.5.5

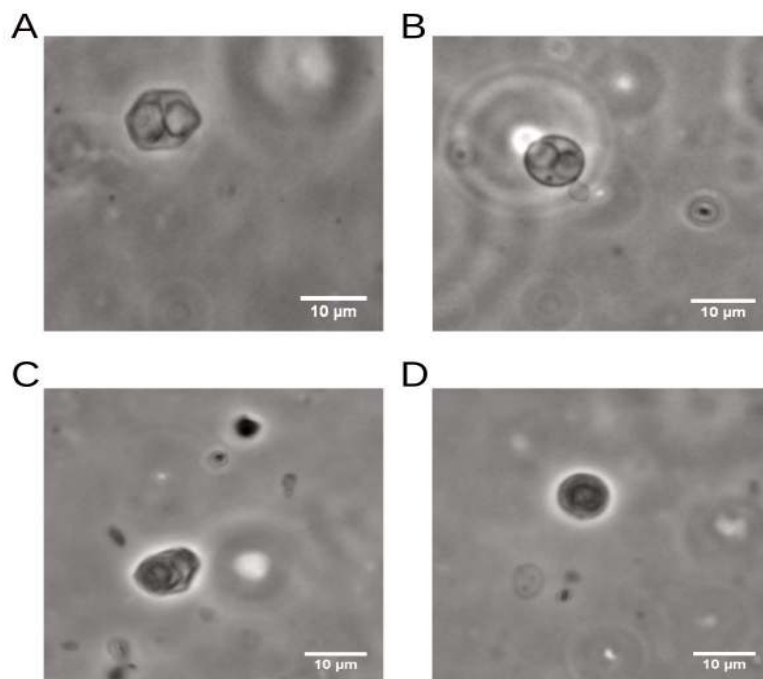


Figure 4.5.5: Snapshots of optical microscopy of DHDAC in Tris/HCl at (A) 20°C and (B) 37°C; and DHImC in Tris/HCl at (C) 40°C and (D) 55°C.

It is possible to observe formation of vesicles for both surfactants. Previous studies on DHImC showed formation of gels for in concentrations above 4.2 wt% (Hu et al., 2015) but the concentration used here was lower, around 0.5 wt%. The vesicles changed shape close to the phase transition temperatures determined by DSC (see below). The images in Figure 4 show that the vesicles are more fluid after the transition temperature, with a rounder shape.

5.3.5 Determination of the phase transition temperature. We used differential scanning calorimetry to determine the phase transition temperatures (T_c) from the gel to the liquid crystalline phase. The values of T_c s for giant vesicles in Tris/HCl (Fig. 4.5.6 A and 4.5.6 B) and LUVs in water (Fig. 4.5.6 C and 4.5.6 D) are summarized in Table 4.5.2.

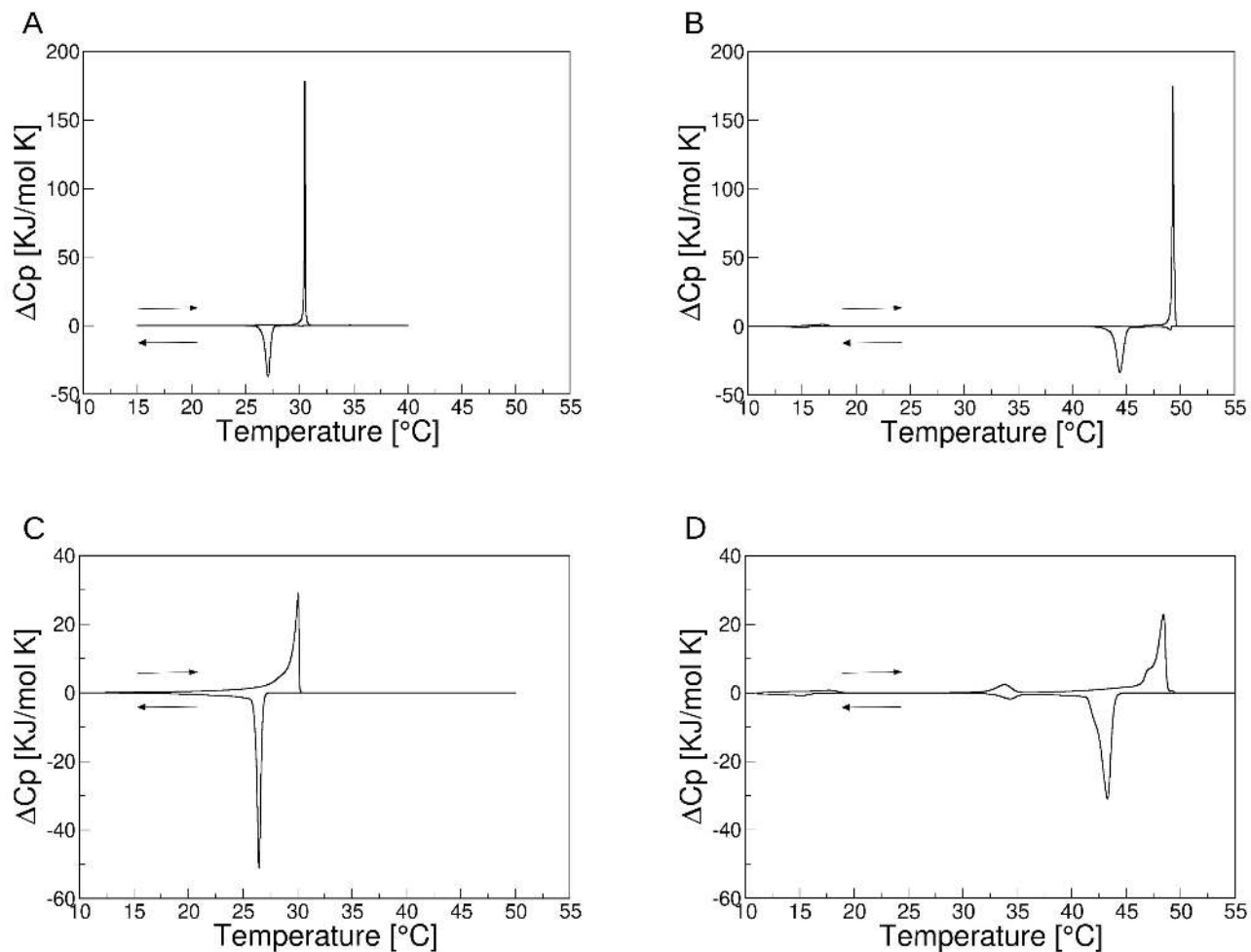


Figure 4.5.6: Thermograms for (A) DHDAC non-extruded in Tris/HCl 10 mM, pH 8 (B) DHImC non-extruded in Tris/HCl 10 mM, pH 8 (C) DHDAC extruded and (D) DHImC extruded in water.

Table 4.5.2: Transition temperature and Enthalpies from DSC data for DHDAC and DHImC in both media

Media	Tris/HCl			Water (extruded)		
Surfactant	T_m [°C]	$T_{1/2}$ [°C]	ΔH [KJ/mol]	T_m [°C]	$T_{1/2}$ [°C]	ΔH [KJ/mol]
DHDAC	30.5	0.1	24.3	30.1	0.5	30.4
DHImC	49.3	0.1	38.3	48.5	0.6	41.4

Although the hydrocarbon tail length for both surfactants was the same, T_c 's were significantly different, probably because of head group interactions. Downscan temperatures in Tris/HCl were 43.2 °C for DHImC and 27.1 °C for DHDAC, respectively.

For a similar SAIL, 1,3- dimethyl-4,5-dipentadecylimidazolium iodide (C15IMe.HI), the DSC scan showed two transition peaks: one at 29.3 and another at 32.5°C, although they were not assigned to phase transitions (Wang et al., 2016).

This difference in transition temperature can probably be related to the structure of the imidazolium headgroup, which shows a higher tendency for hydrogen bonding (Dong et al., 2006) compared to the quaternary ammonium cation (Luczak et al., 2009).

5.3.6 Bilayer structure and temperature effects. We obtained information on the bilayer structure using the spin labels spectra of Methyl X-Doxyl-stearate, with X = 5 or 16. Due to their hydrocarbon chain, these molecules can intercalate in the surfactant bilayer, and their dynamics reflect the environment in which they are inserted (Schreier et al., 1978). Spectra were measured in three temperatures: room temperature ($22^\circ\text{C} \pm 2$), 10°C below the transition temperature (20°C for DHDAC and 40°C for DHImC), and 10°C above the transition temperature (40°C for DHDAC and 60°C for DHImC). For comparison, the spectra before and after transition temperature are in Figure 4.5.7.

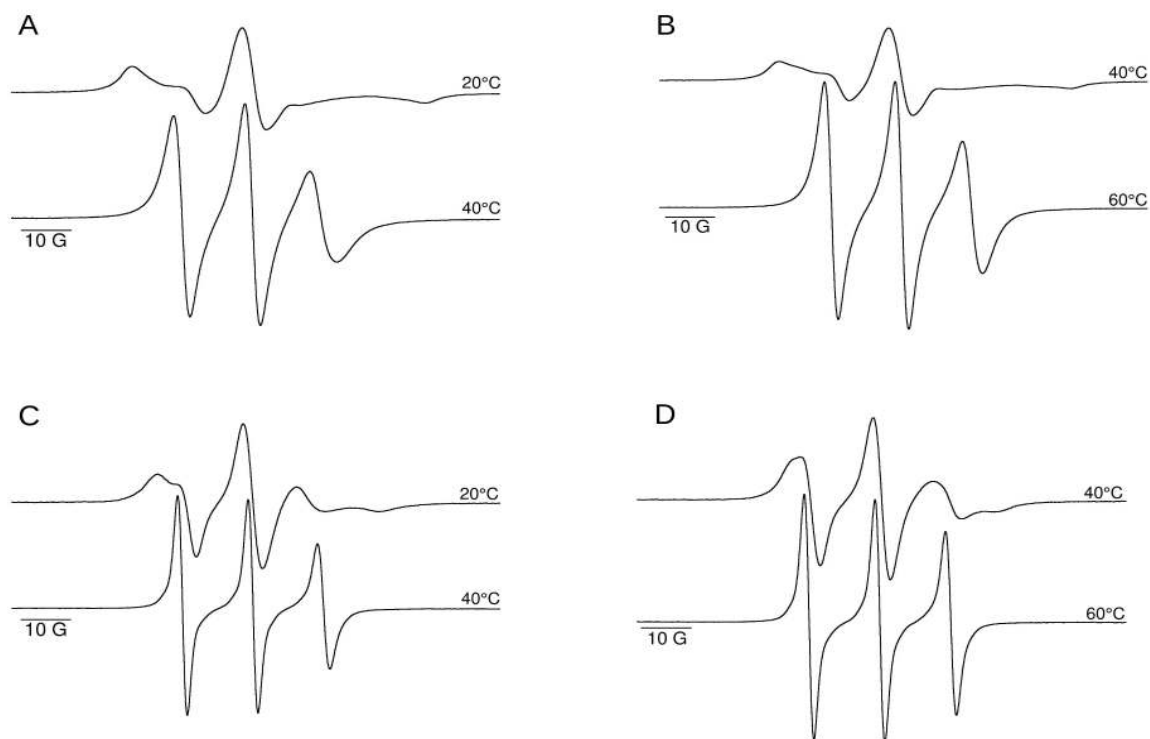


Figure 4.5.7: EPR spectra for (A) 5-MeSL in DHDAC (B) 5-MeSL in DHImC (C) 16-MeSL in DHDAC and (D) 16-MeSL in DHImC.

We calculated label mobility using the ratio of the amplitudes at the low field and central line ($h+1/h_0$) (Table 3). The order parameter decreases towards the terminal methyl group in both model and biological membranes (Schreier et al., 1978), as seen here through the higher mobility of the spin label 16-MeSL compared to 5-MeSL. The transition from a more ordered phase (gel) to a fluid phase (liquid crystalline) can also be appreciated from the $h+1/h_0$ ratio at different temperatures. Both surfactants show very similar ratios below and above the T_c .

Table 4.5.3: Ratio of the amplitudes of the low and central field lines (h+1/h0)

Condition	Label	DHDAC	DHImC
Room temperature	5-MeSL	0.43	0.47
	16-MeSL	0.59	0.56
Pre-transition temperature	5-MeSL	0.46	0.45
	16-MeSL	0.57	0.67
Pos-transition temperature	5-MeSL	0.91	0.96
	16-MeSL	1.00	1.01

5.3.7 Counterion dissociation from DHDAC and DHImC vesicles. The degree of counterion dissociation (α) was determined for both vesicles with Equation 4.5.1.

$$\alpha = \frac{\left(\frac{d\lambda}{dc}\right)_{agg}}{\left(\frac{d\lambda}{dc}\right)_{mon}} \quad (4.5.1)$$

Where $(d\lambda/dc)_{agg}$ is the slope of conductance vs total surfactant above the critical aggregate concentration and $(d\lambda/dc)_{mon}$ is the slope before the critical aggregate concentration (Carpena et al., 2002).

The critical aggregation concentration (cac) for surfactants with two long hydrocarbon tails is expected to be very low (Tucker et al., 2008). Thus we used the hexadecyltrimethyl ammonium chloride (CTAC) pre-aggregation slope. And because approximately half of the surfactants are on the inner core of the vesicle, the concentration was divided by 2. With those approximations, the values of α were 0.10 +/-0.01 for DHDAC e 0.14 +/-0.01 for DHImC. The values of α were lower than those for single tailed surfactants with comparable headgroups, where α is 0.42 (Sarac et al., 2017), 0.45 (Jungnickel et al., 2008) for 1-

hexadecyl-3-methylimidazolium chloride and 0.32 (Maximiano et al., 2006), 0.38 (Zhang et al., 2017) for hexadecyltrimethylammonium chloride.

5.4 Conclusion

We showed the formation of vesicles composed of DHImC. The thermotropic phase behavior of these vesicles was studied using EPR, DSC and optical microscopy and the results were compared to another vesicle composed of an analog quaternary ammonium surfactant. Vesicles formed by DHImC had very similar pressure vs area behaviour, and very similar degree of counterion ionization, but a higher transition temperature of 49°C, compared to 30°C for DHDAC.

5 Conclusions

This thesis evaluated the specific anion effect on zwitterionic aggregates with sulfobetaine as the headgroup, focusing on hydrotrope anions, determined experimentally and by molecular dynamics the relative binding of chloride and bromide to positively charged surfactant monolayers, evaluated the effect of salts on the micellization thermodynamics and demonstrated the formation of vesicle-like aggregates with a new imidazolium-based double-tailed surfactant.

In the first chapter, we showed that the overall micelle hydration, as estimated using dielectric relaxation spectroscopy, is not anion specific. The addition of salt did not change the hydration number of the micelle. However, it slowed the water molecules near the surfactant by simultaneous interaction between water and surfactant/ions. This result is very different from the obtained for cationic micelles (DTA⁺), where the interfacial concentration of counterions is large, and the micelle is severely dehydrated (Lima et al., 2013b). The difference between positively charged and zwitterionic micelles is not surprising since, differently from DTATf, the aggregation number of DPS micelles did not significantly increase upon salt addition (Lima et al., 2013a). In this study, we saw a significant effect on the critical micelle concentration (cmc). However, I want to note that the salt ratio used in the DRS experiments (0.15 M DPS and 0.125 M NaX) was much lower compared to the ratio used at the cmc, where the salt concentrations were the same, but DPS concentration was very low, close to the cmc (~ 4 mM). On the other hand, a recent study showed that the aggregation numbers for a similar sulfobetaine surfactant (with 16 carbons in the tail instead of 12) increase very moderately even at very high NaClO₄ concentrations (Patiño-Agudelo and Quina, 2022). Perchlorate anion interacts strongly at the sulfobetaine interface (Gerola et al., 2017b).

Molecular Dynamics simulations were used to model the DPS micelles in the different salts solutions. In the first chapter, we showed that MD results were similar to experimental ones (Mortara et al., 2018). In the second chapter, we looked deeper at the simulations with exciting results. We saw that anion like triflate, benzoate, benzenesulfonate, and perchlorate have a high interfacial concentration in DPS, although they do not significantly affect the orientation of the head group dipole (Mortara et al., 2020). When these salts are present, a closer look into the number of hydration waters for carbons close to the micellar core is smaller than for the bare micelle or other salts like bromide. However, the headgroup hydration is more extensive, explaining why the overall hydration is the same.

Also, in the second chapter, we showed that the degree of dehydration of the hydrophobic moieties of hydrotropic anions can be correlated to the interfacial concentration. This result is similar to that obtained for cationic micelles (Lima et al., 2017).

In the next chapter, we evaluated the influence of salts on the thermodynamics of micelle formation. As pointed out above, the studied salt/DPS ratios in this study were much higher than for the first two chapters, which explains the much higher effect observed. Cmc order was NaAc ~ NaMs ~ NaCl > NaBr > NaTFA > NaBZO > NaBZS > NaTf > NaClO₄. In the previous chapter NaBZS and NaBZO showed a higher degree of counterion binding than NaTf. However, the overall effect on the micelle (like head group dipole orientation) was slightly higher for NaTf. We do not exclude the possibility of a problem in the anions force field. However, the trend remains very similar, and the theoretical result established in the second chapter remains valid.

The evaluation of the thermodynamics of micellization also showed an exciting difference in the entropic component between triflate and perchlorate. Although both anions showed a similar cmc- that can be correlated to the free energy of micellization-, the enthalpy

was very different, resulting in a lower entropic contribution for perchlorate in the micellization. The origin of this difference has yet to be directly explained.

In the following chapter, we studied cationic surfactants with two alkyl chains that, due to the packing parameter (Israelachvili et al., 1977), should form vesicles in aqueous solutions.

In the fourth chapter, monolayers of DHDA⁺ and DODA⁺ were studied, and the preferential interaction between bromide and chloride was evaluated. We quantified an interfacial concentration of 80%/20% for Br⁻/Cl⁻ at an equimolar concentration in the solution. The bromide interaction also led to a more packed bilayer than chloride. MD studies on this system reproduced the preferential interaction, and interestingly this was done by tuning the polar head group interaction based on the osmotic coefficient of the tetramethylammonium salts.

Lastly, an imidazolium-based surfactant was characterized and compared to a similar well-studied ammonium quaternary. We observed a similar degree of counterion (Cl⁻) association at the interface, but a very different main transition temperature, from gel to liquid crystalline. This difference was explained based on the headgroup interactions, where the imidazolium headgroup can form hydrogen bonds.

The experimental and MD results obtained here contribute to specific ion effects: For the zwitterionic DPS, macroscopic properties like micelle hydration number and aggregation number do not show much specificity, but we could show that micellization captures the anion-specific interaction. For cationic monolayers, we showed that bromides bind more strongly than chloride at the interface, and ion-head group pairing was significant in the model. The aggregate formation of imidazolium-based surfactant was also shown.

6 References

- Abezgauz L, Kuperkar K, Hassan PA, Ramon O, Bahadur P, Danino D. Effect of Hofmeister anions on micellization and micellar growth of the surfactant cetylpyridinium chloride. *J Colloid Interface Sci* 2010;342:83–92. <https://doi.org/10.1016/j.jcis.2009.08.045>.
- Abraham MJ, Murtola T, Schulz R, Páll S, Smith JC, Hess B, et al. Gromacs: High performance molecular simulations through multi-level parallelism from laptops to supercomputers. *SoftwareX* 2015;1–2:19–25. <https://doi.org/10.1016/j.softx.2015.06.001>.
- Ahuja RC, Caruso PL, Möbius D. Counterion specific interactions in dioctadecyldimethylammonium bromide monolayers at the monolayer/subphase interface. *Thin Solid Films* 1994;242:195–200. [https://doi.org/10.1016/0040-6090\(94\)90529-0](https://doi.org/10.1016/0040-6090(94)90529-0).
- Alargova RG, Kochijashky II, Sierra ML, Zana R. Micelle Aggregation Numbers of Surfactants in Aqueous Solutions: A Comparison between the Results from Steady-State and Time-Resolved Fluorescence Quenching. *Langmuir* 1998;14:5412–8. <https://doi.org/10.1021/la980565x>.
- Aroti A, Leontidis E, Dubois M, Zemb T, Brezesinski G. Monolayers, bilayers and micelles of zwitterionic lipids as model systems for the study of specific anion effects. *Colloids Surf Physicochem Eng Asp* 2007;303:144–58. <https://doi.org/10.1016/j.colsurfa.2007.03.011>.
- Baar C, Buchner R, Kunz W. Dielectric relaxation of cationic surfactants in aqueous solution. 2. Solute relaxation. *J Phys Chem B* 2001;105:2914–22. <https://doi.org/10.1021/jp004450p>.
- Baptista M da S, Cuccovia I, Chaimovich H, Politi MJ, Reed WF. Electrostatic properties of zwitterionic micelles. *J Phys Chem* 1992;96:6442–9. <https://doi.org/10.1021/j100194a063>.
- Bayly CI, Cieplak P, Cornell WD, Kollman PA. A well-behaved electrostatic potential based method using charge restraints for deriving atomic charges: The RESP model. *J Phys Chem* 1993;97:10269–80. <https://doi.org/10.1021/j100142a004>.
- Bearden JA. X-ray wavelengths. *Rev Mod Phys* 1967;39:78–124. <https://doi.org/10.1088/0031-9120/5/2/001>.
- Beber RC, Bunton C, Savelli G, Nome F. Incorporation and differential reactivity of anions in zwitterionic sulfobetaine micelles. *Prog Colloid Polym Sci* 2004;128:249–54. <https://doi.org/10.1007/b97097>.
- Benedetto A. Room-temperature ionic liquids meet bio-membranes: the state-of-the-art. *Biophys Rev* 2017;9:309–20. <https://doi.org/10.1007/s12551-017-0279-1>.
- Ben-Naim A. Statistical Mechanics of “Waterlike” Particles in Two Dimensions. I. Physical Model and Application of the Percus–Yevick Equation. *J Chem Phys* 1971;54:3682–95. <https://doi.org/10.1063/1.1675414>.
- Benraou M, Bales BL, Zana R. Effect of the nature of the counterion on the properties of anionic surfactants. 1. Cmc, ionization degree at the Cmc and aggregation number of micelles of sodium, cesium, tetramethylammonium, tetraethylammonium, tetrapropylammonium, and tetrabutylammonium. *J Phys Chem B* 2003;107:13432–40. <https://doi.org/10.1021/jp021714u>.
- Berendsen HJC, Grigera JR, Straatsma TP. The missing term in effective pair potentials. *J Phys Chem* 1987;91:6269–71. <https://doi.org/10.1021/j100308a038>.
- Bergström PÅ, Lindgren J. An infrared spectroscopic study of the hydration of the triflate ion (CF₃SO₃⁻) in aqueous solution. *J Mol Struct* 1990;239:103–11. [https://doi.org/10.1016/0022-2860\(90\)80205-X](https://doi.org/10.1016/0022-2860(90)80205-X).
- Bernhardt MP, Nagata Y, Van Der Vegt NFA. Where Lennard-Jones Potentials Fail: Iterative Optimization of Ion-Water Pair Potentials Based on Ab Initio Molecular Dynamics Data. *J Phys Chem Lett* 2022;13:3712–7. <https://doi.org/10.1021/acs.jpcllett.2c00121>.
- Bhattacharjee S, Chen J, Landers J, Baker JR. Zwitterionic Surfactant as a Promising Non-Cytotoxic Carrier for Nanoemulsion-Based Vaccine Development. *ChemistrySelect* 2019;4:9027–32. <https://doi.org/10.1002/slct.201902737>.
- Bijma K, Engberts JBFN. Effect of Counterions on Properties of Micelles Formed by Alkylpyridinium Surfactants. 1. Conductometry and ¹H-NMR Chemical Shifts. *Langmuir* 1997;13:4843–9.
- Bostrom M, Williams DRM, Ninham BW. Ion Specificity of Micelles Explained by Ionic Dispersion Forces 2002:6010–4. <https://doi.org/10.1021/la0201220>.

- Brandes E, Stage C, Motschmann H, Rieder J, Buchner R. Is surface layering of aqueous alkali halides determined by ion pairing in the bulk solution? *J Chem Phys* 2017;141.
- Brezesinski G, Schneck E. Investigating Ions at Amphiphilic Monolayers with X-ray Fluorescence. *Langmuir* 2019;35:8531–42. <https://doi.org/10.1021/acs.langmuir.9b00191>.
- Brinatti C, Mello LB, Loh W. Thermodynamic study of the micellization of zwitterionic surfactants and their interaction with polymers in water by isothermal titration calorimetry. *Langmuir* 2014;30:6002–10. <https://doi.org/10.1021/la5012346>.
- Bruce CD, Berkowitz ML, Perera L, Forbes MDE. Molecular dynamics simulation of sodium dodecyl sulfate micelle in water: Micellar structural characteristics and counterion distribution. *J Phys Chem B* 2002;106:3788–93. <https://doi.org/10.1021/jp013616z>.
- Bruce EE, Bui PT, Rogers BA, Cremer PS, Van Der Vegt NFA. Nonadditive Ion Effects Drive Both Collapse and Swelling of Thermoresponsive Polymers in Water. *J Am Chem Soc* 2019;141:6609–16. <https://doi.org/10.1021/jacs.9b00295>.
- Buchner R, Baar C, Fernandez P, Schrödle S, Kunz W. Dielectric spectroscopy of micelle hydration and dynamics in aqueous ionic surfactant solutions. *J Mol Liq* 2005;118:179–87. <https://doi.org/10.1016/j.molliq.2004.07.035>.
- Buchner R, Hefter G. Interactions and dynamics in electrolyte solutions by dielectric spectroscopy. *Phys Chem Chem Phys* 2009;11:8984–99. <https://doi.org/10.1039/b906555p>.
- Buchner R, Hölzl C, Stauber J, Barthel J. Dielectric spectroscopy of ion-pairing and hydration in aqueous tetra-n-alkylammonium halide solutions. *Phys Chem Chem Phys* 2002;4:2169–79. <https://doi.org/10.1039/b110361j>.
- Bussi G, Donadio D, Parrinello M. Canonical sampling through velocity rescaling. *J Chem Phys* 2007;126. <https://doi.org/10.1063/1.2408420>.
- Cao H, Hu Y, Xu W, Wang Y, Guo X. Recent progress in the assembly behavior of imidazolium-based ionic liquid surfactants. *J Mol Liq* 2020;319:114354. <https://doi.org/10.1016/j.molliq.2020.114354>.
- Carpena P, Aguiar J, Bernaola-Galvan P, Carnero Ruiz C. Problems Associated with the Treatment of Conductivity-Concentration Data in Surfactant Solutions: Simulations and Experiments. *Langmuir* 2002;18:6054–8. <https://doi.org/10.1021/la025770y>.
- Case DA, Aktulga HM, Belfon K, Ben-Shalom IY, Brozell SR, Cerutti DS, et al. AmberTools21 2021.
- Cavalli A, Dynarowicz-Latka P, Oliveira ON, Feitosa E. Using an effective surface charge to explain surface potentials of Langmuir monolayers from dialkyldimethylammonium halides with the Gouy-Chapman theory. *Chem Phys Lett* 2001;338:88–94. [https://doi.org/10.1016/S0009-2614\(01\)00272-X](https://doi.org/10.1016/S0009-2614(01)00272-X).
- Cavell EAS, Knight PC, Sheikh MA. Dielectric relaxation in non aqueous solutions. Part 2. - Solutions of tri(n-butyl)ammonium picrate and iodide in polar solvents. *Trans Faraday Soc* 1971;67:2225–33. <https://doi.org/10.1039/TF9716702225>.
- Chandler D. Interfaces and the driving force of hydrophobic assembly. *Nature* 2005;437:640–7. <https://doi.org/10.1038/nature04162>.
- Chapman D, Urbina J, Keough KM. Biomembrane Phase Transitions. *J Biol Chem* 1974;249:2512–21. [https://doi.org/10.1016/S0021-9258\(19\)42760-9](https://doi.org/10.1016/S0021-9258(19)42760-9).
- Cheng CJ, Qu GM, Wei JJ, Yu T, Ding W. Thermodynamics of micellization of sulfobetaine surfactants in aqueous solution. *J Surfactants Deterg* 2012;15:757–63. <https://doi.org/10.1007/s11743-012-1374-8>.
- Collins KD. Ions from the Hofmeister series and osmolytes: effects on proteins in solution and in the crystallization process. *Methods* 2004;34:300–11. <https://doi.org/10.1016/j.ymeth.2004.03.021>.
- Corrin ML, Harkins WD. The Effect of Salt on the Critical Concentration for the Formation of Micelles in Colloidal Electrolytes. *J Am Chem Soc* 1947;69:683–8. <https://doi.org/10.1021/ja01195a065>.
- Cuccovia IM, Chaimovich H, Lissi E, Abuin E. Selectivity Coefficients for Iodide/Bromide and Iodide/Chloride Counterion Exchanges at the Surfaces of Dioctadecyldimethylammonium Vesicles. *Langmuir* 1990;6:1601–4. <https://doi.org/10.1021/la00100a013>.
- Darden T, York D, Pedersen L. Particle mesh Ewald: An $N \cdot \log(N)$ method for Ewald sums in large systems. *J Chem Phys* 1993;98:10089–92. <https://doi.org/10.1063/1.464397>.

- De Neve L, Vermeir L, Sabatino P, Saveyn P, Denon Q, Martins J, et al. Quantification of counterion binding to and its effects on aqueous dispersions of dialkyl cationic surfactants. *Colloids Surf Physicochem Eng Asp* 2017;532:458–63. <https://doi.org/10.1016/j.colsurfa.2017.04.031>.
- Dickson CJ, Rosso L, Betz RM, Walker RC, Gould IR. GAFFlipid: A General Amber Force Field for the accurate molecular dynamics simulation of phospholipid. *Soft Matter* 2012;8:9617–27. <https://doi.org/10.1039/c2sm26007g>.
- Dong K, Zhang S, Wang D, Yao X. Hydrogen bonds in imidazolium ionic liquids. *J Phys Chem A* 2006;110:9775–82. <https://doi.org/10.1021/jp054054c>.
- Drinkel E, Souza FD, Fiedler HD, Nome F. The chameleon effect in zwitterionic micelles: Binding of anions and cations and use as nanoparticle stabilizing agents. *Curr Opin Colloid Interface Sci* 2013;18:26–34. <https://doi.org/10.1016/j.cocis.2013.01.001>.
- Dutt S, Siril PF, Remita S. Swollen liquid crystals (SLCs): a versatile template for the synthesis of nano structured materials. *RSC Adv* 2017;7:5733–50. <https://doi.org/10.1039/C6RA26390A>.
- Eeman M, Deleu M. From biological membranes to biomimetic model membranes. *Biotechnol Agron Soc Environ* 2010;14:719–36.
- Eiberweiser A, Buchner R. Ion-pair or ion-cloud relaxation? on the origin of small-amplitude low-frequency relaxations of weakly associating aqueous electrolytes. *J Mol Liq* 2012;176:52–9. <https://doi.org/10.1016/j.molliq.2012.03.025>.
- Eiberweiser A, Nazet A, Hefter G, Buchner R. Ion hydration and association in aqueous potassium phosphate solutions. *J Phys Chem B* 2015;119:5270–81. <https://doi.org/10.1021/acs.jpcc.5b01417>.
- El Seoud OA, Blasko A, Bunton CA. Proton NMR studies on the structure of water at interfaces of aqueous micelles. Part 4: effects of cationic and zwitterionic headgroups. *Berichte Bunsen-Ges Fuer Phys Chem* 1995;99:1214–20.
- Evans DF, Mitchell DJ, Ninham W. Ion Binding and Dressed Micelles. *J Phys Chem* 1984;88:6344–8. <https://doi.org/10.1021/j150669a057>.
- Fabre H, Kamenka N, Khan A, Lindblom G, Lindman B, Tiddy GJT. Self-diffusion and NMR studies of chloride and bromide ion binding in aqueous hexadecyltrimethylammonium salt solutions. *J Phys Chem* 1980;84:3428–33. <https://doi.org/10.1021/j100462a023>.
- Feitosa E, Alves FR. The role of counterion on the thermotropic phase behavior of DODAB and DODAC vesicles. *Chem Phys Lipids* 2008;156:13–6. <https://doi.org/10.1016/j.chemphyslip.2008.08.001>.
- Fendler J. *Membrane Mimetic Membrane Chemistry: Characterization and Applications of Micelles, Microemulsions, Monolayers, Bilayers, Vesicles, Host-Guests Systems, and Polyions*. N.Y.: Wiley; 1982.
- Florenzano FH, Dias LG. Critical Micelle Concentration and Average Aggregation Number Estimate of Zwitterionic Amphiphiles: Salt Effect. *Langmuir* 1997;13:5756–8. <https://doi.org/10.1021/la970176n>.
- Frank HS, Evans MW. Free volume and entropy in condensed systems III. Entropy in binary liquid mixtures; Partial molal entropy in dilute solutions; Structure and thermodynamics in aqueous electrolytes. *J Chem Phys* 1945;13:507–32. <https://doi.org/10.1063/1.1723985>.
- Friesen S, Buchecker T, Cognigni A, Bica K, Buchner R. Hydration and Counterion Binding of [C12MIM] Micelles. *Langmuir* 2017;33:9844–56. <https://doi.org/10.1021/acs.langmuir.7b02201>.
- Frisch MJ, Trucks GW, Schlegel HB, Scuseria GE, Robb MA, Cheeseman JR, et al. *Gaussian 09, Revision D.01* 2016:Gaussian, Inc., Wallingford CT.
- Fukasawa T, Sato T, Watanabe J, Hama Y, Kunz W, Buchner R. Relation between dielectric and low-frequency Raman spectra of hydrogen-bond liquids. *Phys Rev Lett* 2005;95:1–4. <https://doi.org/10.1103/PhysRevLett.95.197802>.
- Fyta M, Netz RR. Ionic force field optimization based on single-ion and ion-pair solvation properties: Going beyond standard mixing rules. *J Chem Phys* 2012;136. <https://doi.org/10.1063/1.3693330>.
- Gallagher KR, Sharp KA. A New Angle on Heat Capacity Changes in Hydrophobic Solvation. *J Am Chem Soc* 2003;125:9853–60. <https://doi.org/10.1021/ja029796n>.

- Gamboa C, Sepúlveda L. High Viscosities of Cationic and Anionic Micellar Solutions in the Presence of Added Salts. *J Colloid Interface Sci* 1986;113:566–76.
- Geng Y, Romsted LS, Froehner S, Zanette D, Magid LJ, Cuccovia IM, et al. Origin of the Sphere-to-Rod Transition in Cationic Micelles with Aromatic Counterion

- Jackson AJ, Li ZX, Thomas RK, Penfold J. The structures of micelles of alkytrimethylammonium perfluorocarboxylates and of their adsorbed layers at the air/water interface. *Phys Chem Chem Phys* 2002;4:3022–31. <https://doi.org/10.1039/b201562p>.
- Jämbeck JPM, Lyubartsev AP. Derivation and systematic validation of a refined all-atom force field for phosphatidylcholine lipids. *J Phys Chem B* 2012;116:3164–79. <https://doi.org/10.1021/jp212503e>.
- Joung IS, Cheatham TE. Determination of alkali and halide monovalent ion parameters for use in explicitly solvated biomolecular simulations. *J Phys Chem B* 2008;112:9020–41. <https://doi.org/10.1021/jp8001614>.
- Jungnickel C, Luczak J, Ranke J, Fernández JF, Müller A, Thöming J. Micelle formation of imidazolium ionic liquids in aqueous solution. *Colloids Surf Physicochem Eng Asp* 2008;316:278–84. <https://doi.org/10.1016/j.colsurfa.2007.09.020>.
- Kaur R, Kumar H, Singla M. Micellization studies of selected imidazolium based ionic liquid in aqueous solution and in presence of different additives: A review. *J Ion Liq* 2022;2:100036. <https://doi.org/10.1016/j.jil.2022.100036>.
- Kauzmann W. Some Factors in the Interpretation of Protein Denaturation. *Adv Protein Chem* 1959;14:1–63. [https://doi.org/10.1016/S0065-3233\(08\)60608-7](https://doi.org/10.1016/S0065-3233(08)60608-7).
- Király Z, Dekány I. A thermometric titration study on the micelle formation of sodium decyl sulfate in water. *J Colloid Interface Sci* 2001;242:214–9. <https://doi.org/10.1006/jcis.2001.7777>.
- Klockenkamper R, Knoth J, Prange A, Schwenke H. Fluorescence Spectroscopy Total-Reflection X-Ray. *Anal Chem* 1992;64:1115A-1123A.
- Kodama M, Seki S. Thermodynamical investigations on phase transitions of surfactant-water systems: thermodynamic stability of gel and coagel phases and the role of water molecules in their appearance. *Adv Colloid Interface Sci* 1991;35:1–30. [https://doi.org/10.1016/0001-8686\(91\)80019-G](https://doi.org/10.1016/0001-8686(91)80019-G).
- Kohns M, Reiser S, Horsch M, Hasse H. Solvent activity in electrolyte solutions from molecular simulation of the osmotic pressure. *J Chem Phys* 2016;144. <https://doi.org/10.1063/1.4942500>.
- Kresheck GC. Isothermal Titration Calorimetry Studies of Neutral Salt Effects on the Thermodynamics of Micelle Formation Isothermal Titration Calorimetry Studies of Neutral Salt Effects on the Thermodynamics of Micelle Formation 2009:6732–5.
- Kroflič A, Šarac B, Bešter-Rogač M. Thermodynamic Characterization of 3-[(3-Cholamidopropyl)-dimethylammonium]-1-propanesulfonate (CHAPS) Micellization Using Isothermal Titration Calorimetry: Temperature, Salt, and pH Dependence. *Langmuir* 2012;28:10363–71. <https://doi.org/10.1021/la302133q>.
- Kroflič A, Šarac B, Bešter-Rogač M. Influence of the alkyl chain length, temperature, and added salt on the thermodynamics of micellization: Alkytrimethylammonium chlorides in NaCl aqueous solutions. *J Chem Thermodyn* 2011;43:1557–63. <https://doi.org/10.1016/j.jct.2011.05.015>.
- Krog N, Larsson K. Phase Behaviour and Rheological Properties of Aqueous Systems of Industrial Distilled Monoglycerides. *Chem Phys Lipids* 1968:129–43.
- Kunz W, Henle J, Ninham BW. 'Zur Lehre von der Wirkung der Salze' (about the science of the effect of salts): Franz Hofmeister's historical papers. *Curr Opin Colloid Interface Sci* 2004;9:19–37. <https://doi.org/10.1016/j.cocis.2004.05.005>.
- Kunz W, Neueder R. Specific ion effects - an attempt of a general overview. *Specif. Ion Eff.*, 2009, p. 3–54.
- Laage D, Hynes JT. A molecular jump mechanism of water reorientation. *Science* 2006;311:832–5. <https://doi.org/10.1126/science.1122154>.
- Laage D, Stirnemann G, Hynes JT. Why water reorientation slows without iceberg formation around hydrophobic solutes. *J Phys Chem B* 2009;113:2428–35. <https://doi.org/10.1021/jp809521t>.
- Lei Z, Chen B, Koo Y-M, MacFarlane DR. Introduction: Ionic Liquids. *Chem Rev* 2017;117:6633–5. <https://doi.org/10.1021/acs.chemrev.7b00246>.
- Leontidis E. Investigations of the Hofmeister series and other specific ion effects using lipid model systems. *Adv Colloid Interface Sci* 2017;243:8–22. <https://doi.org/10.1016/j.cis.2017.04.001>.

- Leontidis E. Chaotropic salts interacting with soft matter: Beyond the lyotropic series. *Curr Opin Colloid Interface Sci* 2016;23:100–9. <https://doi.org/10.1016/j.cocis.2016.06.017>.
- Leontidis E, Aroti A, Belloni L, Dubois M, Zemb T. Effects of Monovalent Anions of the Hofmeister Series on DPPC Lipid Bilayers Part II: Modeling the Perpendicular and Lateral Equation-of-State. *Biophys J* 2007;93:1591–607. <https://doi.org/10.1529/biophysj.107.109264>.
- Lima FS, Andrade MFC, Mortara L, Gustavo Dias L, Cuccovia IM, Chaimovich H. Ion dehydration controls adsorption at the micellar interface: hydrotropic ions. *Phys Chem Chem Phys* 2017;19:30658–66. <https://doi.org/10.1039/C7CP05283A>.
- Lima FS, Chaimovich H, Cuccovia IM, Buchner R. Dielectric relaxation spectroscopy shows a sparingly hydrated interface and low counterion mobility in triflate micelles. *Langmuir* 2013a;29:10037–46. <https://doi.org/10.1021/la401728g>.
- Lima FS, Chaimovich H, Cuccovia IM, Horinek D. Molecular Dynamics Shows That Ion Pairing and Counterion Anchoring Control the Properties of Triflate Micelles: A Comparison with Triflate at the Air/Water Interface. *Langmuir* 2014;30:1239–49. <https://doi.org/10.1021/la404260y>.
- Lima FS, Cuccovia IM, Buchner R, Antunes FE, Lindman B, Miguel MG, et al. Sodium Triflate Decreases Interaggregate Repulsion and Induces Phase Separation in Cationic Micelles. *Langmuir* 2015;31:2609–14. <https://doi.org/10.1021/la5049216>.
- Lima FS, Cuccovia IM, Horinek D, Amaral LQ, Riske KA, Schreier S, et al. Effect of Counterions on the Shape, Hydration, and Degree of Order at the Interface of Cationic Micelles: The Triflate Case. *Langmuir* 2013b;29:4193–203. <https://doi.org/10.1021/la304658e>.
- Lima FS, Maximiano FA, Cuccovia IM, Chaimovich H. Surface Activity of the Triflate Ion at the Air/Water Interface and Properties of N,N,N -Trimethyl- N -Dodecylammonium Triflate Aqueous Solutions. *Langmuir* 2011;27:4319–23. <https://doi.org/10.1021/la2004613>.
- Lindenbaum S, Boyd GE. Osmotic and activity coefficients for the symmetrical tetraalkyl ammonium halides in aqueous solution at 25°. *J Phys Chem* 1964;68:911–7. <https://doi.org/10.1021/j100786a038>.
- Lo Nostro P, Ninham BW. Hofmeister phenomena: An update on ion specificity in biology. *Chem Rev* 2012;112:2286–322. <https://doi.org/10.1021/cr200271j>.
- Luczak J, Jungnickel C, Joskowska M, Thöming J, Hupka J. Thermodynamics of micellization of imidazolium ionic liquids in aqueous solutions. *J Colloid Interface Sci* 2009;336:111–6. <https://doi.org/10.1016/j.jcis.2009.03.017>.
- Magid LJ, Han Z, Warr GG, Cassidy MA, Butler PD, Hamilton WA. Effect of Counterion Competition on Micellar Growth Horizons for Cetyltrimethylammonium Micellar Surfaces: Electrostatics and Specific Binding. *J Phys Chem B* 1997;101:7919–27. <https://doi.org/10.1021/jp970864f>.
- Maibaum L, Dinner AR, Chandler D. Micelle formation and the hydrophobic effect. *J Phys Chem B* 2004;108:6778–81. <https://doi.org/10.1021/jp037487t>.
- Marcus Y. Effect of Ions on the Structure of Water: Structure Making and Breaking. *Chem Rev* 2009;109:1346–70. <https://doi.org/10.1021/cr8003828>.
- Martínez L, Andrade R, Birgin EG, Martínez JM. Packmol: A Package for Building Initial Configurations. *J Comput Chem* 2009;30:2157–64. <https://doi.org/10.1002/jcc>.
- Matero A. Hydrotropes. *Handb. Appl. Surf. Colloid Chem.*, vol. 1, 2002, p. 407–19.
- Maximiano FA, Chaimovich H, Cuccovia IM. Decarboxylation of 6-Nitrobenzisoazole-3-carboxylate in Mixed Micelles of Zwitterionic and Positively Charged Surfactants. *Langmuir* 2006;22:8050–5. <https://doi.org/10.1021/la061042p>.
- Mehring J, Kunz W. Carl Neuberg's hydrotropic appearances (1916). *Adv Colloid Interface Sci* 2021;294:102476. <https://doi.org/10.1016/j.cis.2021.102476>.
- Miyamoto S, Kollman PA. SETTLE: An Analytical Version of the SHAKE and RATTLE Algorithm for Rigid Water Models. *J Comput Chem* 1992;13:952–62.
- Mora S, Dailant J, Luzet D, Struth B. X-ray surface scattering investigation of Langmuir films: Phase transitions and elastic properties. *Europhys Lett* 2004;66:694–700. <https://doi.org/10.1209/epl/i2003-10252-6>.

- Moroi Y, Matuura R. Relationship between Solubility and Micellization of Surfactants; Micelle Temperature Range (MTR) Instead of Krafft Point. *Bull Chem Soc Jpn* 1988;61:333–9. <https://doi.org/10.1246/bcsj.61.333>.
- Mortara L, Chaimovich H, Cuccovia IM, Horinek D, Lima FS. Dehydration Determines Hydrotropic Ion Affinity for Zwitterionic Micelles. *J Chem Inf Model* 2020;60:604–10. <https://doi.org/10.1021/acs.jcim.9b00870>.
- Mortara L, Lima FDS, Cuccovia IM, Nazet A, Horinek D, Buchner R, et al. Specific Ion Effects on Zwitterionic Micelles Are Independent of Interfacial Hydration Changes. *Langmuir* 2018;34:11049–57. <https://doi.org/10.1021/acs.langmuir.8b02115>.
- Mukerjee P. Salt Effects on Nonionic Association Colloids. *J Phys Chem* 1965;69:4038–40.
- Mukerjee P, Mysels KJ. Critical Micelle Concentration of Aqueous Surfactant Systems. National Bureau of Standards: 1971.
- Mukerjee P, Mysels KJ, Kapauan P. Counterion Specificity in the Formation of Ionic Micelles-Size, Hydration and Hydrophobic Bonding Effects. *J Phys Chem* 1966;3803:4166–75.
- Mukhina T, Brezesinski G, Shen C, Schneck E. Phase behavior and miscibility in lipid monolayers containing glycolipids. *J Colloid Interface Sci* 2022a;615:786–96. <https://doi.org/10.1016/j.jcis.2022.01.146>.
- Mukhina T, Pabst G, Ruyschaert JM, Brezesinski G, Schneck E. pH-Dependent physicochemical properties of ornithine lipid in mono- and bilayers. *Phys Chem Chem Phys* 2022b;24:22778–91. <https://doi.org/10.1039/d2cp01045c>.
- Muller N. Search for a Realistic View of Hydrophobic Effects. *Acc Chem Res* 1990;23:23–8. <https://doi.org/10.1021/ar00169a005>.
- Nagarajan R, Ruckenstein E. Theory of Surfactant Self-Assembly: A Predictive Molecular Thermodynamic Approach. *Langmuir* 1991;7:2934–69. <https://doi.org/10.1021/la00060a012>.
- Nagle JF, Tristram-nagle S. Structure of lipid bilayers 2000;1469.
- Nakama Y. Surfactants. *Cosmet. Sci. Technol.*, Elsevier; 2017, p. 231–44. <https://doi.org/10.1016/B978-0-12-802005-0.00015-X>.
- Nascimento DB, Rapuano R, Lessa MM, Carmona-Ribeiro AM. Counterion Effects on Properties of Cationic Vesicles. *Langmuir* 1998;14:7387–91. <https://doi.org/10.1021/la980845c>.
- Nazet A, Sokolov S, Sonnleitner T, Makino T, Kanakubo M, Buchner R. Densities, Viscosities, and Conductivities of the Imidazolium Ionic Liquids [Emim][Ac], [Emim][FAP], [Bmim][BETI], [Bmim][FSI], [Hmim][TFSI], and [Omim][TFSI]. *J Chem Eng Data* 2015;60:2400–11. <https://doi.org/10.1021/acs.jced.5b00285>.
- Neuberg C. Hydrotropische Erscheinungen. *Biochem Z* 1916;76:107–8.
- Nihonyanagi S, Yamaguchi S, Tahara T. Counterion effect on interfacial water at charged interfaces and its relevance to the hofmeister series. *J Am Chem Soc* 2014;136:6155–8. <https://doi.org/10.1021/ja412952y>.
- Nijmeijer MJP, Bruin C, Bakker AF, Van Leeuwen MJ. Wetting and drying of an inert wall by a fluid in a molecular-dynamics simulation. *Phys Rev A* 1990;42:6052–9. <https://doi.org/10.1103/PhysRevA.42.6052>.
- O'Flaherty SM, Wiegart L, Konovalov O, Struth B. Observation of zinc phthalocyanine aggregates on a water surface using grazing incidence x-ray scattering. *Langmuir* 2005;21:11161–6.
- Okada T, Patil JM. Ion uptake by zwitterionic surfaces. *Langmuir* 1998;14:6241–8. <https://doi.org/10.1021/la980442c>.
- Okur HI, Hladílková J, Rembert KB, Cho Y, Heyda J, Dzubiella J, et al. Beyond the Hofmeister Series: Ion-Specific Effects on Proteins and Their Biological Functions. *J Phys Chem B* 2017;121:1997–2014. <https://doi.org/10.1021/acs.jpcc.6b10797>.
- Oliveira ACN, Martens TF, Raemdonck K, Adati RD, Feitosa E, Botelho C, et al. Dioctadecyldimethylammonium:monoolein nanocarriers for efficient in vitro gene silencing. *ACS Appl Mater Interfaces* 2014;6:6977–89. <https://doi.org/10.1021/am500793y>.
- Paleos C, Dais P. Ready Reduction of Some Nitroxide Free Radicals with Ascorbic Acid. *J Chem Soc Chem Commun* 1977:345–6.

- Paredes S, Tribout M, Sepulveda L. Enthalpies of micellization of quaternary tetradecyl- and cetyltrimethylammonium. *J Phys Chem* 1984;88:1871–5. <https://doi.org/10.1021/j150653a040>.
- Parrinello M, Rahman A. Polymorphic transitions in single crystals: A new molecular dynamics method. *J Appl Phys* 1981;52:7182–90. <https://doi.org/10.1063/1.328693>.
- Patiño-Agudelo AJ, Quina FH. Thermodynamics of anion binding to zwitterionic sulfobetaine micelles. *J Colloid Interface Sci* 2022;611:39–45. <https://doi.org/10.1016/j.jcis.2021.12.062>.
- Perger TM, Bešter-Rogač M. Thermodynamics of micelle formation of alkyltrimethylammonium chlorides from high performance electric conductivity measurements. *J Colloid Interface Sci* 2007;313:288–95. <https://doi.org/10.1016/j.jcis.2007.04.043>.
- Phukon A, Sahu K. How do the interfacial properties of zwitterionic sulfobetaine micelles differ from those of cationic alkyl quaternary ammonium micelles? An excited state proton transfer study. *Phys Chem Chem Phys* 2017;19:31461–8. <https://doi.org/10.1039/C7CP06339C>.
- Pottel R, Kaatze U, Mueller S. Dielectric Relaxation in Aqueous Solutions of Zwitterionic Surfactant Micelles. *Berichte BunsengesellschaftPhysical Chem Chem Phys* 1978;82:1086–93. <https://doi.org/10.1002/bbpc.19780821013>.
- Preston W. Some Correlating Principles of Detergent Action. *J Phys Colloid Chem* 1948;52:84–97. <https://doi.org/10.1021/j150457a010>.
- Priebe JP, Satnami ML, Tondo DW, Souza BS, Priebe JM, Micke GA, et al. The chameleon-like nature of zwitterionic micelles: The intrinsic relationship of anion and cation binding in sulfobetaine micelles. *J Phys Chem B* 2008;112:14373–8. <https://doi.org/10.1021/jp801337n>.
- Priebe JP, Souza FD, Silva M, Tondo DW, Priebe JM, Micke GA, et al. The chameleon-like nature of zwitterionic micelles: Effect of cation binding. *Langmuir* 2012;28:1758–64. <https://doi.org/10.1021/la2043735>.
- Pusterla J, Scoppola E, Appel C, Mukhina T, Shen C, Brezesinski G, et al. Characterization of lipid bilayers adsorbed to functionalized air/water interfaces. *Nanoscale* 2022;14:15048–59. <https://doi.org/10.1039/d2nr03334h>.
- Rahman HMA. Dielectric Spectroscopy of The Hydration of Organic Anions as Models for Anionic Residues of Biomolecules. PhD Thesis. Universität Regensburg, 2012.
- Rahman HMA, Buchner R. Hydration and sodium-ion binding of trifluoroacetate in aqueous solution. *J Mol Liq* 2012;176:93–100. <https://doi.org/10.1016/j.molliq.2012.05.017>.
- Rahman HMA, Hefter G, Buchner R. Hydrophilic and hydrophobic hydration of sodium propanoate and sodium butanoate in aqueous solution. *J Phys Chem B* 2013;117:2142–52. <https://doi.org/10.1021/jp310029c>.
- Rahman HMA, Hefter G, Buchner R. Hydration of formate and acetate ions by dielectric relaxation spectroscopy. *J Phys Chem B* 2012;116:314–23. <https://doi.org/10.1021/jp207504d>.
- Ray A, Némethy G. Effects of Ionic Protein Denaturants on Micelle Formation by Nonionic Detergents. *J Am Chem Soc* 1971;93:6787–93. <https://doi.org/10.1021/ja00754a014>.
- Rehage H, Hoffmann H. Viscoelastic Detergent Solutions. *Faraday Discuss Chem Soc* 1983;76:363–73.
- Rodríguez A, del Mar Graciani M, Muñoz M, Moyá ML. Influence of the nature of the cation on the reaction DDT + OH⁻ in sulfobetaine micellar solutions in the presence of added salts. *Langmuir* 2001;17:1860–3. <https://doi.org/10.1021/la001437n>.
- Ropers MH, Czichocki G, Brezesinski G. Counterion effect on the thermodynamics of micellization of alkyl sulfates. *J Phys Chem B* 2003;107:5281–8. <https://doi.org/10.1021/jp0264329>.
- Santos DP, Longo RL. Molecular Dynamics Simulations of Specific Anion Adsorption on Sulfobetaine (SB3-14) Micelles. *J Phys Chem B* 2016;120:2771–80. <https://doi.org/10.1021/acs.jpcc.5b12475>.
- Šarac B, Bešter-Rogač M. Temperature and salt-induced micellization of dodecyltrimethylammonium chloride in aqueous solution: A thermodynamic study. *J Colloid Interface Sci* 2009;338:216–21. <https://doi.org/10.1016/j.jcis.2009.06.027>.
- Sarac B, Medos Z, Cognigni A, Bica K, Chen L, Bester-Rogac M. Thermodynamic study for micellization of imidazolium based surface active ionic liquids in water: Effect of alkyl chain

- length and anions. *Colloids Surf Physicochem Eng Asp* 2017;532:609–17. <https://doi.org/10.1016/j.colsurfa.2017.01.062>.
- Sarac B, Mériguet G, Ancian B, Bester-Rogac M. Salicylate Isomer-Specific Effect on the Micellization of Dodecyltrimethylammonium Chloride: Large Effects from Small Changes. *Langmuir* 2013;29:4460–9. <https://doi.org/10.1021/la400161n>.
- Scarpa MV, Maximiano FA, Chaimovich H, Cuccovia IM. Interfacial concentrations of chloride and bromide and selectivity for ion exchange in vesicles prepared with dioctadecyldimethylammonium halides, lipids, and their mixtures. *Langmuir* 2002;18:8817–23. <https://doi.org/10.1021/la025652a>.
- Schales O, Schales SS. A Simple and Accurate Method for the Determination of Chloride in Biological Fluids. *J Biol Chem* 1941;140:879–84. [https://doi.org/10.1016/s0021-9258\(18\)72872-x](https://doi.org/10.1016/s0021-9258(18)72872-x).
- Schneider CA, Rasband WS, Eliceiri KW. NIH Image to ImageJ: 25 years of image analysis. *Nat Methods* 2012;9:671–5. <https://doi.org/10.1038/nmeth.2089>.
- Schreier S, Polnaszek CF, Smith ICP. Spin Labels in Membranes Problems in Practice. *Biochim Biophys Acta BBA* 1978;515:375–436.
- Schreier-Muccillo S, Marsh D, Smith ICP. Monitoring the permeability profile of lipid membranes with spin probes. *Arch Biochem Biophys* 1976;172:1–11. [https://doi.org/10.1016/0003-9861\(76\)90041-2](https://doi.org/10.1016/0003-9861(76)90041-2).
- Schwierz N, Horinek D, Sivan U, Netz RR. Reversed Hofmeister series—The rule rather than the exception. *Curr Opin Colloid Interface Sci* 2016;23:10–8. <https://doi.org/10.1016/j.cocis.2016.04.003>.
- Sepúlveda L, Cortés J. Ionization degrees and critical micelle concentrations of hexadecyltrimethylammonium and tetradecyltrimethylammonium micelles with different counterions. *J Phys Chem* 1985;89:5322–4. <https://doi.org/10.1021/j100270a040>.
- Shapovalov VL, Dittrich M, Konovalov OV, Brezesinski G. Use of total reflection X-ray fluorescence (TRXF) for the quantification of DNA binding to lipid monolayers at the air-water interface. *Langmuir* 2010;26:14766–73. <https://doi.org/10.1021/la102472u>.
- Shapovalov VL, Ryskin ME, Konovalov OV, Hermelink A, Brezesinski G. Elemental analysis within the electrical double layer using total reflection X-ray fluorescence technique. *J Phys Chem B* 2007;111:3927–34. <https://doi.org/10.1021/jp066894c>.
- Shimizu S, Booth JJ, Abbott S. Hydrotropy: Binding models vs. statistical thermodynamics. *Phys Chem Chem Phys* 2013;15:20625–32. <https://doi.org/10.1039/c3cp53791a>.
- Shinoda K. Correlation between Melting Points of Alkanoic Acids and Krafft Points of Their Sodium Salts. *J Phys Chem* 1987;80:1987–8. <https://doi.org/10.1021/j100559a007>.
- Sonnleitner T, Turton DA, Waselikowski S, Hunger J, Stoppa A, Walther M, et al. Dynamics of RTILs: a comparative dielectric and OKE study. *J Mol Liq* 2014;19–25.
- Southall NT, Dill KA. The mechanism of hydrophobic solvation depends on solute radius. *J Phys Chem B* 2000;104:1326–31. <https://doi.org/10.1021/jp992860b>.
- Southall NT, Dill KA, Haymet ADJ. A view of the hydrophobic effect. *J Phys Chem B* 2002;106:521–33. <https://doi.org/10.1021/jp015514e>.
- Souza FD, Souza BS, Tondo DW, Leopoldino EC, Fiedler HD, Nome F. Imidazolium-based zwitterionic surfactants: Characterization of normal and reverse micelles and stabilization of nanoparticles. *Langmuir* 2015;31:3587–95. <https://doi.org/10.1021/la504802k>.
- Stefaniu C, Latza VM, Gutowski O, Fontaine P, Brezesinski G, Schneck E. Headgroup-ordered monolayers of uncharged glycolipids exhibit selective interactions with ions. *J Phys Chem Lett* 2019;10:1684–90.
- Stephenson BC, Goldsipe A, Beers KJ, Blankschtein D. Quantifying the hydrophobic effect. 1. A computer simulation-molecular-thermodynamic model for the self-assembly of hydrophobic and amphiphilic solutes in aqueous solution. *J Phys Chem B* 2007;111:1025–44. <https://doi.org/10.1021/jp065696i>.
- Sung W, Wang W, Lee J, Vaknin D, Kim D. Specificity and variation of length scale over which monovalent halide ions neutralize a charged interface. *J Phys Chem C* 2015;119:7130–7. <https://doi.org/10.1021/jp512233g>.

- Tanford C. The hydrophobic effect: formation of micelles and biological membranes 2d ed. J. Wiley.; 1980.
- Tanford C. Interfacial free energy and the hydrophobic effect. *Proc Natl Acad Sci U S A* 1979;76:4175–6. <https://doi.org/10.1073/pnas.76.9.4175>.
- Tanford C. Theory of micelle formation in aqueous solutions. *J Phys Chem* 1974;78:2469–79. <https://doi.org/10.1021/j100617a012>.
- Tapia MJ, Burrows HD, Azenha MDG, Miguel M da G, Pais AACC, Sarraguça JMG. Cation Association with Sodium Dodecyl Sulfate Micelles As Seen by Lanthanide Luminescence. *J Phys Chem B* 2002;106:6966–72. <https://doi.org/10.1021/jp014083x>.
- Tardieu A, Luzzati V, Reman FC. Structure and polymorphism of the hydrocarbon chains of lipids: A study of lecithin-water phases. *J Mol Biol* 1973;75:711–33. [https://doi.org/10.1016/0022-2836\(73\)90303-3](https://doi.org/10.1016/0022-2836(73)90303-3).
- Taylor KMG, Morris RM. Thermal analysis of phase transition behaviour in liposomes. *Thermochim Acta* 1995;248:289–301. [https://doi.org/10.1016/0040-6031\(94\)01884-J](https://doi.org/10.1016/0040-6031(94)01884-J).
- Tiddy GJT. Surfactant-water liquid crystal phases. *Phys Rep* 1980;57:1–46. [https://doi.org/10.1016/0370-1573\(80\)90041-1](https://doi.org/10.1016/0370-1573(80)90041-1).
- Tielrooij KJ, Garcia-Araez N, Bonn M, Bakker HJ. Cooperativity in ion hydration. *Science* 2010;328:1006–9. <https://doi.org/10.1126/science.1183512>.
- Tori K, Nakagawa T. Colloid chemical properties of ampholytic surfactants. *Kolloid-Z Z Für Polym* 1963;187:44–51. <https://doi.org/10.1007/bf01622716>.
- Tucker I, Penfold J, Thomas RK, Grillo I, Barker JG, Mildner DFR. The Surface and Solution Properties of Dihexadecyl Dimethylammonium Bromide. *Langmuir* 2008;24:6509–20.
- Van Der Spoel D, Lindahl E, Hess B, Groenhof G, Mark AE, Berendsen HJC. GROMACS: Fast, flexible, and free. *J Comput Chem* 2005;26:1701–18. <https://doi.org/10.1002/jcc.20291>.
- Van Swaay D, deMello A. Microfluidic methods for forming liposomes. *Lab Chip* 2013;13:752. <https://doi.org/10.1039/c2lc41121k>.
- Vega C, De Miguel E. Surface tension of the most popular models of water by using the test-area simulation method. *J Chem Phys* 2007;126. <https://doi.org/10.1063/1.2715577>.
- Voet A. Quantitative Lyotropy. *Chem Rev* 1937;20:169–79.
- Wachter W, Kunz W, Buchner R, Hefter G. Is There an Anionic Hofmeister Effect on Water Dynamics ? Dielectric Spectroscopy of. *J Phys Chem* 2005;109:8675–83. <https://doi.org/10.1021/jp053299m>.
- Wang D, De Jong DH, Rühling A, Lesch V, Shimizu K, Wulff S, et al. Imidazolium-Based Lipid Analogues and Their Interaction with Phosphatidylcholine Membranes. *Langmuir* 2016;32:12579–92. <https://doi.org/10.1021/acs.langmuir.6b02496>.
- Wang J, Wang W, Kollman PA, Case DA. Development and testing of a general amber force field. *J Comput Chem* 2004;25:1157–74. <https://doi.org/10.1002/jcc.20035>.
- Wang X, Liu J, Yu L, Jiao J, Wang R, Sun L. Surface adsorption and micelle formation of imidazolium-based zwitterionic surface active ionic liquids in aqueous solution. *J Colloid Interface Sci* 2013;391:103–10. <https://doi.org/10.1016/j.jcis.2012.09.073>.
- Wojciechowski K, Gutberlet T, Konovalov O. Anion-specificity at water-air interface probed by total reflection X-ray fluorescence (TRXF). *Colloids Surf Physicochem Eng Asp* 2012;413:184–90. <https://doi.org/10.1016/j.colsurfa.2012.06.045>.
- Wu A, Gao Y, Zheng L. Zwitterionic amphiphiles : their aggregation behavior and applications. *Green Chem* 2019;4290–312. <https://doi.org/10.1039/c9gc01808e>.
- X-ray data booklet. <https://Xdb.Lbl.Gov/Xdb.Pdf>: 2001.
- Zhang C, Geng T, Jiang Y, Zhao L, Ju H, Wang Y. Impact of NaCl concentration on equilibrium and dynamic surface adsorption of cationic surfactants in aqueous solution. *J Mol Liq* 2017;238:423–9. <https://doi.org/10.1016/j.molliq.2017.05.033>.
- Zhang L, Somasundaran P, Maltesh C. Electrolyte effects on the surface tension and micellization of n-dodecyl β -D-maltoside solutions. *Langmuir* 1996;12:2371–3. <https://doi.org/10.1021/la950670w>.

Zhao Y, Bharadwaj S, van der Vegt NFA. Nonadditive ion effects on the coil–globule equilibrium of PNIPAM: a computer simulation study. *Phys Chem Chem Phys* 2022;24:10346–55. <https://doi.org/10.1039/D2CP00057A>.

7 Appendix

Force Field Parameters

Table S1. Non-Bonded parameters force field.

Atoms	σ (nm)	Epsilon (KJ/mol)	Charge (q)
C1	0.339	0.457	-0.471
C2	0.339	0.457	0.082
C3	0.339	0.457	-0.008
C4, C5, C6	0.339	0.457	-0.310
S	0.356	1.046	1.234
O	0.295	0.878	-0.679
N	0.325	0.711	0.232
H1	0.247	0.657	0.149
H2	0.265	0.657	0.042
H3	0.196	0.66	0.069
H4, H5, H6	0.196	0.66	0.154

Table S2. Ryckaert-Bellemans dihedral parameter for the polar head.

Dihedral	C0	C1	C2	C3	C4	C5
S-C1-C2-H	0.524	1.227	-0.707	-1.377	0.730	-0.280
O-S-C1-C2	0.997	3.381	0.131	-4.562	-0.131	0.049
O-S-C1-H	0.522	1.796	0.000	-2.517	0.000	0.149
C1-C2-C3-N	0.902	4.525	0.543	-5.824	-0.465	-0.262

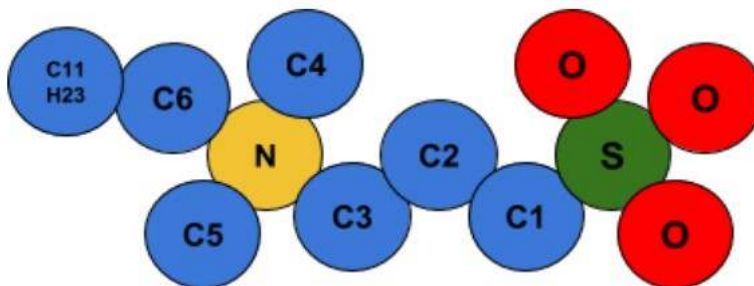


Figure S1. Representation for the naming of atoms in the polar head.

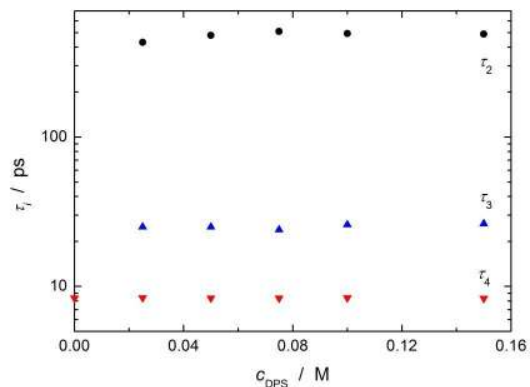


Figure S2. Relaxation times, τ_i ($i = 2$ (● black), 3 (▲ blue), 4 (▼ red), of aqueous DPS solutions at 25 °C.

c) DRS parameters

Table S3. DRS parameters DPS concentration

Conc (mol x L ⁻¹)	S ₂	α	τ ₂	S ₃	τ ₃	S ₄	τ ₄	ε _∞	ε
0.025	2.15	0.198	430.1	0.78	25	71.2	8.38	80.01	5.85
0.05	3.88	0.119	479	1.49	25	69.77	8.34	81	5.86
0.075	5.76	0.118	509	1.82	24	68.37	8.32	81.94	5.98
0.1	7.38	0.102	493	2.09	25	67.5	8.37	82.99	5.99
0.15	10.14	0.092	489	3.18	26	64.9	8.30	84.24	5.94

Table 4. DRS parameters 0.050 M salt

Salt	S ₁	τ ₁	S ₂	α	τ ₂	S ₃	τ ₃	S ₄	τ ₄	ε _∞	ε
NaBr	3.14	2721	10.04	0.1	486	2.63	26.86	63.80	8.3	6.34	85.92
NaTf	4.31	4895	9.39	0.1	517	2.62	36.00	64.21	8.3	6.06	86.61
NaTFA	2.33	3909	10.18	0.1	519	2.55	32.34	64.34	8.3	6.02	85.42
NaMs	3.77	2530	10.67	0.1	543	2.69	30.54	64.40	8.3	5.97	87.49

Table S5. DRS parameters 0.075 M salt

Salt	S ₁	τ ₁	S ₂	α	τ ₂	S ₃	τ ₃	S ₄	τ ₄	ε _∞	ε
NaBr	4.58	3559	9.14	0.1	495	2.63	27.1	63.8	8.3	6	86.09
NaTf	4.58	3559	9.14	0.1	468	2.05	29.4	64.32	8.3	6	86.09

Table S6. DRS parameters 0.100 M salt

Salt	S ₁	τ ₁	S ₂	α	τ ₂	S ₃	τ ₃	S ₄	τ ₄	ε _∞	ε
NaBr	6.05	3990	8.39	0.1	485	2.55	33.3	63.98	8.3	6.05	87.31
NaTf	6.34	3990	8.39	0.1	485	2.55	33.3	63.98	8.3	6.05	87.31
NaTFA	4.48	2896	9.49	0.1	5.02	2.92	34	63.44	8.3	6.07	86.41
NaMs	4.88	3474	12.72	0.1	646	3.29	30.70	62.87	8.3	6.52	90.3

Table S7. DRS parameters 0.125 M salt

Salt	S ₁	τ ₁	S ₂	α	τ ₂	S ₃	τ ₃	S ₄	τ ₄	ε _∞	ε
NaBr	7.29	3864	8.58	0.1	459	2.29	33	63.53	8.3	6.1	87.8
NaTf	6.34	3990	8.39	0.1	485	2.55	33.33	63.98	8.3	6.05	87.3

For DPS concentration the amplitude can be described by the power law

$$S_2(c_{\text{DPS}}) = 51.7 \times (c_{\text{DPS}})^{0.854} \quad (\sigma_{\text{fit}} = 0.14) \quad (\text{S1})$$

The amplitude of bulk-like water, S_b , decreases linearly (Fig. 5a) according to

$$S_b(c_{\text{DPS}}) = 74.848 - 50.3 \times c_{\text{DPS}} \quad (\sigma_{\text{fit}} = 0.17) \quad (\text{S2})$$

where the fit was forced through the pure-water value , $S_b(0) = 74.848$.

The amplitude of slow water, S_3 , increases (Fig. 5b) but the obtained values are rather small, $S_3(c_{\text{DPS}}) < 2.5$, and thus prone to systematic errors. Since a linear increase of $S_3(c_{\text{DPS}})$ is expected for low DPS concentrations, we used the data at 100 mM and 150 mM together with (0, 0) to get

$$S_3(c_{\text{DPS}}) = 21.15 \times c_{\text{DPS}} \quad (\sigma_{\text{fit}} = 0.02) \quad (\text{S3})$$

from the solid red line in Fig. 5b.

For salt-containing solutions, the amplitudes can be correlated to the salt concentration linearly yielding

$$S_1(c) = 57.9 \times c_{\text{salt}} \quad (\sigma_{\text{fit}} = 0.7) \quad (\text{S4})$$

$$S_2(c) = 10.1 - 6.9 \times c_{salt} \quad (\sigma_{fit} = 1.1) \quad (S5)$$

$$S_3(c) = 3.2 - 7.2 \times c_{salt} \quad (\sigma_{fit} = 0.4) \quad (S6)$$

$$S_b(c) = 67.4 - 10.9 \times c_{salt} \quad (\sigma_{fit} = 0.2) \quad (S7)$$

The fraction of bound water (f_t), slow water (f_s) and ib water (f_{ib}) are linearly correlated to the concentration of salt with the equations

$$f_t(c) = 0.0542 + 0.142 \times c_{salt} \quad (\sigma_{fit} = 0.004) \quad (S8)$$

$$f_s(c) = 0.0447 - 0.101 \times c_{salt} \quad (\sigma_{fit} = 0.005) \quad (S9)$$

$$f_{ib}(c) = 0.0095 + 0.243 \times c_{salt} \quad (\sigma_{fit} = 0.004) \quad (S10)$$

with the intercepts clamped to the interpolated values for salt-free 150 mM DPS.

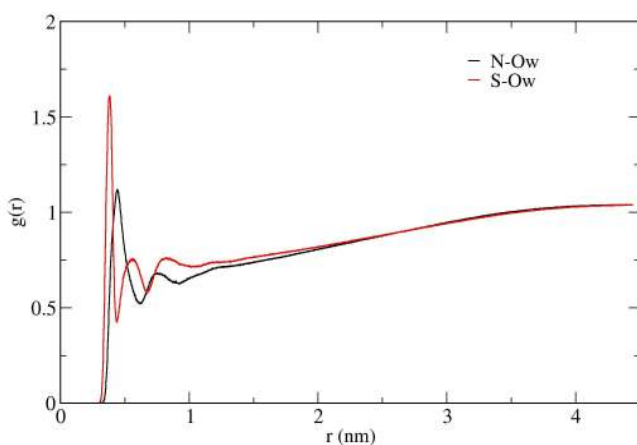


Figure S3. RDF of oxygen atoms of water in relation to nitrogen or sulfur atoms for DPS atoms in water.

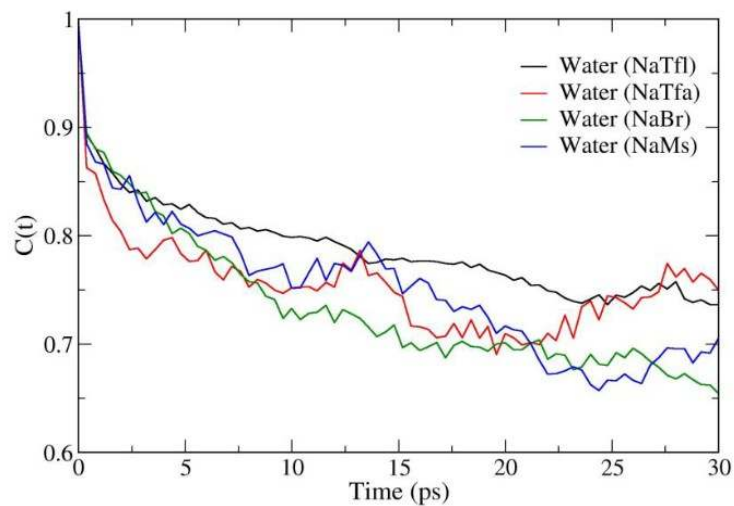


Figure S4. Autocorrelation function of water molecules bound to DPS+salt.

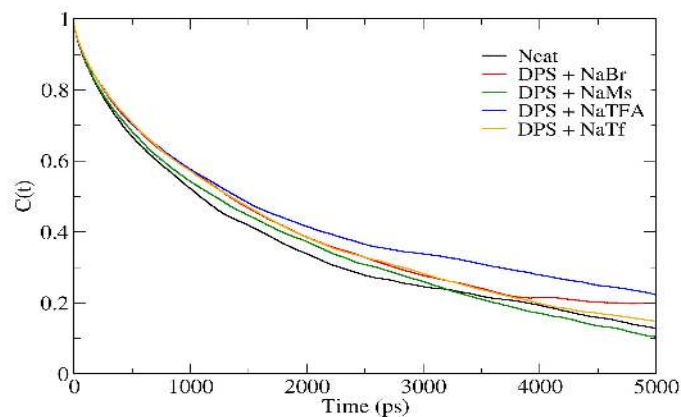


Figure S5. Autocorrelation function of N-S in DPS molecule for all systems.

Table S8. Thermodynamic parameters for DPS micellization in 100 mM salt solutions, in three temperatures.

Temperature / °C	cmc / mmol/L	ΔG / KJ.mol ⁻¹	ΔH / KJ.mol ⁻¹	T ΔS / KJ.mol ⁻¹
No Salt				
10	4.30 ± 0.05	-22.27 ± 0.02	9.49 ± 0.11	31.76 ± 0.11
25	3.69 ± 0.14	-23.86 ± 0.10	2.97 ± 0.16	26.83 ± 0.25
35	3.41 ± 0.05	-24.83 ± 0.02	-1.05 ± 0.01	23.78 ± 0.02
NaAc				

10	4.06 ± 0.05	-22.41 ± 0.01	9.11 ± 0.29	31.52 ± 0.30
25	3.85 ± 0.13	-23.76 ± 0.08	2.45 ± 0.16	26.21 ± 0.18
35	3.48 ± 0.11	-24.78 ± 0.08	-1.11 ± 0.05	23.67 ± 0.10
NaMs				
10	3.91 ± 0.05	-22.49 ± 0.03	9.44 ± 0.37	31.94 ± 0.38
25	3.51 ± 0.10	-23.99 ± 0.07	2.74 ± 0.09	26.52 ± 0.11
35	3.19 ± 0.05	-25.00 ± 0.03	-1.44 ± 0.05	23.56 ± 0.05
NaCl				
10	4.05 ± 0.14	-22.41 ± 0.08	9.47 ± 0.35	31.88 ± 0.37
25	3.37 ± 0.10	-24.09 ± 0.06	2.74 ± 0.27	26.83 ± 0.10
35	3.41 ± 0.17	-24.83 ± 0.12	-1.15 ± 0.07	23.68 ± 0.14
NaBr				
10	3.58 ± 0.05	-22.70 ± 0.04	7.9 ± 0.30	30.68 ± 0.30
25	3.21 ± 0.06	-24.21 ± 0.05	1.69 ± 0.04	25.90 ± 0.10
35	3.04 ± 0.05	-25.13 ± 0.04	-2.19 ± 0.03	22.94 ± 0.10
NaTFA				
10	2.84 ± 0.05	-23.25 ± 0.04	8.32 ± 0.18	31.57 ± 0.18
25	2.61 ± 0.06	-24.73 ± 0.05	1.50 ± 0.07	26.23 ± 0.10
35	2.43 ± 0.05	-25.70 ± 0.06	-2.58 ± 0.03	23.12 ± 0.10
NaBzo				
10	2.51 ± 0.07	-23.53 ± 0.07	7.14 ± 0.25	30.68 ± 0.26
25	2.25 ± 0.11	-25.10 ± 0.13	0.48 ± 0.08	25.58 ± 0.15
35	2.25 ± 0.07	-25.89 ± 0.08	-3.86 ± 0.15	22.03 ± 0.17
NaBzs				
10	2.23 ± 0.05	-23.81 ± 0.06	5.26 ± 0.08	29.07 ± 0.10
25	1.95 ± 0.05	-25.45 ± 0.05	-1.14 ± 0.04	24.31 ± 0.10
35	2.10 ± 0.13	-26.07 ± 0.16	-5.06 ± 0.38	21.01 ± 0.32
NaTf				
10	1.30 ± 0.06	-25.09 ± 0.10	3.22 ± 0.56	28.31 ± 0.57
25	1.28 ± 0.10	-26.51 ± 0.18	-3.11 ± 0.24	23.40 ± 0.30
35	1.41 ± 0.05	-27.09 ± 0.07	-6.51 ± 0.37	20.58 ± 0.37
NaClO ₄				
10	1.12 ± 0.05	-25.43 ± 0.10	-2.43 ± 0.35	23.00 ± 0.36

25	1.16 ± 0.05	-26.74 ± 0.10	-7.21 ± 0.20	19.52 ± 0.22
35	1.29 ± 0.05	-27.32 ± 0.10	-10.76 ± 0.40	16.57 ± 0.41

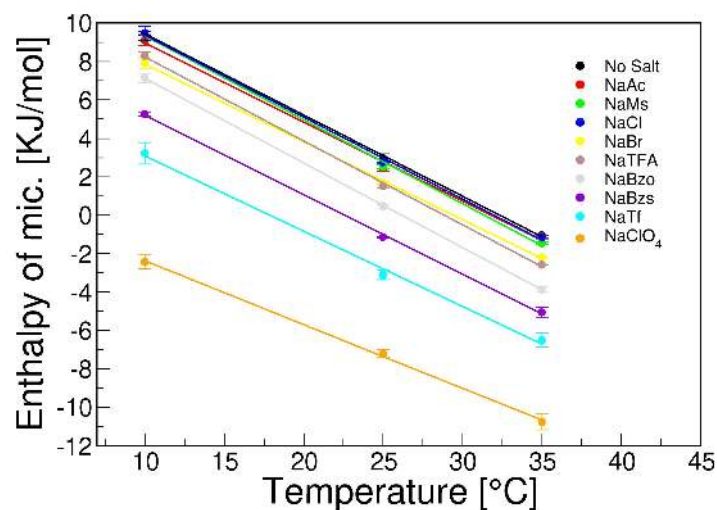


Figure S6. Linear regression micellization enthalpy vs temperature.

Table S9. cmc and enthalpy for DPS in higher salt concentrations

Salt concentration/ mM	cmc / mmol/L	$\Delta H / \text{KJ.mol}^{-1}$
NaBr		
50	3.35	2.14
100	3.2	1.70
200	2.83	1.35
300	2.67	0.90
500	2.37	0.68
NaTFA		
50	2.8	2.13
100	2.6	1.5
200	1.98	0.75
400	1.44	-0.92
1000	0.78	-5.26
NaBzo		

50	2.64	1.35
100	2.16	0.54
200	1.8	-1.21
300	1.63	-2.91
500	1.26	-6.19
1000	1.04	-12.95
NaBzs		
50	2.46	0.20
100	1.93	-1.20
200	1.63	-3.24
300	1.39	-4.66
500	1.17	-8.81
1000	1.11	-13.2
NaTf		
50	1.67	-1.95
100	1.21	-3.28
200	0.92	-5.41
300	0.7	-7.24
500	0.503	-9.42
1000	0.308	-11.93
NaClO ₄		
50	1.45	-6.38
100	1.19	-8.2
200	0.82	-10.4
300	0.64	-13.22
500	0.55	-15.1
1000	0.36	-17.87

Synthesis of DHImC:

Potassium hydroxide (2 mol) was added to a dimethyl sulfoxide (DMSO) solution (500 mL) containing imidazole (1 mol). The mixture was then stirred for 30 min at 70°C and 1-bromo hexadecane (1.1 mol) was added drop wise under vigorous stirring. After 6 h, the mixture was

cooled at room temperature and 100 mL of water were added in order to allow the precipitation of intermediary compound 1-Hexadecyl-1H-imidazole. The precipitate was filtered and washed twice with water.

A mixture of 1-Hexadecyl-1H-imidazole and 1-bromo hexadecane (0.01 mol) was ground in mortar using a pestle for uniform mixing. This mixture was microwaved at 100 W and 90°C for 1.30 h, with stirring. Completion of reaction was checked by TLC. The product was purified by neutral alumina column chromatography using chloroform/methanol (1:1). DHImB was prepared exchanging bromide to chloride in a Dowex 21K anion-exchange resin.

Analytical Data for Dihexadecyl-imidazolium Bromide (C₃₅H₆₉N₂Br)

Mol. wt. C₃₅H₆₉N₂Br = 579.84

Melting Point: 64-66 °C

Elementary Analysis: C: 70.29; H: 11.65; N: 4.71

Found: C: 70.32; H: 11.63; N: 4.69

Mass spectra:

Amazon Speed ETD – Bruker Daltonics

Capillary: 4500V

Nebulizer: 12 Psi

Dry gas: 5 L/min

Temp: 200°C

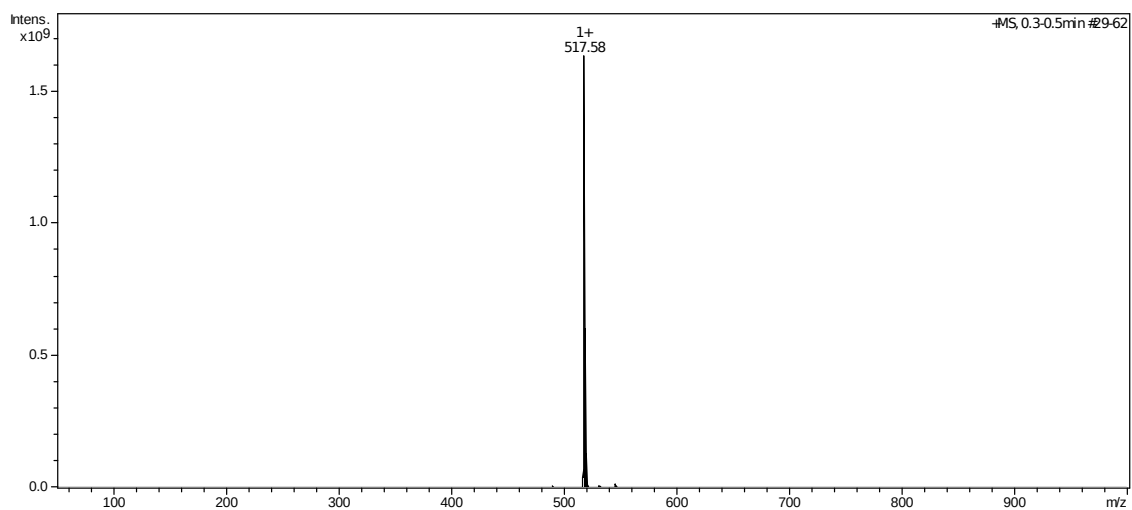


Figure S7. Mass spectra for DHImC in methanol

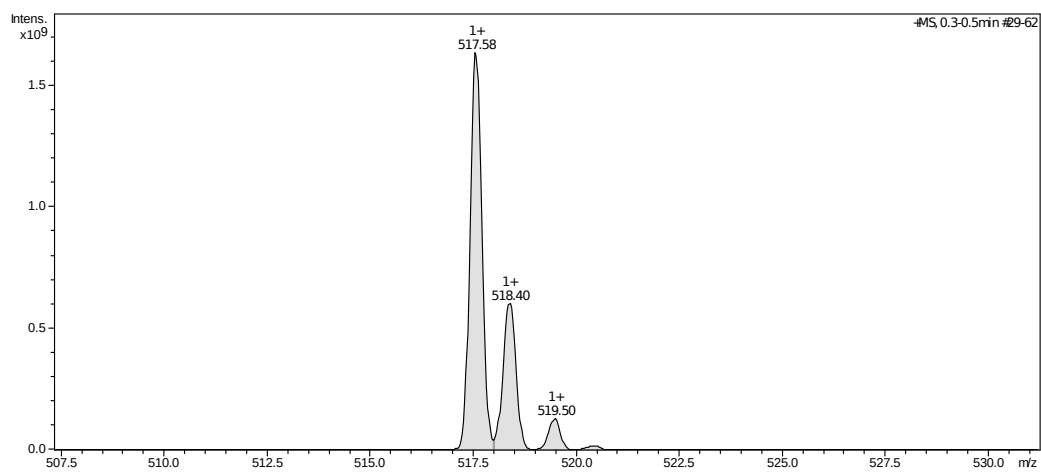
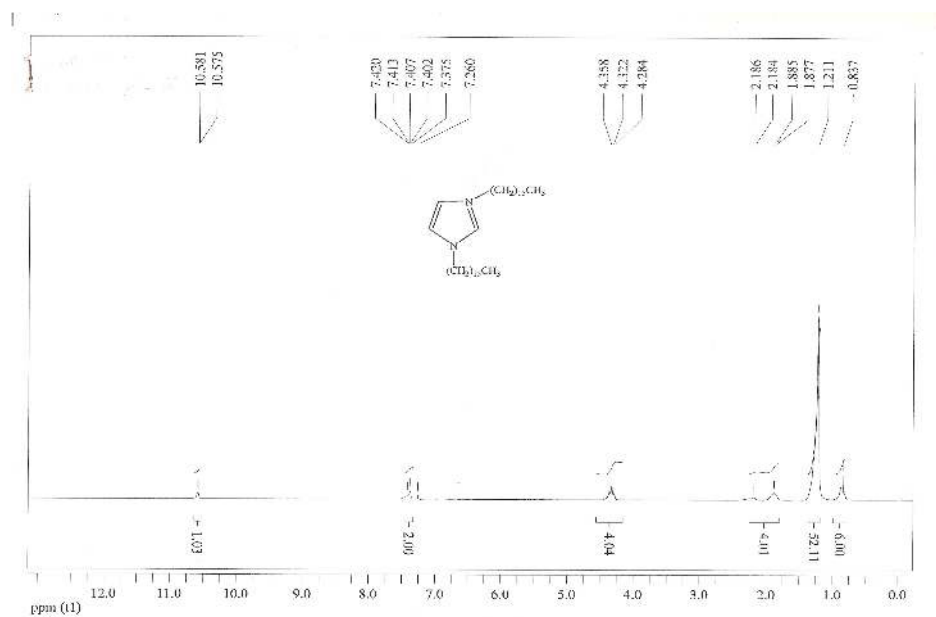
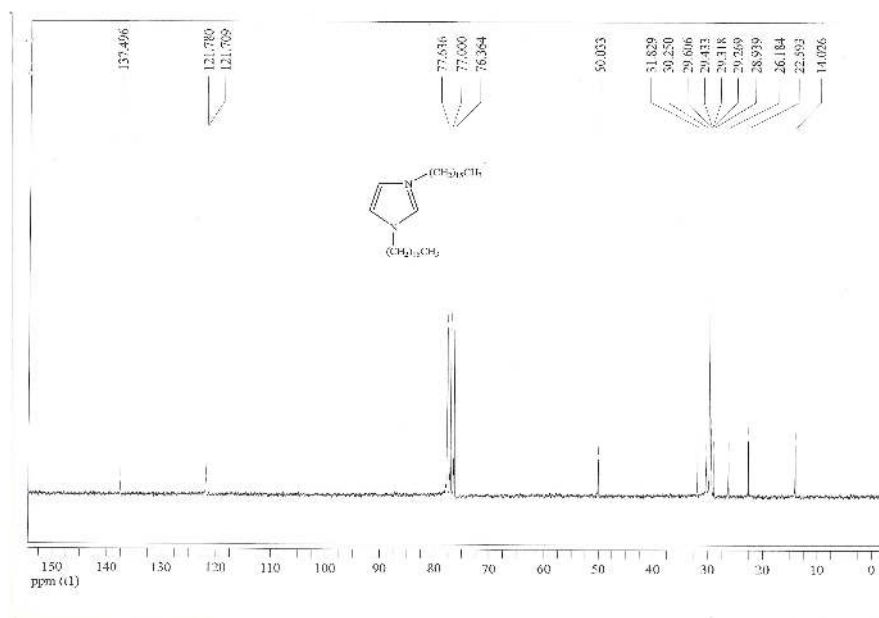


Figure S8. Mass spectra for DHImC in methanol



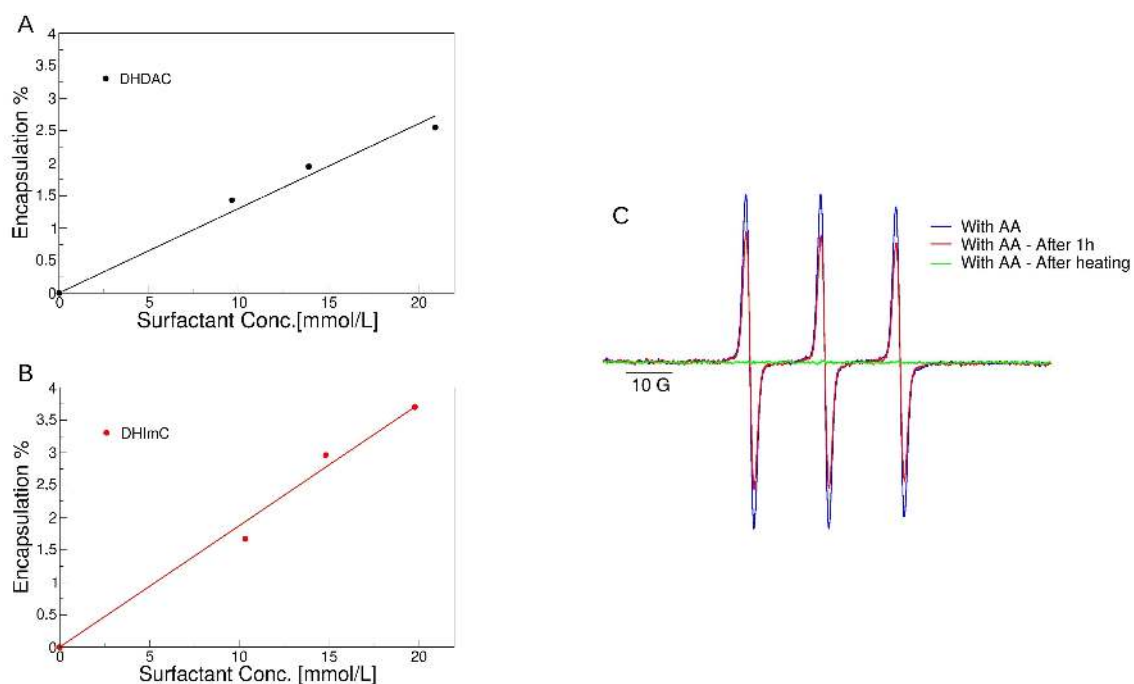


Figure S11. Encapsulation percentage with different surfactant concentration for (A) DHDAC and (B) DHImC and (C) EPR spectra for CAT encapsulated in DHDAC vesicles right after ascorbic acid, after 1h, and after heating the sample at 40°C for 10 minutes.

Table S10. Relative heights (h) and width (w) of the EPR peaks for the systems pos-transition.

Surfactant	DHDAC	DHImC	DHDAC	DHImC
Label	5-MeSL		16-MeSL	
h+1/h0	0.91	0.96	1.03	1.01
h+1/h-1	2.21	1.80	1.75	1.34
h0/h1	2.44	1.87	1.70	1.32
w+1	3.33	2.84	2.01	2.01
w0	3.17	2.83	2.05	1.96
w-1	5.61	4.10	2.54	2.25

Table S11. $A_{||}$, A_{\perp} and Order parameter (S) for molecules pre-transition.

Surfactant	DHDAC	DHImC	DHDAC	DHImC
Label	5-MeSL		16-MeSL	
$A_{ }$	30.11	30.11	22.67	20.61
A_{\perp}	8.27	8.76	10.31	10.73
S	0.84	0.82	0.48	0.38

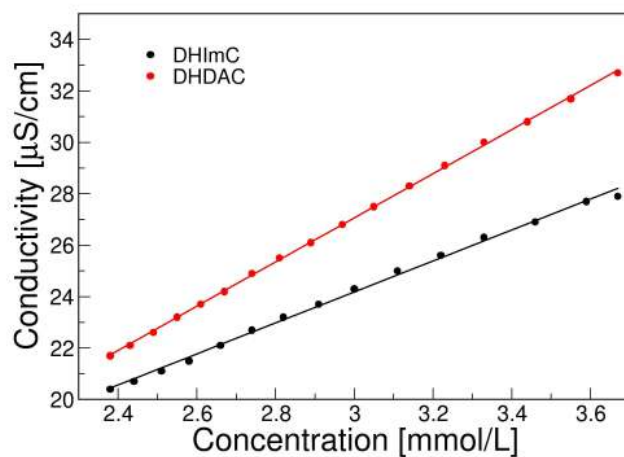


Figure S14. Conductivity for DHImC and DHDAC LUVs

8 Attachment 1 – Curricular Summary

1. Dados Pessoais

Laura Mortara
Jundiaí-SP Brasil, 18/05/1993

2. Educação

Ser Universitário, Jundiaí, 2010.

Universidade de São Paulo, São Paulo, 2016.
Graduação em Química

Universidade de São Paulo, São Paulo, 2017.
Licenciatura em Química

3. Áreas de especialização

1. Dinâmica Molecular
2. Físico-Química de Colóides
3. Biofísica de Membranas

4. Ocupação

Bolsista de Doutorado, FAPESP, 2017-2023

4. Publicações

Artigos completos publicados em periódicos

Lima FS, Andrade MFC, **Mortara L**, Gustavo Dias L, Cuccovia IM, Chaimovich H. Ion dehydration controls adsorption at the micellar interface: hydrotropic ions. *Phys Chem Chem Phys* 2017;19:30658–66. <https://doi.org/10.1039/C7CP05283A>.

Mortara L, Lima FDS, Cuccovia IM, Nazet A, Horinek D, Buchner R, et al. Specific Ion Effects on Zwitterionic Micelles Are Independent of Interfacial Hydration Changes. *Langmuir* 2018;34:11049–57. <https://doi.org/10.1021/acs.langmuir.8b02115>.

Cauz ACG, Carretero GPB, Saraiva GKV, Park P, **Mortara L**, Cuccovia IM, et al. Violacein Targets the Cytoplasmic Membrane of Bacteria. *ACS Infect Dis* 2019;5:539–49. <https://doi.org/10.1021/acsinfectdis.8b00245>.

Mortara L, Chaimovich H, Cuccovia IM, Horinek D, Lima FS. Dehydration Determines Hydrotropic Ion Affinity for Zwitterionic Micelles. *J Chem Inf Model* 2020;60:604–10. <https://doi.org/10.1021/acs.jcim.9b00870>.

Oseliero Filho PL, Gerbelli BB, Fornasier F, Chaves Filho AB, Yoshinaga MY, Miyamoto S, **Mortara, L**, Lacerda, CD, Cuccovia, IM, Pimentel, AS, Oliveira, CLP. Structure and Thermotropic Behavior of Bovine- And Porcine-Derived Exogenous Lung Surfactants. *Langmuir* 2020;36:14514–29. <https://doi.org/10.1021/acs.langmuir.0c02224>.

Resumos publicados em anais de congressos

Mortara, Laura, Muckina, Tetiana, Cuccovia, Iolanda M, Chaimovich, H, Hernan Chamovich, Brezesinski, Gerald, van der Vegt, Nico, and Schneck, Emanuel. Quantifying the Bromide vs. Chloride Adsorption at Cationic Surfactant Interfaces. [36th European Colloid & Interface Society Conference](#), Chania 2022.

Mortara, Laura; Lacerda, C. D. ; Cuccovia, Iolanda Midea ; Lima, Filipe Da Silva ; Chaimovich, H. . Micellization Thermodynamics Of A Zwitterionic Micelle In The Presence Of Hydrotropic Salts. In: XLIV Congresso da Sociedade Brasileira de Biofísica, 2019, Santos. XLIV Congresso da Sociedade Brasileira de Biofísica, 2019.

Mortara, Laura; Lima, Filipe Da Silva ; Cuccovia, Iolanda Midea ; Nazet, Andreas ; Horinek, Dominik ; Buchner, R. ; Chaimovich, H. . Specific anion binding to zwitterionic micelles does not depends on interfacial dehydration. In: Sao Paulo School of Advanced Science on Colloids, 2018, Campinas. Sao Paulo School of Advanced Science on Colloids, 2018.

Mortara, Laura; Redy, S. N. ; Carretero, G. ; Chaimovich, Hernan ; Cuccovia, Iolanda Midea . Characterization of liposomes formed by a new imidazolium compound. In: Sao Paulo School of Advanced Science - Biophysical Methods to Study Biomolecular Interactions, 2017, São Paulo. Sao Paulo School of Advanced Science - Biophysical Methods to Study Biomolecular Interactions, 2017.

Mortara, Laura; Lima, Filipe Da Silva ; Chaimovich, Hernan ; Cuccovia, Iolanda Midea . Caracterização Por Dinâmica Molecular De Micelas Zwitteriônicas Com Adição De Sais De Sódio. In: 24° Simpósio Internacional de Iniciação Científica e Tecnológica da USP, 2016, São Paulo. 24° Simpósio Internacional de Iniciação Científica e Tecnológica da USP, 2016.

Mortara, Laura; Lima, F. S. ; Buchner, Richard ; Chaimovich, Hernan ; Cuccovia, Iolanda Midea . Hydration of 3-(N,N-Dimethyldodecylammonio)propanesulfonate micelles using Dielectric Relaxation Spectroscopy. In: 45th Annual Meeting of the Brazilian Society for Biochemistry and Molecular Biology (SBBq), 2016, Natal. 45th Annual Meeting of the Brazilian Society for Biochemistry and Molecular Biology (SBBq), 2016.

Mortara, Laura; Lima, Filipe Da Silva ; Horinek, Dominik ; Chaimovich, Hernan ; Cuccovia, Iolanda Midea . Efeito da Adição de Sais a Micelas Zwitteriônicas. In: 23° Simpósio Internacional dd Iniciação Científica da USP, 2015, São Paulo. 23° Simpósio Internacional dd Iniciação Científica da USP, 2015.